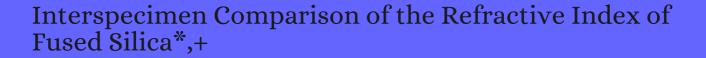
## CITATION REPORT List of articles citing



DOI: 10.1364/josa.55.001205 Journal of the Optical Society of America, 1965, 55, 1205.

Source: https://exaly.com/paper-pdf/8726062/citation-report.pdf

Version: 2024-04-03

This report has been generated based on the citations recorded by exaly.com for the above article. For the latest version of this publication list, visit the link given above.

The third column is the impact factor (IF) of the journal, and the fourth column is the number of citations of the article.

#	Paper IF	Citations
2286	Spectral restoration for femtosecond spectral interferometry with attosecond accuracy. <b>2010</b> , 27, 1104	
2285	High efficiency excitation of plasmonic waveguides with vertically integrated resonant bowtie apertures. <b>2009</b> , 17, 8036	
2284	Cylindrical beam propagation modelling of perturbed whispering-gallery mode microcavities. <b>2013</b> , 21, 30243	
2283	Cylindrical beam propagation modelling of perturbed whispering-gallery mode microcavities. <b>2013</b> , 21, 30243	
2282	Generalized full-vector multi-mode matching analysis of whispering gallery microcavities. <b>2014</b> , 22, 13507	
2281	Flexible tool for simulating the bulk optical properties of polydisperse spherical particles in an absorbing host: experimental validation. <b>2014</b> , 22, 20223	
2280	Evolution of modes in a metal-coated nano-fiber. <b>2011</b> , 19, 25206	
2279	Evolution of modes in a metal-coated nano-fiber. <b>2011</b> , 19, 25206	
2278	Evolution of modes in a metal-coated nano-fiber. <b>2011</b> , 19, 25206	
2277	Cylindrical beam propagation modelling of perturbed whispering-gallery mode microcavities. <b>2013</b> , 21, 30243	
2276	Quantitative phase microscopy via optimized inversion of the phase optical transfer function. <b>2015</b> , 54, 8566	
2275	References. 558-604	
2274	Symmetric Raman Tensor Contributes to Chiral Vibrational Sum-Frequency Generation from Binaphthyl Amphiphile Monolayers on Water: Study of Electronic Resonance Amplitude and Phase Profiles.	
2273	Probing Charged Aqueous Interfaces Near Critical Angles: Effect of Varying Coherence Length.	
2272	Reduced Near-Resonant Vibrational Coupling at the Surfaces of Liquid Water and Ice.	
2271	Polarization-Dependent Optical Response in Anisotropic NanoparticleDNA Superlattices.	
2270	Optoelectronic Synapses Based on Hot-Electron-Induced Chemical Processes.	

Tunable Visibly Transparent Optics Derived from Porous Silicon.	
2268 High Internal Emission Efficiency of Silicon Nanoparticles Emitting in the Visible Range.	
Optically Induced Structural Instability in GoldSilica Nanostructures: A Case Study.	
Water Structure at the Buried Silica/Aqueous Interface Studied by Heterodyne-Detected Vibrational Sum-Frequency Generation.	
Probing Hydrogen-Bonding Interactions of Water Molecules Adsorbed on Silica, Sodium Calcium Silicate, and Calcium Aluminosilicate Glasses.	
Using a FabryPerot Cavity to Augment the Enhancement Factor for Surface-Enhanced Raman Spectroscopy.	
Quantitative Measurements of the pH-Sensitive Quantum Yield of Fluorophores in Mesoporous Silica Thin Films Using a Drexhage-Type Experiment.	
The Topmost Water Structure at a Charged Silica/Aqueous Interface Revealed by Heterodyne-Detected Vibrational Sum Frequency Generation Spectroscopy.	
Beyond the GouyChapman Model with Heterodyne-Detected Second Harmonic Generation.	
Weakly Trapped, Charged, and Free Excitons in Single-Layer MoS2 in the Presence of Defects, Strain, and Charged Impurities.	
2259 Dynamic Plasmonic Pixels.	
2258 Ultrafast All-Optical Light Control with Tamm Plasmons in Photonic Nanostructures.	
Effects of a simulated high-energy space environment on the ultraviolet transmittance of optical materials between 1050 A and 3000 A. <b>1966</b> , 5, 937-43	107
2256 The effect of the earth's radiation belts on an optical system. <b>1966</b> , 5, 1838-42	5
Determination of silicon oxide thickness. <b>1966</b> , 9, 331-332	10
2254 The optical constants of lithium-ammonia solutions in the metallic range. <b>1967</b> , 16, 439-447	14
Some Properties of SiO2Films Deposited by the Reaction of SiH4with Water Vapor. <b>1967</b> , 6, 1176-1183	4
2252 Refractive-Index Interpolation for Fused Silica*. <i>Journal of the Optical Society of America</i> , <b>1967</b> , 57, 674	52

2251	Optical thickness measurement of SiO2?Si3N4 films on silicon. <b>1967</b> , 10, 625-632	52
2250	Phase-shift corrections in determining the thicknesses of transparent films on reflective substrates. <b>1968</b> , 11, 957-963	6
2249	Optical Waveguides Formed by Proton Irradiation of Fused Silica* Journal of the Optical Society of America, <b>1968</b> , 58, 1171	130
2248	Photoinjection into SiO2: Use of Optical Interference to Determine Electron and Hole Contributions. <b>1969</b> , 40, 5093-5101	83
2247	Index of Refraction of Single-Crystal Selenium. Journal of the Optical Society of America, 1969, 59, 72	24
2246	Refractive Index of Several Glasses as a Function of Wavelength and Temperature*. <i>Journal of the Optical Society of America</i> , <b>1969</b> , 59, 774	141
2245	Spectrophotometric Thickness Measurement for Very Thin SiO2 Films on Si. <b>1970</b> , 41, 787-790	13
2244	Transmissivity and Absorption of Fused Quartz Between 0.22 mu and 3.5 mu from Room Temperature to 1500 degrees C. <b>1971</b> , 10, 2263-8	63
2243	Ellipsometry using imperfect polarizers. <b>1971</b> , 10, 2679-84	3
2242	Generalized Ellipsometric Method for the Absorbing Substrate Covered with a Transparent-Film System Optical Constants of Silicon at 3655 . <i>Journal of the Optical Society of America</i> , <b>1972</b> , 62, 16	42
2241	Ellipsometric Data Analysis of the Oxidation of Thin Molybdenum Films*. <i>Journal of the Optical Society of America</i> , <b>1972</b> , 62, 1524	4
2240	Calibration of instruments measuring reflectance and transmittance. <b>1972</b> , 11, 1749-55	10
2239	Reflection spectroscopy of optically active materials. <b>1973</b> , 1, 277-296	10
2238	Variation of refractive index with wavelength in fused silica optical fibers and preforms. <b>1974</b> , 24, 422-424	5
2237	Correction to the velocity-per-fringe relationship for the VISAR interferometer. <b>1974</b> , 45, 3692-3693	146
2236	Pulse broadening in graded-index optical fibers. <b>1976</b> , 15, 483-91	<b>29</b> 0
2235	Binary silica optical fibers: refractive index and profile dispersion measurements. <b>1976</b> , 15, 3029-36	77
2234	Material and Mode Dispersion in GeO2[B2O3[SiC2 Glasses. <b>1976</b> , 59, 503-507	100

2233 Photocurrents in MOS devices. <b>1976</b> , 36, 243-246	1
2232 Elastic and elasto-optic constants of rutile from a Brillouin scattering study. <b>1976</b> , 14, 1670-1682	48
Optical frequency dependence of the photoelastic coefficients of fused silica. <b>1976</b> , 47, 4024-4025	3
<sub>2230</sub> Glass fibers as optical waveguides. <b>1977</b> , 25, 322-342	2
Experimental and Theoretical Investigation of Subnanosecond Pulse Propagation in Graded Index Fibers. <b>1977</b> ,	
2228 Light drag in a ring laser: An improved determination of the drag coefficient. <b>1977</b> , 16, 313-319	25
Profile synthesis in multicomponent glass optical fibers. <b>1977</b> , 16, 108-12	21
2226 Optical constants of crystalline and fused quartz in the far ultraviolet. <b>1977</b> , 16, 2212-4	28
Temperature and wavelength dependent properties of multiplate reflectors. <b>1977</b> , 13, 950-954	3
A proposal on optical fibre transmission systems in a low-loss 1.0¶.4 h wavelength region. <b>1977</b> , 9, 33-42	56
Silica-based binary glass systems: wavelength dispersive properties and composition in optical fibres. <b>1978</b> , 10, 163-170	19
2222 Wavelength dependent propagation in optical multimode fibers. <b>1978</b> , 24, 213-216	1
Optical Fiber Communication-The State of the Art. <b>1978</b> , 26, 946-955	16
2220 Measurements of the absorption edge in fused silica. <b>1978,</b> 32, 98-99	43
Generation of pulse bursts at 212.8 nm by intracavity modulation of an Nd:YAG laser. <b>1978</b> , 14, 527-532	22
2218 Optical fiber (800-Mbit/sec) transmission experiment at 1.05 microm. <b>1978</b> , 17, 2420-6	15
Propagation in graded-index fibers: comparison between experiment and three theories. <b>1978</b> , 17, 2831	-5 16
Pulse broadening in long-span single-mode fibers around a material-dispersion-free wavelength.  1978, 2, 106	12

Total dispersion in step-index monomode fibres. <b>1979</b> , 15, 394	20
2214 Optical Materials <b>R</b> efractive. <b>1979</b> , 47-77	
Dispersion minimisation in single-mode fibres between 1.3 fh and 1.7 fh. <b>1979</b> , 15, 478	19
2212 Dispersion-free single-mode fibre in 1.5 th wavelength region. <b>1979</b> , 15, 476	50
Mode dispersion, material dispersion and profile dispersion in graded-index single-mode fibre 1979, 3, 239	es. 42
2210 Radiation forces on small particles in the solar system. <b>1979</b> , 40, 1-48	1074
Investigation of spectral absorption coefficient of KI and KV quartz glasses in IR region to upp temperature limit. <b>1979</b> , 31, 1157-1160	per 2
2208 Thermal History Dependence of Refractive Index Dispersion of Fused Silica. <b>1979</b> , 62, 526-526	5 4
Pulse spreading in a single-mode fiber due to third-order dispersion. <b>1979</b> , 18, 678-82	91
2206 Multiple-alpha index profiles. <b>1979</b> , 18, 683-9	17
Sensitivity analysis of the Sagnac-effect optical-fiber ring interferometer. <b>1979</b> , 18, 915-31	63
2204 Minimum dispersion in a single-mode step-index optical fiber. <b>1979</b> , 18, 2516-22	18
Dispersion in step-index silicone-clad fibers. <b>1979</b> , 18, 4000-2	3
2202 Beam-splitter and cell-window errors in fluorescence spectrometry. <b>1979</b> , 18, 4134-7	2
2201 Thermal variation of attenuation for optical fibers. <b>1979</b> , 30, 359-370	41
2200 The ATR spectra of multipole surface plasmons. <b>1979</b> , 84, 75-105	65
2199 Propagation in glass optical waveguides. <b>1979</b> , 51, 341-367	140
2198 Effect of Temperature on Transmission in Lightguides. <b>1979</b> , 58, 945-951	53

Optical Properties of the Interface between Si and Its Thermally Grown Oxide. <b>1979</b> , 43, 1046-1050	102
Definitive profile-dispersion data for germania-doped silica fibres over an extended wavelength range. <b>1979</b> , 15, 469	15
The Absorption Spectra of Monolayers of Fat-soluble Vitamins and the Orientations of Their Chromophores. <b>1980</b> , 53, 1817-1824	9
2194 The ultraviolet absorption spectrum of liquid water. <b>1980</b> , 72, 4416-4428	177
2193 The Calibration of Gloss Reference Standards. <b>1980</b> , 16, 89-93	21
2192 Benchmark cross sections for electron-impact excitation of n S1 levels of He. <b>1980</b> , 22, 1916-1929	101
2191 Characteristics of dispersion free single-mode fiber in the 1.5 µm wavelength region. <b>1980</b> , 16, 1052-1058	21
2190 Wavelength dispersion characteristics of single-mode fibers in low-loss region. <b>1980</b> , 16, 215-225	37
2189 Analytical Models for Thermal Radiation in Fibrous Insulations. <b>1980</b> , 4, 27-44	67
Temperature variation of the refractive indices of yttrium lithium fluoride. <i>Journal of the Optical Society of America</i> , <b>1980</b> , 70, 1244	30
2187 Calibration technique for refracted near-field scanning of optical fibers. <b>1980</b> , 19, 2479-80	8
2186 The electrical and optical properties of amorphous germanium-gallium alloys. <b>1980</b> , 37, 231-240	3
Interferometric method for chromatic dispersion measurement in a single-mode optical fiber. <b>1981</b> , 17, 404-407	83
2184 Optical fiber index profiles by the refracted-ray method (refracted near-field scanning). <b>1981</b> , 20, 3415-22	2 49
2183 Material dispersion of fluorozirconate-type glasses. <b>1981</b> , 20, 3688-90	16
2182 Accurate Wavelength Calibration of an Etalon-Tuned Dye Laser. <b>1981</b> , 35, 593-598	5
2181 Refractive index dispersion of lightguide glasses at high temperature. <b>1981</b> , 17, 310	33
2180 Optical properties of phosphorus-doped polycrystalline silicon layers. <b>1981</b> , 52, 6870-6878	77

2179	Material dispersion evaluation in a fluoride glass. <b>1981</b> , 17, 808	13
2178	OPTICAL FIBER WAVEGUIDES. <b>1981</b> , 1-107	2
2177	Effects of thermal stress on group delay in jacketed single mode fibres. <b>1981</b> , 17, 813	2
2176	Discrete time MRAS with reduced implementation complexity. <b>1981</b> , 17, 809	5
2175	Numerical Analysis of Pulse Broadening in Graded Index Optical Fibers. 1981, 29, 348-352	57
2174	Computer controlled Fabry-Perot wavemeter. <b>1981</b> , 39, 277-282	39
2173	A New Method of Pulse Dispersion Analysis for Simple-Mode Optical Fibers.	
2172	Nondestructive analysis of Si3N4/SiO2/Si structures using spectroscopic ellipsometry. <b>1981</b> , 52, 6788-6797	27
2171	Characterization of low-pressure chemical-vapor-deposited and thermally-grown silicon nitride films. <b>1982</b> , 53, 404-415	57
2170	Optical constants for silicon at 300 and 10 K determined from 1.64 to 4.73 eV by ellipsometry. <b>1982</b> , 53, 3745-3753	160
2169	Computerized refractive index measurements for bulk materials at UV, visible, and IR wavelengths. <b>1982</b> , 53, 43-47	17
2168	Physics of photon-flux measurements with silicon photodiodes. <i>Journal of the Optical Society of America</i> , <b>1982</b> , 72, 1068	23
2167	Optical nature of interface layers: a comparative study of the SiBiO_2 interface. <i>Journal of the Optical Society of America</i> , <b>1982</b> , 72, 1253	19
2166	Optical properties of fiber optics materials. <b>1982</b> , 47, 135-146	2
2165	Repeater spacing of 280 Mbit/s single-mode fiber-optic transmission system using 1.55 µm laser diode source. <b>1982</b> , 18, 264-273	10
2164	Pulse delay measurements in single-mode fibers using sum-frequency mixing as a picosecond shutter. <b>1982</b> , 18, 278-282	3
2163	Single-mode fiber design for long haul transmission. <b>1982</b> , 18, 727-732	18
2162	An overview of the modified chemical vapor deposition (MCVD) process and performance. <b>1982</b> , 18, 459-476	169

2161	Use of polarization-optical time domain reflectometry for observation of the Faraday effect in single-mode fibers. <b>1982</b> , 18, 455-456	5
2160	Comparison of measured and predicted bandwidth of graded-index multimode fibers. <b>1982</b> , 18, 825-838	7
2159	An Overview of the Modified Chemical Vapor Deposition (MCVD) Process and Performance. <b>1982</b> , 30, 305-322	39
2158	Single-Mode Fiber Design for Long Haul Transmission. <b>1982</b> , 30, 573-578	4
2157	Wavelength dependence of the numerical aperture of optical fibers. <b>1982</b> , 41, 99-101	1
2156	Single-Mode Fiber Design for Minimum Dispersion. <b>1983</b> , 31, 959-962	1
2155	Time Domain Optical Spectrometry with Fiber Optic Waveguides. <b>1983</b> , 19, 325-362	2
2154	Silicon photodiode device with 100% external quantum efficiency. <b>1983</b> , 22, 2867	175
2153	Refractive index dispersion and related properties in fluorine doped silica. <b>1983</b> , 22, 3102	80
2152	The stress-optic effect in optical fibers. <b>1983</b> , 19, 834-839	110
2151	An inexpensive, feedback-controlled dye laser intensity stabilisation system. <b>1983</b> , 16, 759-763	2
2150	An enhanced sensitivity null ellipsometry technique for studying films on substrates: Application to silicon nitride on gallium arsenide. <b>1983</b> , 54, 1559-1569	18
2149	Radiative Heat Transfer in Fibrous InsulationsPart I: Analytical Study. <b>1983</b> , 105, 70-75	114
2148	The temperature dependence of the refractive indices of fused silica and crystal quartz. <b>1983</b> , 16, L97-L100	77
2147	An on-line ultraviolet radiation monitoring system for control of photosensitivity test dose. <b>1984</b> , 29, 407-17	2
2146	Determination of the Refractive Indices of Soot Particles from the Reflectivities of Compressed Soot Pellets. <b>1984</b> , 37, 263-283	49
2145	Measurement of dispersion using short lengths of an optical fiber and picosecond pulses from semiconductor film lasers. <b>1984</b> , 2, 464-468	6
2144	Unambiguous determination of thickness and dielectric function of thin films by spectroscopic ellipsometry. <b>1984</b> , 113, 101-113	137

2143	Some new developments on coupled radiative-conductive heat transfer in glasses experiments and modelling. <b>1984</b> , 27, 2307-2319	26
2142	Structural and Chemical Analysis of a Silicon Nitride Film on GaAs by Null Ellipsometry. <b>1984</b> , 85, 69-76	1
2141	Photoacoustic spectroscopy of thin SiO2 films grown on (100) crystalline Si substrates. <b>1984</b> , 33, 153-159	24
2140	Multiple determination of the optical constants of thin-film coating materials. <b>1984</b> , 23, 3571	184
2139	Fitting refractive-index data with the Sellmeier dispersion formula. <b>1984</b> , 23, 4477	212
2138	Dispersion in GeO2-SiO2 glasses. <b>1984</b> , 23, 4486	353
2137	Dielectric properties of heavily doped crystalline and amorphous silicon from 1.5 to 6.0 eV. <b>1984</b> , 29, 768-779	294
2136	Wavelength of distributed feedback dye lasers as a function of the pump-laser wavelength. <b>1985</b> , 17, 457-461	4
2135	Routine determination of the absorption and dispersion spectra of solids with a Fourier-transform infrared spectrometer. <b>1985</b> , 172, 101-110	17
2134	A study of the microstructure of a-Si:H using spectroscopic ellipsometry measurements. <b>1985</b> , 129, 127-138	24
2133	Optical characterization of polycrystalline silicon before and after thermal oxidation. <b>1985</b> , 125, 235-241	13
2132	Harthannia of Sanithanad CdC Silva Sanada adll andiantiana 4005 43 245 252	
	Heat treatment of rf sputtered CdS films for solar cell applications. <b>1985</b> , 12, 345-352	21
2131	MODIFIED CHEMICAL VAPOR DEPOSITION. <b>1985</b> , 1-64	9
	MODIFIED CHEMICAL VAPOR DEPOSITION. <b>1985</b> , 1-64	9
2130	MODIFIED CHEMICAL VAPOR DEPOSITION. <b>1985</b> , 1-64  Silicon Dioxide (SiO2) (Glass). <b>1985</b> , 749-763	9
2130	MODIFIED CHEMICAL VAPOR DEPOSITION. 1985, 1-64  Silicon Dioxide (SiO2) (Glass). 1985, 749-763  An ellipsometry study of a hydrogenated amorphous silicon based n-i structure. 1985, 57, 4566-4571	9 115 33

2125	Single-mode optical fiber with arbitrary refractive index profile: Propagation solution by the Numerov method. <b>1985</b> , 3, 619-627	13
2124	Optical properties and microstructure of gold-fluorocarbon-polymer composite films. <b>1985</b> , 32, 719-732	86
2123	Opto-elastic constant in single mode optical fibers. <b>1985</b> , 3, 1078-1083	34
2122	Application of the Clausius-Mossotti equation to dispersion calculations in optical fibers. <b>1985</b> , 3, 1123-1124	5
2121	Refractive-index measurements of 1.8 cineole (eucalyptole) in the 0.6-1.7-Mum range. <b>1985</b> , 24, 990	1
2120	Heat mirrors for greenhouses. <b>1985</b> , 24, 2651	10
2119	Interpretation of the nonbulklike optical density of thin copper films grown under ion bombardment. <b>1985</b> , 24, 3335	17
2118	Study of refractive index of GeO2:SiO2 mixtures using deposited-thin-film optical waveguides. 1985, 24, 4404	9
2117	Multiple determination of the optical constants of thin-film coating materials: a Rh sequel. <b>1986</b> , 25, 1299	15
2116	Column-density meter: a high precision technique for measuring line-of-sight vapor densities. <b>1986</b> , 25, 4476	12
2115	The nucleation and growth of glow-discharge hydrogenated amorphous silicon. <b>1986</b> , 59, 1160-1166	33
2114	High Resolution Chromatic Dispersion Measurements For Single-Mode Fibers. <b>1986</b> , 0584, 215	
2113	Velocity Interferometer System For Any Reflector (VISAR). <b>1986</b> , 0648, 301	2
2112	Optical Soliton Communication With Wavelength Division Multiplexing. 1986,	
2111	Corona-Discharge-Induced Stress Relaxation in Silicon Dioxide Films on Silicon. <b>1986</b> , 75, 803	2
2110	Variable wavelength, variable angle ellipsometry including a sensitivities correlation test. <b>1986</b> , 138, 27-41	89
2109	Antireflection coatings for planar silicon solar cells. <b>1986</b> , 18, 93-114	25
2108	Determination of the Thickness and Refractive Index of Cu2O Thin Film Using Thermal and Optical Interferometry. <b>1986</b> , 93, 613-620	33

Spectral and temporal investigations of nonlinearities in a non-polarization preserving single-mode optical fibre. <b>1986</b> , 41, 235-240	14
Methods for reducing the fresnel reflection in an optical-fiber connector with index matching material. <b>1986</b> , 69, 94-102	2
2105 Intracavity skew-Brewster-angle plates as a calibrated attenuator for gas lasers. <b>1986</b> , 19, 943-956	4
2104 Stress relaxation technique for thermally grown SiO2. <b>1986</b> , 49, 143-145	15
2103 . <b>1986</b> , 4, 1393-1401	
2102 Temperature dependence of the optical spectra of Si, Ge, and Ge-Si alloys. <b>1986</b> , 33, 1092-1101	15
2101 Examination of the Radiative Properties of Coated Silica Fibers. <b>1987</b> , 11, 7-31	3
2100 Temperature Dependence of the Spectral Attenuation of a Silica-Based Fiber. <b>1987</b> , 8,	1
The ultraviolet calibration system for the UK XUV telescope to be flown on the ROSAT satellite. <b>1987</b> , 20, 1261-1264	6
Refractive index, relaxation times and the viscoelastic model in dry-grown SiO2 films on Si. <b>1987</b> , 51, 1416-1418	56
2097 Nondestructive analysis of silicon-on-insulator wafers. <b>1987</b> , 50, 1900-1902	23
2096 Perturbation correction for refraction in interferometric tomography. <b>1987</b> , 26, 774-6	3
Measurement technique for determining the temperature distribution in a transparent solid using holographic interferometry. <b>1987</b> , 26, 954-8	11
Temperature dependence of the extinction coefficient of fused silica for CO(2) laser wavelengths.  1987, 26, 1728-31	94
Temperature-dependent transmittance of luminous and solar radiation for quartz fibers immersed in carbon tetrachloride. <b>1987</b> , 26, 2164-70	10
2092 Dispersion approximation using higher-order Taylor series terms. <b>1987</b> , 26, 4043-5	2
2091 The Measurement of UV/VIS Transmission Characteristics of Intraocular Lenses. <b>1987</b> , 41, 334-336	3
2090 Time-resolved fluorescence with an optical-fiber probe. <b>1987</b> , 192, 145-153	17

2089	Optical properties of thermally stabilized ion implantation amorphized silicon. <b>1987</b> , 19-20, 577-581	7
2088	300 Femtosecond pulses at 497 nanometer generated by an excimer laser pumped cascade of distributed feedback dye lasers. <b>1988</b> , 47, 299-302	9
2087	Characterization of thin films and materials used in semiconductor technology by spectroscopic ellipsometry. <b>1988</b> , 164, 43-50	8
2086	Dispositif original de mesures des facteurs de rflexion d'une couche mfallique paisse en lumife polarise. <b>1988</b> , 165, 211-216	1
2085	Distortion of Femtosecond Laser Pulses in Lenses and Lens Systems. <b>1988</b> , 35, 1907-1918	154
2084	Temperature dependence of bend- and twist-induced birefringence in a low-birefringence fiber. <b>1988</b> , 13, 62-4	27
2083	Measurement of Fresnel drag in moving media using a ring-resonator technique. <b>1988</b> , 5, 674	26
2082	Laser wavemeter with solid Fizeau wedge interferometer. <b>1988</b> , 27, 3656-60	15
2081	Attenuated Total Reflection FT-IR Spectroscopy to Measure Interfacial Reaction Kinetics at Silica Surfaces. <b>1988</b> , 42, 997-1004	19
2080	Nondestructive characterization of oxygen-ion-implanted silicon- on-insulator using multiple-angle ellipsometry. <b>1988</b> , 64, 2754-2756	7
2079	Infrared optical constants of coal slags - Dependence on chemical composition. <b>1989</b> , 3, 53-60	36
2078	Disorder effects on optical spectra and band structure of Si induced by ion implantation. <b>1989</b> , 66, 5261-5266	19
2077	Reduction of radiative heat transfer in thermal insulations by use of dielectric coated fibers. <b>1989</b> , 16, 851-860	14
2076	KrF laser system with corrected pulse front and compressed pulse duration. <b>1989</b> , 49, 239-244	29
2075	. <b>1989</b> , 1, 142-145	23
2074	Optical properties of mixed yttria-silica films. <b>1989</b> , 28, 5229-32	17
2073	Interaction of optical solitons with a forward Raman pump wave. <b>1989</b> , 14, 84-6	8
2072	Distortion of femtosecond laser pulses in lenses. <b>1989</b> , 14, 119-21	160

2071 . 1989, 7, 1181-1186 9 Spectroscopic Ellipsometry as a Non-Destructive Technique for Characterization of Atomic-Scale Interfaces. 1989, 159, 459 2069 Ellipsometric Characterization Of Optical Constants For Transparent Materials. 1989, 0970, 62 2068 In-Situ Spectroscopic Ellipsometry Investigation Of Ion Beam Damage: A Kinetic Study. 1990, 1188, 162 10 Improving the performance of porous radiant burners through use of sub-micron size fibers. 1990, 2067 27 33. 1339-1346 2066 Near IR optical properties of sputtered InN films. 1990, 192, 227-234 17 2065 Spectroscopic ellipsometry of E1-like transitions in nanometer-thickness Ge layers. 1990, 64, 315-318 25 Comparison of the (B) values of crystalline and amorphous thin films of 2064 17 4-butoxy-carbonyl-methyl-urethane polydiacetylene at 1.06 and 1.3 fh. 1990, 67, 7199-7203 2063 Comparison of Radiative Heat Transfer in Several Fibrous Insulations. 1990, 14, 107-122 2062 . **1990**, 8, 1856-1865 7 Characterization of the interface between Ge+-implanted crystalline silicon and its thermally grown 2061 17 oxide by spectroscopic ellipsometry. 1990, 67, 599-603 Fitting of transmission data for determining the optical constants and thicknesses of optical films. 2060 **1990**, 67, 2056-2059 2059 Dispersion formula for the thermo-optic coefficient of optical glasses. 1990, 10 2058 Deep ultraviolet microscope. **1990**, 29, 495-501 13 2057 Fiber optic delay line memory. **1990**, 29, 627-37 31 2056 Two-channel polarization modulation ellipsometer. **1990**, 29, 959-74 72 2055 Ultrashort-soliton interactions in optical fibers. 1990, 15, 1061-3 5 2054 Constant-dispersion grism spectrometer for channeled spectra. 1990, 7, 1779 24

2053	Active mode locking of broad band continuous-wave lasers. <b>1991</b> , 27, 1048-1060	12
2052	Electronic and chemical changes in shocked liquid carbon disulfide inferred from time resolved reflection experiments and analysis. <b>1991</b> , 95, 451-466	12
2051	. <b>1991</b> , 9, 18-21	6
2050	. 1991,	
2049	Analytic solution for the three-layer multiple beam interferometer. <b>1991</b> , 30, 59-65	45
2048	Laser interferometric thermometry for substrate temperature measurement. <b>1991</b> , 30, 1221-6	25
2047	Use of the biased estimator in the interpretation of spectroscopic ellipsometry data. <b>1991</b> , 30, 3354-60	96
2046	Determination of the optical functions of transparent glasses by using spectroscopic ellipsometry. <b>1991</b> , 30, 4310-5	36
2045	Low-cost wavemeter with a solid Fizeau interferometer and fiber-optic input. <b>1991</b> , 30, 5254-9	6
2044	Examination of thin SiO2 films on Si using spectroscopic polarization modulation ellipsometry. <b>1991</b> , 69, 7627-7634	75
2043	Large second-order nonlinearity in poled fused silica. <b>1991</b> , 16, 1732-4	560
2042	Generating dark solitons through cross-phase modulation in optical fibers. 1991, 8, 464	5
2041	Interactions between femtosecond solitons in optical fibers. <b>1991</b> , 8, 1114	15
2040	Refractive index, dispersion and absorption of fluorine-doped silica glass in the deep UV region.  1991, 127, 191-196	16
2039	Temperature dependence of refractive index of SiO2 glass. <b>1991</b> , 135, 86-89	83
2038	Optical third-harmonic generation in layered perovskite-type material (C10H21NH3)2PbI4. <b>1991</b> , 79, 245-248	53
2037	Optical and microstructural properties of hafnium dioxide thin films. <b>1991</b> , 203, 227-250	84
2036	Infrared and ellipsometric studies of reactive-ion-beam-sputtered hydrogenated amorphous silicon (a-Si:H), germanium (a-Ge:H) and Si?Ge alloy (a-Si28Ge72:H) films correlation. <b>1991</b> , 197, 269-277	4

2035	Determination of properties of thin thermal SiO2 on silicon by spectroscopic ellipsometry. <b>1991</b> , 195, 185-192	17
2034	Two-channel spectroscopic polarization modulation ellipsometry: A new technique for the analysis of thin SiO2 films. <b>1991</b> , 206, 294-299	6
2033	Real time spectroscopic ellipsometry for characterization of thin film optical properties and microstructural evolution. <b>1991</b> , 206, 374-380	15
2032	Determination of thickness and refractive index of SiO2 films on silicon wafers using an Abbe refractometer. <b>1991</b> , 85, 381-384	6
2031	Formation of particles in a H2?O2 counterflow diffusion flame doped with SiH4 or SiCl4. <b>1991</b> , 85, 134-142	22
2030	Laboratory reflectance measurements of analogues to dirtylice surfaces on atmosphereless solar system bodies. <b>1991</b> , 94, 209-217	10
2029	LPCVD Si3N4growth retardation on silicon native oxide compared with in situ HF vapour-deglazed silicon substrates. <b>1991</b> , 6, 1100-1102	13
2028	Radiometric Aspects of an Experiment to Determine the Melting/Freezing Temperature of Gold. <b>1991</b> , 28, 221-227	11
2027	Determination of the refractive index dispersion of liquid nitrobenzene in the visible and ultraviolet. <b>1992</b> , 25, 525-529	36
2026	The improvement of phase modulated spectroscopic ellipsometry. <b>1992</b> , 63, 2958-2966	19
2025	. <b>1992</b> , 28, 479-487	14
2024	. <b>1992</b> , 28, 1533-1538	3
2023	Cross-polarization cross-phase modulation of femtosecond pulses in erbium-doped fiber amplifiers. <b>1992</b> , 9, 682	3
2022	Highly stable, monochromatic and tunable optical radiation source and its application to high accuracy spectrophotometry. <b>1992</b> , 31, 536-45	47
2021	Scanning differential interferometer to measure index heterogeneity. <b>1992</b> , 31, 6622-31	1
2020	Determination of the optical constants of an inhomogeneous transparent LaF(3) thin film on a transparent substrate by spectroscopic ellipsometry. <b>1992</b> , 17, 538-40	26
2019	Space - time focusing: breakdown of the slowly varying envelope approximation in the self-focusing of femtosecond pulses. <b>1992</b> , 17, 1340	158
2018	Formation of SiO2, Al2O3, and 3Al2O3. 2SiO2 Particles in a Counterflow Diffusion Flame. <b>1992</b> , 75, 117-123	16

2017	Interferometric fibre sensors for measurement of surface heat transfer rates on turbine blades. <b>1992</b> , 16, 207-221	9
2016	Characterization of SiGe multiple quantum wells by spectroscopic ellipsometry and photoluminescence. <b>1992</b> , 222, 69-72	6
2015	Optical functions of silicon determined by two-channel polarization modulation ellipsometry. <b>1992</b> , 1, 41-47	275
2014	Scattering by closely-spaced radially-stratified parallel cylinders. <b>1992</b> , 48, 119-130	40
2013	. <b>1992</b> , 39, 541-545	25
2012	Conjugated polymers with degenerate ground state. The route to high performance third-order nonlinear optical response. <b>1992</b> , 200, 364-368	49
2011	Third harmonic generation spectra of degenerate ground state derivatives of poly (1,6-heptadiyne). <b>1993</b> , 212, 85-89	11
2010	Spectroscopic ellipsometry studies on ion beam sputter deposited Pb(Zr, Ti)O3 films on sapphire and Pt-coated silicon substrates. <b>1993</b> , 230, 15-27	41
2009	Characterization of very thin Ge epilayers on (100) Si by spectroscopic ellipsometry. <b>1993</b> , 223, 14-18	5
2008	A fiber-optic chemical sensor based on surface plasmon resonance. <b>1993</b> , 12, 213-220	839
2007	Spectral broadening of picosecond laser pulses in optical fibres. <b>1993</b> , 25, 1-25	41
2006	Wavelength dispersion in fiber optical detection of time-resolved fluorescence. <b>1993</b> , 346, 560-563	3
2005	Evolution of the optical functions of thin-film aluminum: A real-time spectroscopic ellipsometry	66
	study. <b>1993</b> , 47, 3947-3965	
2004	Characterization of silicon on insulator multilayers using ex situ spectroscopic ellipsometry and in situ monochromatic ellipsometry during plasma etching. <b>1993</b> , 233, 214-217	3
2004	Characterization of silicon on insulator multilayers using ex situ spectroscopic ellipsometry and in	3
2003	Characterization of silicon on insulator multilayers using ex situ spectroscopic ellipsometry and in situ monochromatic ellipsometry during plasma etching. <b>1993</b> , 233, 214-217  Studies on inhomogeneous transparent optical coatings on transparent substrates by	
2003	Characterization of silicon on insulator multilayers using ex situ spectroscopic ellipsometry and in situ monochromatic ellipsometry during plasma etching. 1993, 233, 214-217  Studies on inhomogeneous transparent optical coatings on transparent substrates by spectroscopic ellipsometry. 1993, 234, 439-442	16

1999 Optimized design of an antireflection coating for textured silicon solar cells. <b>1993</b> , 32, 5557-60	12
Determination of the optical function n $\P$ of vitreous silica by spectroscopic ellipsometry with an achromatic compensator. <b>1993</b> , 32, 6391-8	24
1997 Heat scan: a simple technique to study gratings in fibers. <b>1993</b> , 18, 1016-8	14
1996 Temperature effects in a Brillouin fiber ring laser. <b>1993,</b> 18, 2123	21
1995 Refractive index of densified silica glass. <b>1993</b> , 159, 241-245	31
Conjugated polymers with degenerate ground state: The route to high performance third-order nonlinear optical response. <b>1993</b> , 57, 3961-3967	14
1993 Formation of optical slab waveguides using thermal oxidation of SiOx. <b>1993</b> , 29, 714	7
Novel calibration technique employing a spread-spectrum tone for mobile satellite systems. <b>1993</b> , 29, 716	2
Present State of the Comparison between Radiometric Scales Based on Three Primary Standards. <b>1991 1993</b> , 30, 439-449	37
Spectroscopic ellipsometry characterization of strained and relaxed Si1\(\mathbb{U}\)Gex epitaxial layers. <b>1993</b> , 73, 239-250	71
1989 Interaction of light with an accelerating dielectric. <b>1993</b> , 48, 1082-1088	7
1988 Optical fiber refractometer for measuring the dispersion of turbid fluids. <b>1993</b> , 1796, 383	1
1987 Heat treatment of spun-on acid-catalyzed sol-gel silica films. <b>1994</b> , 9, 723-730	46
1986 . <b>1994</b> , 41, 2277-2283	12
Relationship between radiation response and density of buried oxide in separation-by-implantation-of-oxygen material. <b>1994</b> , 65, 2993-2995	4
1984 Optical design of a beam Cherenkov counter: chromatic corrections. <b>1994</b> , 342, 364-382	
1983 Analysis of Si/Six Ge1 lk/Si microstructures by spectroscopic ellipsometry. <b>1994</b> , 248, 140-144	5
1982 Third harmonic generation in standard and erbium-doped fibers. <b>1994</b> , 110, 435-444	16

Automated refractive index measurement of catalyst-laden edible oils undergoing partial hydrogenation. <b>1994</b> , 71, 1339-1342	5
1980 Temperature dispersion of refractive indexes in some silicate fiber glasses. <b>1994</b> , 6, 431-433	60
1979 . <b>1994</b> , 12, 1338-1342	205
Characterization of inhomogeneous transparent thin films on transparent substrates by spectroscopic ellipsometry: refractive indices n() of some fluoride coating materials. <b>1994</b> , 33, 2664-	71 <sup>22</sup>
1977 Tunable four-wave mixing in low-mode-number optical fibers. <b>1994</b> , 33, 3203-8	3
1976 Rainbow-enhanced forward glory from fused-silica spheres. <b>1994</b> , 33, 4672-6	2
1975 Interpretation of Infrared Transmittance Spectra of SiO2 Thin Films. <b>1994</b> , 48, 113-120	28
1974 Ultrabroadband femtosecond lasers. <b>1994</b> , 30, 1100-1114	148
1973 Dielectric function spectra of strained and relaxed Si1⊠Gex alloys (x=00.25). 1994, 75, 4642-4647	47
Effect of Power on the Properties of Sio2 Films Produced by Plasma-Enhanced Chemical Vapour Deposition. <b>1994</b> , 338, 57	3
Optical Characterization of Inhomogeneous Transparent Films on Transparent Substrates by Spectroscopic Ellipsometry. <b>1994</b> , 191-247	15
1970 Strain-rate sensor based on in-fiber Doppler velocimetry. <b>1995</b> ,	1
1969 Laser based spectrometry. <b>1995</b> , 6, 337-354	
Properties of Gate-Quality SiO2 Films Prepared by Electron Cyclotron Resonance Chemical Vapour Deposition in an Ultrahigh Vacuum Processing System. <b>1995</b> , 386, 255	1
Composition Profiling of Graded Dielectric Function Materials by Spectroscopic Ellipsometry. <b>1995</b> , 411, 185	2
Silicon (Oxy)Nitride Thin Films Deposited by LPCVD from SiCl2H2-NH3-N2O Mixtures of Variable Composition. <b>1995</b> , 417, 187	
1965 The calculation of dispersion forces for engineering applications. <b>1995</b> , 56, 201-243	74
Dynamic ultrafiltration model for charged colloidal dispersions: A Wigner-Seitz cell approach. <b>1995</b> , 50, 1707-1736	125

1963	Third harmonic generation spectra of degenerate ground state poly(dipropargyl) amines. <b>1995</b> , 232, 149-153	4
1962	Third harmonic generation spectrum of a degenerate ground state conjugated polymer. Direct evidence of simultaneous two- and three-photon resonance. <b>1995</b> , 247, 221-226	2
1961	Characterization of Optical Thin Films by Spectroscopic Ellipsometry. <b>1995</b> , 78, 2412-2416	5
1960	Locking of soliton pulses with different carrier frequencies through parametric interaction. <b>1995</b> , 206, 187-194	3
1959	Surface chemistry and tip-sample interactions in atomic force microscopy. <b>1995</b> , 94, 29-51	202
1958	Determination of oxide thickness on an Si2N2O?ZrO2 composite by spectroscopic ellipsometry. <b>1995</b> , 15, 313-318	5
1957	Determination of thickness, refractive indices, optical anisotropy of, and stresses in SiO2 films on silicon wafers. <b>1995</b> , 117, 1-7	26
1956	Plasma-enhanced growth, composition, and refractive index of silicon oxy-nitride films. <b>1995</b> , 77, 6616-6623	35
1955	Oxide growth, refractive index, and composition depth profiles of structures formed by 2 MeV oxygen implantation into silicon. <b>1995</b> , 77, 577-586	5
1954	A spectroscopic ellipsometry study of the interfacial stresses and their correlation with microvoids in very thin thermally grown SiO2 films. <b>1995</b> , 78, 5362-5365	5
1953	Femtosecond solvation dynamics determining the band shape of stimulated emission from a polar styryl dye. <b>1995</b> , 102, 2691-2700	122
1952	. <b>1995</b> , 13, 109-114	2
1951	Transient conductive and radiative heat transfer in a silica window. <b>1995</b> , 9, 370-373	18
1950	Diffusely scattering phantoms for optical tomography. <b>1995</b> ,	2
1949	Optical power and transmittance measurements and their use in detector-based realization of the luminous intensity scale. <b>1995</b> , 34, 2611	24
1948	. <b>1995</b> , 13, 1-5	2
1947	. <b>1995</b> , 13, 1445-1451	19
1946	Balancing optical path lengths in broadband fiber interferometers. <b>1995</b> , 34, 2194-201	9

1945	High-accuracy spectrometer for measurement of regular spectral transmittance. <b>1995</b> , 34, 3686-92	31
1944	Optical-constant calculation over an extended spectral region: application to titanium dioxide film. <b>1995</b> , 34, 7355-60	24
1943	The optical and magnetic properties of Ni+-implanted silica. <b>1995</b> , 189, 173-180	51
1942	. <b>1995</b> , 7, 795-797	9
1941	Polarization effects in coherent optical frequency-domain reflectometry. <b>1996</b> , 8, 1513-1515	7
1940	Optical properties of ZnSe and its modeling. <b>1996</b> , 53, 1475-1484	86
1939	. <b>1996</b> , 7, 605-611	4
1938	Improved Two-Fiber Probe for in Situ Spectroscopic Measurement. <b>1996</b> , 68, 3098-3103	12
1937	Measurement of mode times of flight in multimode fibers by an interferometric method using polychromatic light: theoretical approach and experimental results. <b>1996</b> , 35, 1129-34	3
1936	Realization of a scale of absolute spectral response using the National Institute of Standards and Technology high-accuracy cryogenic radiometer. <b>1996</b> , 35, 4392-403	92
1935	Scattering of polarized radiation by an arbitrary collection of closely spaced parallel nonhomogeneous tilted cylinders. <b>1996</b> , 13, 2256	13
1934	Modeling of absorption data complicated by Fabry <b>B</b> erot interference in germanosilicate thin-film waveguides. <b>1996</b> , 13, 268	7
1933	Numerical solutions of Maxwell equations for nonlinear-optical pulse propagation. <b>1996</b> , 13, 1135	57
1932	Reanalysis of Laub drag effects in a ring cavity. <b>1996</b> , 13, 2065	3
1931	Electric potential-related reflection from transparent metal/v-SiO2/metal interfaces. 1996, 203, 109-113	7
1930	A fiber-optic autocollimation refractometric method for dispersion measurement of bulk optical materials using a widely tunable fiber Raman laser. <b>1996</b> , 32, 1897-1902	5
1929	Return loss characteristics of optical fiber connectors. <b>1996</b> , 14, 1986-1991	13
1928	Preparation of solid phantoms with defined scattering and absorption properties for optical tomography. <b>1996</b> , 41, 1823-44	41

1927	Optical-to-electrical wavelength demultiplexing detector: design, fabrication, and analysis. <b>1996</b> , 14, 534-541	6
1926	Dispersion compensation based on dual-mode optical fiber with inhomogeneous profile core. <b>1996</b> , 14, 2387-2394	21
1925	The effect of propagation delay uncertainty on the speed of time-of-flight digital optoelectronic circuits. <b>1996</b> , 14, 2698-2713	1
1924	Angle of Incidence and Size Effects on Dependent Scattering in Fibrous Media. <b>1996</b> , 118, 931-936	7
1923	Water-quality measurement using fiber optics at wavelengths below 230 nm. <b>1996</b> , 2836, 186	1
1922	Microstructural Analysis and Modelling of Thin Porous Silicon Layers with Variable Angle Spectroscopic Ellipsometry. <b>1996</b> , 431, 259	1
1921	Geo2 concentration dependence of nonlinear refractive index coefficients of silica-based optical fibers. <b>1996</b> , 79, 12-19	13
1920	Tuneable THz beat frequency generation in optical fibers. <b>1996</b> , 130, 25-28	3
1919	Passive-Oxidation Kinetics of High-Purity Silicon Carbide from 800° to 1100°C. <b>1996</b> , 79, 2897-2911	106
1918	Ultra-low values of the absorption coefficient for bandBand transitions in moderately doped Si obtained from luminescence. <b>1996</b> , 80, 5325-5331	21
1917	Formation and characterization of Si/SiO2 multilayer structures by oxygen ion implantation into silicon. <b>1996</b> , 80, 4960-4970	5
1916	Properties and Applications of Ultra-Short Electromagnetic Mono- and Sub-Cycle Waves. <b>1996</b> , 65, 2020-2032	29
1915	Transient Temperature During the Vaporization of Liquid on a Pulsed Laser-Heated Solid Surface. <b>1996</b> , 118, 702-708	30
1914	Quartz-Fiber Thermal Insulation: Infrared Radiative Properties and Calculation of Radiative-Conductive Heat Transfer. <b>1996</b> , 118, 408-414	30
1913	Time-resolved polarimetry on an optical fibre ammeter. <b>1996</b> , 5, 323-330	
1912	Organic <b>i</b> horganic dielectric multilayer systems as high reflectivity distributed Bragg reflectors. <b>1997</b> , 71, 732-734	26
1911	Silicon Dioxide (SiO2) (Glass). <b>1997</b> , 749-763	24
1910	Liquid-core fused silica capillary lightguides for applications in the UV/VIS and NIR spectral range. <b>1997</b> , 2977, 58	5

1909	Preparation and characterization of Nd3+ and Er3+-doped silica sol-gel coatings by Rutherford backscattering spectroscopy and spectroscopic ellipsometry. <b>1997</b> , 12, 2779-2783	7
1908	Pigment mass density and refractive index determination from optical measurements. <b>1997</b> , 9, 1661-1670	18
1907	Refractive Index. <b>1997</b> , 5-114	1
1906	Accurate measurement of refraction and dispersion of a solid by a double-layer interferometer. <b>1997</b> , 36, 779-85	8
1905	Characterization of a polarization-independent transmission trap detector. <b>1997</b> , 36, 2807-12	23
1904	Application of tunable excimer lasers to combustion diagnostics: a review. <b>1997</b> , 36, 3971-4033	86
1903	Development of a detector-based absolute spectral irradiance scale in the 380-900-nm spectral range. <b>1997</b> , 36, 8909-18	36
1902	Liquid-core light guides for near-infrared applications. <b>1997</b> , 36, 9075-82	14
1901	Self-focusing in the presence of small time dispersion and nonparaxiality. <b>1997</b> , 22, 1379-81	56
1900	Faraday effect in TiO2?SiO2 glasses. <b>1997</b> , 222, 391-395	6
	Faraday effect in TiO2?SiO2 glasses. 1997, 222, 391-395  Thermo-Optic Coefficients. 1997, 115-261	6 4
1899		
1899 1898	Thermo-Optic Coefficients. <b>1997</b> , 115-261	4
1899 1898 1897	Thermo-Optic Coefficients. <b>1997</b> , 115-261  Smart-sensor approach for a fibre-optic-based residual chlorine monitor. <b>1997</b> , 39, 380-385	23
1899 1898 1897	Thermo-Optic Coefficients. 1997, 115-261  Smart-sensor approach for a fibre-optic-based residual chlorine monitor. 1997, 39, 380-385  In-fiber doppler velocimeter for velocity measurements of moving surfaces. 1997, 37, 328-332	4 23 8
1899 1898 1897	Thermo-Optic Coefficients. 1997, 115-261  Smart-sensor approach for a fibre-optic-based residual chlorine monitor. 1997, 39, 380-385  In-fiber doppler velocimeter for velocity measurements of moving surfaces. 1997, 37, 328-332  The mean polarizability and density of glasses. 1997, 229, 217-224	4 23 8 50
1899 1898 1897 1896	Thermo-Optic Coefficients. 1997, 115-261  Smart-sensor approach for a fibre-optic-based residual chlorine monitor. 1997, 39, 380-385  In-fiber doppler velocimeter for velocity measurements of moving surfaces. 1997, 37, 328-332  The mean polarizability and density of glasses. 1997, 229, 217-224  Faraday effect in silica glasses. 1997, 233, 1-7  Two-wave mixing of the fundamental and its third-harmonic: eigenmodes, spatial instabilities and	4 23 8 50 28

1891 Three-photon absorption cross-section of simple molecular liquids. <b>1998</b> , 153, 32-38	27
$_{ m 1890}$ Protection coatings for polycarbonates based on PECVD from organosilicon feeds. <b>19</b>	<b>98</b> , 50, 19-21 25
Spectroscopic ellipsometry with compensator and X-ray specular reflectivity for characteristic thin optical layers on transparent substrates. <b>1998</b> , 313-314, 68-72	acterization of 8
Composition profiling of graded dielectric function materials by spectroscopic ellipso 313-314, 389-393	metry. <b>1998,</b> 3
Infrared spectroscopic ellipsometry for residual water detection in annealed solgel th <b>1998</b> , 313-314, 722-726	in layers.
Optical properties of fluorinated silicon oxide films by liquid phase deposition for opt waveguides. <b>1998</b> , 47, 698-702	ical 10
1885 Propagation of optical pulses in periodic nonlinear fibers. <b>1998</b> , 41, 698-705	
1884 Optical properties of densified silica glasses. <b>1998</b> , 252, 28-33	36
Optical characterization of layers for silicon microelectronics. <b>1998</b> , 40, 263-274	5
Linear and nonlinear optical spectra of polyazomethines fabricated by chemical vapor <b>1998</b> , 95, 101-105	deposition. 32
Ellipsometric determination of optical constants for silicon and thermally grown silicon a multi-sample, multi-wavelength, multi-angle investigation. <b>1998</b> , 83, 3323-3336	on dioxide via 822
Determination of refractive index of silica glass for infrared wavelengths by IR spectro 223, 158-163	oscopy. <b>1998</b> ,
1879 Water-related IR absorption spectra for alkali zinc pyrophosphate glasses. <b>1998</b> , 238,	124-142 29
$_{ m 1878}$ Review and analysis of refractive index temperature dependence in amorphous SiO2.	<b>1998,</b> 238, 30-36 <sub>37</sub>
1877 Large-bandwidth frequency conversion in high-NA step index optical fibers. <b>1998</b> , 34,	660-665 10
Single crystallites in planar polycrystalline bligothiophene films: Determination of orie thickness by polarization microscopy. <b>1998</b> , 83, 3816-3824	entation and 42
1875 Cerenkov radiation as a UV and visible light source for time-resolved fluorescence. <b>19</b>	<b>98</b> , 70, 3426-33 8
Optical time-of-flight chemical detection: spatially resolved analyte mapping with ext continuous chemically modified optical fibers. <b>1998</b> , 70, 1453-61	ended-length 16

1873	Radiation-induced wave-front aberrations: a new approach. <b>1998</b> , 37, 643-8	8
1872	Spectral reflectance of silicon photodiodes. <b>1998</b> , 37, 729-32	35
1871	Modified white-light Mach-Zehnder interferometer for direct group-delay measurements. <b>1998</b> , 37, 4105-11	28
1870	Absolute Refractive Indices and Thermal Coefficients of Fused Silica and Calcium Fluoride Near 193 nm. <b>1998</b> , 37, 5964-8	23
1869	Light scattering by closely spaced parallel cylinders embedded in a semi-infinite dielectric medium. <b>1998</b> , 15, 163	28
1868	Rotating-compensator multichannel ellipsometry: Applications for real time Stokes vector spectroscopy of thin film growth. <b>1998</b> , 69, 1800-1810	161
1867	Characterization of photodiodes as transfer detector standards in the 120 nm to 600 nm spectral range. <b>1998</b> , 35, 355-362	36
1866	Hydrogen Concentration Dependence of Bragg Wavelength of UV-Written Fiber Grating. <b>1998</b> , 15, 886-888	7
1865	New one-parameter fits of sub-bandgap optical properties of crystals. <b>1998</b> , 10, 10283-10289	1
1864	Neutron reflectometry, x-ray reflectometry, and spectroscopic ellipsometry characterization of thin SiO2 on Si. <b>1998</b> , 73, 2131-2133	38
1863	Three-Dimensional Optical Data Storage in Vitreous Silica. <b>1998</b> , 37, L1527-L1530	101
1862	Direct measurement of refractive-index dispersion using a time-delayed technique. <b>1998</b> , 69, 1472-1475	5
1861	Measurements of index of refraction in the deep and vacuum ultraviolet using the minimum-deviation method. <b>1998</b> ,	2
1860	Measurement of the refractive index of transparent materials using null polarimetry near Brewster's angle. <b>1998</b> ,	
1859	AC phase measuring interferometer for measuring dn/dT of fused silica and calcium fluoride at 193 nm. <b>1998</b> , 3425, 172	
1858	Direct group-delay measurement and 3D profilometry using a white-light interferometer. <b>1998</b> ,	
1857	. 1999,	366
1856	Quantum efficiency of a back-illuminated CCD imager: an optical approach. <b>1999</b> , 3649, 80	21

1855	Electromagnetic shocks on the optical cycle of ultrashort pulses in triple-resonance Lorentz dielectric media with subfemtosecond nonlinear electronic Debye relaxation. <b>1999</b> , 60, 1051-9	24
1854	Second-harmonic spectroscopy of interband excitations at the interfaces of strained Si(100)Bi0.85Ge0.15BiO2 heterostructures. <b>1999</b> , 59, 2915-2926	36
1853	Analysis of specular and textured SnO2:F films by high speed four-parameter Stokes vector spectroscopy. <b>1999</b> , 85, 2015-2025	83
1852	Wavelength dependence of the Faraday effect in glassy SiO2. <b>1999</b> , 60, 1689-1692	19
1851	Characterization and production metrology of thin transistor gate oxide films. <b>1999</b> , 2, 103-147	51
1850	Optical phase change on reflection at v-SiO2/Sn interface. <b>1999</b> , 262, 98-103	8
1849	Far-field diffraction of pulsed optical beams in dispersive media. <b>1999</b> , 167, 15-22	56
1848	High-accuracy measurement of specular spectral reflectance and transmittance. <b>1999</b> , 380, 317-325	8
1847	Rapid melting dynamics of amorphous Si films. <b>1999</b> , 5, 525-532	6
1846	Ellipsometric approach for determination of the pseudodielectric function of the Si <b>I</b> hterface in the Si <b>B</b> iO2 structure. <b>1999</b> , 443, 186-194	1
1845	Solgel derived porous silica films. <b>1999</b> , 243, 75-79	46
1844	Optical interference and refractive index of silica glass in the infrared absorption region. <b>1999</b> , 249, 51-54	15
1843	Operational stability of a spectrally encoded optical CDMA system using inexpensive transmitters without spectral control. <b>1999</b> , 11, 916-918	13
1842	Analysis of femtosecond-order optical pulses diffracted by periodic structure. <b>1999</b> , 16, 299	16
1841	Spectrally resolved white-light interferometry for measurement of ocular dispersion. <b>1999</b> , 16, 2092-102	17
1840	High beam quality of ultraviolet radiation generated through resonant enhanced frequency doubling of a diode laser. <b>1999</b> , 16, 2207	5
1839	Mathematical Model of a Laser-Induced Fluorescence Fiber-Optic Sensor Head for Trace Detection of Pollutants in Soil. <b>1999</b> , 53, 49-56	10
1838	Fundamentals of Electromagnetic Waves and Waveguides. 19-93	О

1837 Ocular dispersion. **1999**, 3591, 22

1836	Spectroscopic Ellipsometry of Ta2O5 on Si. <b>1999</b> , 567, 559	4
1835	Extension of Multichannel Spectroscopic Ellipsometry into the Ultraviolet for Real Time Characterization of the Growth of Wide Bandgap Materials from 1.5 to 6.5 eV. <b>1999</b> , 569, 71	6
1834	Spectroscopic Ellipsometry for the Characterization of the Morphology of Ultra-thin Thermal CVD Amorphous and Nanocrystalline Silicon Thin Films. <b>2000</b> , 609, 2431	
1833	Light Scattering in Pigmented Coatings:: Experiments and Theory. <b>2000</b> , 68, 553-561	30
1832	Real-time spectroscopic ellipsometry from 1.5 to 6.5 eV. <b>2000</b> , 364, 16-21	8
1831	Effect of hydrogen ion implantation on the physical properties of SiO2/Si system. <b>2000</b> , 58, 166-173	2
1830	Temperature dependence of refractive index of glassy SiO 2 in the infrared wavelength range. <b>2000</b> , 61, 1315-1320	73
1829	Laser-based measurement of liquid temperature or concentration at a solid I quid interface. <b>2000</b> , 23, 1-9	18
1828	Soliton pulses in two-mode periodic fibers. <b>2000</b> , 88, 560-563	11
1827	New primary standard for specular gloss measurements. <b>2000</b> , 72, 61-66	25
1826	Solar Spectral Irradiance Monitor (SIM). <b>2000</b> , 37, 415-418	14
1825	Spectroscopic Ellipsometry Studies on Ultrathin Hydrogenated Amorphous Silicon Films Prepared by Thermal Chemical Vapor Deposition. <b>2000</b> , 39, 6196-6201	5
1824	Realization of the unit of luminous intensity at the HUT. <b>2000</b> , 37, 131-140	22
1823	Multichannel ellipsometer for real time spectroscopy of thin film deposition from 1.5 to 6.5 eV. <b>2000</b> , 71, 3451-3460	25
1822	Optical and surface properties of oxyfluoride glass. 2000,	
1821	Scattering delay time of Mie scatterers determined from steady-state and time-resolved optical spectroscopy. <b>2000</b> , 17, 745-9	
1820	Interpolation of the spectral responsivity of silicon photodetectors in the near ultraviolet. <b>2000</b> , 39, 9-15	16

1819	Coarse WDM/CDM/TDM concept for optical packet transmission in metropolitan and access networks supporting 400 channels at 2.5 Gb/s peak rate. <b>2000</b> , 18, 1928-1938	26
1818	Ultraviolet-initiated reactions of $H(2)$ with germanosilicate fibers and $H(2)$ concentration dependence of the Bragg wavelength of a fiber grating. <b>2000</b> , 25, 527-9	10
1817	Spectroscopic ellipsometry of oxides and interfaces thermally formed on (100)Si and (111)Si. <b>2000</b> , 454-456, 402-406	4
1816	Interferometric determination of the refractive index of liquid sulphur dioxide. <b>2000</b> , 11, 1714-1720	17
1815	Cross phase modulation artifact in liquid phase transient absorption spectroscopy. <b>2000</b> , 87, 2340-2352	105
1814	Formation of Conducting and Insulating Layered Structures in Si by Ion Implantation: Process Control Using FTIR Spectroscopy. <b>2001</b> , 148, G704	6
1813	Whispering-gallery-mode evanescent-wave microsensor for trace-gas detection. <b>2001</b> , 4265, 102	21
1812	Studies of the fifth-order nonlinear susceptibility of ultraviolet-grade fused silica. <b>2001</b> , 26, 896-8	16
1811	Effect of third-order dispersion on the phases of solitonlike Cr^4+: YAG-laser pulses characterized by the second-harmonic generation frequency-resolved optical gating method. <b>2001</b> , 18, 388	6
1810	Dispersion-compensating dual-mode optical fibers desirable for erbium-doped-fiber-amplified systems. <b>2001</b> , 18, 737	6
1809	Optical pulse compression to 50 fs by use of only a spatial light modulator for phase compensation. <b>2001</b> , 18, 1742	39
1808	Locking a microsphere whispering-gallery mode to a laser. <b>2001</b> , 8, 605-10	40
1807	Comparison between theory and experiment of nonlinear propagation for a-few-cycle and ultrabroadband optical pulses in a fused-silica fiber. <b>2001</b> , 37, 398-404	70
1806	Locking and laser-frequency tracking of a microsphere whispering-gallery mode. 2001,	1
1805	Group refractive index of fused silica and white-light spectral interferometry with a dispersive Michelson interferometer. <b>2001</b> ,	
1804	Planar optical waveguide temperature sensor based on etched bragg gratings considering nonlinear thermo-optic effect. <b>2001</b> , 15, 309-319	4
1803	Refractive index, optical dispersion, and group velocity of infrared waves in silica glass. <b>2001</b> , 62, 1087-1092	20
1802	Optical and microstructural characterization of thin films of photochromic fulgides. <b>2001</b> , 62, 1219-1228	6

## (2002-2001)

1801	Dispersion of the optical constants of quartz and polymethyl methacrylate glasses in a wide spectral range: 0.2日 fb. <b>2001</b> , 188, 129-139	72
1800	Dispersion measurements of microstructured fibers using femtosecond laser pulses. <b>2001</b> , 192, 219-223	34
1799	White-light spectral interferometry with the uncompensated Michelson interferometer and the group refractive index dispersion in fused silica. <b>2001</b> , 193, 1-7	59
1798	Study of thin SiO2 and its interface formed by thermal oxidation of rf hydrogen plasma-cleaned silicon. <b>2001</b> , 61, 263-268	5
1797	Pre-resonance Raman excitation profile of the 3400 cml mode of liquid water. <b>2001</b> , 32, 649-655	6
1796	Structure and magnetic properties of Co+-implanted silica. <b>2001</b> , 178, 144-147	36
1795	Eighty kilometre transmission experiment using an InGaAs/InP SPAD-based quantum cryptography receiver operating at 1.55 fh. <b>2001</b> , 48, 1957-1966	O
1794	Determination of the refractive indices by variable azimuth reflectometry from a single sample face. <b>2001</b> , 3, 108-113	1
1793	Precision spectrometer for measurement of specular reflectance. <b>2002</b> , 73, 2237-2241	1
1792	Optimal wavelength pair selection and accuracy analysis of dual fiber grating sensors for simultaneously measuring strain and temperature. <b>2002</b> , 41, 2456	20
1791	Specifications and performance of UV rotating shadowband spectroradiometer (UV-RSS). <b>2002</b> , 4482, 249	3
1790	Singleshot spectroscopic polarimetry using channeled spectrum. 2002,	7
1789	Data and signal processing of rotating shadowband spectroradiometer (RSS) data. <b>2002</b> , 4815, 58	3
1788	Refractive-index changes caused by proton radiation in silicate optical glasses. <b>2002</b> , 41, 678-84	25
1787	Femtosecond measurements of two-photon absorption coefficients at lambda = 264 nm in glasses, crystals, and liquids. <b>2002</b> , 41, 4365-76	76
1786	Least-mean-squares algorithm to determine submicrometer particle diameter, volume fraction, and size distribution width by elastic light scattering. <b>2002</b> , 41, 4421-31	2
1785	Cauchy's dispersion equation reconsidered: Dispersion in silicate glasses. <b>2002</b> , 157, 823-828	5
1784	Computer simulations of nonlinear propagation of an optical pulse using a finite-difference in the frequency-domain method. <b>2002</b> , 38, 626-629	5

1783 Timing Aspects in SDH Networks. 93-130

1782	. 2002,	86
1781	Effect of particle size on the optically transparent nano meter-order glass particle-dispersed epoxy matrix composites. <b>2002</b> , 62, 1187-1189	81
1780	Dispersive white-light spectral interferometry to measure distances and displacements. <b>2002</b> , 212, 65-70	28
1779	Group velocity dispersion in fused-silica sample measured using white-light interferometry with the equalization wavelength determination. <b>2002</b> , 113, 149-152	8
1778	Dispersive white-light spectral two-beam interference under general measurement conditions. <b>2003</b> , 114, 185-190	4
1777	Slightly dispersive white-light spectral interferometry to measure distances and displacements. <b>2003</b> , 114, 389-393	9
1776	Optical properties of the DIRC fused silica Cherenkov radiator. <b>2003</b> , 515, 680-700	28
1775	Optical properties of AsSe1.5⊠Tex glassy system. <b>2003</b> , 35, 335-340	33
1774	Study of plasma polymerization from acetylene in pulsed r.f. discharges. <b>2003</b> , 425, 72-84	23
1773	Optical absorption threshold of low pressure chemically vapor deposited silicon oxynitride films from SiCl2H2?NH3?N2O mixtures. <b>2003</b> , 437, 266-271	15
1772	Spectral changes of Gaussian Schell-model beams passing through a dispersive lens. <b>2003</b> , 114, 485-490	1
1771	Direct measurement of refractive-index dispersion of transparent media by white-light interferometry. <b>2003</b> , 42, 3910-4	32
1770	Propagation properties of ultrashort pulsed bessel beams in dispersive media. <b>2003</b> , 20, 582-7	10
1769	Development of experimentally validated optical property models for silicon and related materials.	О
1768	Structural change induced in TiO2 by swift heavy ions and its application to three-dimensional lithography. <b>2003</b> , 68,	37
1767	Dispersive white-light spectral two-beam interference under general measurement conditions. <b>2003</b> ,	
1766	Optical design of MOIRCS. 2003,	2

1/03	Measuring distances and displacements using dispersive white-light spectral interferometry. 2003,	1
1764	Spectral interferograms including equalization wavelengths processed by autoconvolution method. <b>2003</b> , 5064, 198	7
1763	Light Intensity Enhancement and Optical Nonlinear Response due to Localized Surface Plasmons in Nanosize Ag Sphere. <b>2004</b> , 43, 6507-6512	9
1762	GeO2-doped SiO2 sputtered thin films: Microstructure, stoichiometry, and optical properties. <b>2004</b> , 22, 2234-2238	6
1761	Highly nonlinear dynamics of third-harmonic generation by focused beams. 2004, 69,	8
1760	Refractive Index, Density and Polarizability of Silica Glass with Various Fictive Temperatures. <b>2004</b> , 43, L743-L745	24
1759	Comparative thickness measurements of SiO2/Si films for thicknesses less than 10 nm. <b>2004</b> , 36, 23-29	6
1758	Finite-difference time-domain analysis of ultrashort laser pulse propagation in a fiber with nonlinear effects. <b>2004</b> , 87, 1-10	1
1757	Validity of separating group-velocity dispersion of photonic-crystal fibers into material and waveguide components. <b>2004</b> , 43, 91-93	
	Measurement of the refractive index and attenuation length of liquid vapon for its scintillation	
1756	Measurement of the refractive index and attenuation length of liquid xenon for its scintillation light. <b>2004</b> , 516, 462-474	37
1756 1755		37
	light. 2004, 516, 462-474  Propagation of ultra-short optical pulses in cubic nonlinear media. 2004, 196, 90-105	
1755	light. 2004, 516, 462-474  Propagation of ultra-short optical pulses in cubic nonlinear media. 2004, 196, 90-105	320
1755 1754	Propagation of ultra-short optical pulses in cubic nonlinear media. 2004, 196, 90-105  Effect of material dispersion on the focusing of isodiffracting ultrashort pulses by a lens. 2004, 51, 645-655  Dispersive spectral-domain two-beam interference analysed by a fibre-optic spectrometer. 2004,	320
1755 1754 1753	Propagation of ultra-short optical pulses in cubic nonlinear media. 2004, 196, 90-105  Effect of material dispersion on the focusing of isodiffracting ultrashort pulses by a lens. 2004, 51, 645-655  Dispersive spectral-domain two-beam interference analysed by a fibre-optic spectrometer. 2004, 51, 537-547	320 2 22
1755 1754 1753 1752	Propagation of ultra-short optical pulses in cubic nonlinear media. 2004, 196, 90-105  Effect of material dispersion on the focusing of isodiffracting ultrashort pulses by a lens. 2004, 51, 645-655  Dispersive spectral-domain two-beam interference analysed by a fibre-optic spectrometer. 2004, 51, 537-547  Electron mean free path in fused silica and optical fiber preform. 2004, 95, 6204-6208	320 2 22 10
1755 1754 1753 1752 1751	Propagation of ultra-short optical pulses in cubic nonlinear media. 2004, 196, 90-105  Effect of material dispersion on the focusing of isodiffracting ultrashort pulses by a lens. 2004, 51, 645-655  Dispersive spectral-domain two-beam interference analysed by a fibre-optic spectrometer. 2004, 51, 537-547  Electron mean free path in fused silica and optical fiber preform. 2004, 95, 6204-6208  Measurements of radiation characteristics of fused quartz containing bubbles. 2004, 21, 149-59  Modelling of microstructured waveguides using a finite-element-based vectorial mode solver with	320 2 22 10

1747	Design of single-polarization PCF at 1300- and 1550-nm bands. <b>2004</b> ,	1
1746	Measurement of the phase spectra of transparent thin films using white-light interferometry. 2004,	
1745	Optical light bullets in a pure Kerr medium. <b>2004</b> , TuC11	
1744	Optical Materials. 2005,	
1743	Radiative Properties of Pattered Wafers With Linewidth Below 100 nm. <b>2005</b> , 793	
1742	Realization of photometric base unit of candela traceable to cryogenic radiometer at UME. <b>2005</b> , 30, 205-213	10
1741	Primary scintillation yield and ratio in liquid xenon. <b>2005</b> , 74, 160-167	7
1740	Effects of dispersion and longitudinal chromatic aberration on the focusing of isodiffracting pulsed Gaussian light beam. <b>2005</b> , 334, 73-80	3
1739	Calibration of silica fibers for the Optical Hawaiian Array for Nanoradian Astronomy (DHANA): Temperature dependence of differential chromatic dispersion. <b>2005</b> , 251, 115-123	9
1738	The group indices of refraction and the group velocities of the e-ray and the o-ray waves in Equartz. <b>2005</b> , 66, 1252-1255	2
1737	Filter-radiometer-based realization of candela and establishment of photometric scale at UME. <b>2005</b> , 43, 1252-1266	11
1736	The Spectral Irradiance Monitor: Measurement Equations and Calibration. <b>2005</b> , 230, 169-204	45
1735	The Spectral Irradiance Monitor: Scientific Requirements, Instrument Design, and Operation Modes. <b>2005</b> , 230, 141-167	85
1734	Modeling of thermal radiation of polymer coating containing hollow microspheres. <b>2005</b> , 43, 247-258	15
1733	Nonlinear Propagation Theory for Few-to-Mono Optical-Cycle Pulses beyond the Slowly-Varying-Envelope Approximation (SVEA). <b>2005</b> , 1-65	
1732	Active Chirp Compensation for Ultrabroadband Optical Pulses. <b>2005</b> , 103-151	
1731	III-nitride-based planar lightwave circuits for long wavelength optical communications. <b>2005</b> , 41, 100-110	27
1730	High accuracy, absolute, cryogenic refractive index measurements of infrared lens materials for JWST NIRCam using CHARMS. <b>2005</b> ,	3

1729	Refractive index and density in F- and Cl-doped silica glasses. 2005, 86, 161907	13
1728	Use of Mie theory to analyze experimental data to identify infrared properties of fused quartz containing bubbles. <b>2005</b> , 44, 7021-31	53
1727	Comparison between finite-difference time-domain calculation with all parameters of Sellmeier's fitting equation and experimental results for slightly chirped 12-fs laser pulse propagation in a silica fiber. <b>2005</b> , 23, 855-863	23
1726	Study of filamentary damage in synthesized silica induced by chirped femtosecond laser pulses. <b>2005</b> , 22, 2437	24
1725	Refractive indices of cubic-phase MgxZn1⊠O thin-film alloys. <b>2005</b> , 97, 023515	32
1724	Phase and amplitude comparison between experiment and calculation of ultrabroad-band pulses generated in a taper fiber. <b>2005</b> , 17, 31-33	2
1723	Dielectrics and Electrooptics. 2005, 817-901	2
1722	Modeling Radiative Properties of Silicon with Coatings and Comparison with Reflectance Measurements. <b>2005</b> , 19, 558-565	33
1721	Electrical and spectroscopic characterization of metal/monolayer/Si devices. 2005, 109, 21836-41	51
1720	Introduction. <b>2006</b> , 1-24	5
1719	Chemical and optical properties of thermally evaporated manganese oxide thin films. <b>2006</b> , 24, 1746-1750	12
1718	Ultrafast third harmonic micro-spectroscopy reveals a two-photon resonance in human hemoglobin. <b>2006</b> ,	1
1717	Effects of Thermal Environment and Surface Roughness on LPRT Surface Temperature Measurements. <b>2006</b> ,	3
1716	Toward nd spectroscopy: Analytic solution of the three-phase model of polarimetry in the thin-film limit. <b>2006</b> , 88, 201107	4
1715	Schlieren Diagnostics of Fused Quartz Heated by Intense Ion Beams. <b>2006</b> , 34, 2414-2418	
1714	Plasmon resonances of gold nanoparticles incorporated inside an optical fibre matrix. <b>2006</b> , 17, 2504-11	40
1713	Optical Properties. <b>2006</b> , 531-607	
1712	Silica, Vitreous. <b>2006</b> ,	

1711	Modeling radiation characteristics of semitransparent media containing bubbles or particles. <b>2006</b> , 23, 1645-56	26
1710	Quantitative investigation of the multiphoton intrapulse interference phase scan method for simultaneous phase measurement and compensation of femtosecond laser pulses. <b>2006</b> , 23, 750	177
1709	Spectroscopy of third-harmonic generation: evidence for resonances in model compounds and ligated hemoglobin. <b>2006</b> , 23, 932	51
1708	Determination of the optical constants (n and k) of inhomogeneous thin films with linear index profiles. <b>2006</b> , 45, 4591-7	7
1707	Thickness optimization of metal films for the development of surface-plasmon-based sensors for nonabsorbing media. <b>2006</b> , 45, 7632-42	63
1706	Assessment of multiphoton absorption in inert gases for the measurement of gas temperatures. <b>2006</b> , 60, 246-53	4
1705	Robust Calculation of Chromatic Dispersion Coefficients of Optical Fibers From Numerically Determined Effective Indices Using Chebyshev[lagrange Interpolation Polynomials. <b>2006</b> , 24, 4411-4416	6
1704	An Extended FDTD Method With Inclusion of Material Dispersion for the Full-Vectorial Analysis of Photonic Crystal Fibers. <b>2006</b> , 24, 4417-4423	10
1703	Interferometric thickness calibration of 300 mm silicon wafers. <b>2006</b> ,	2
1702	Applications of reverse engineering in the fabrication of optical coatings with high performance. <b>2006</b> ,	1
1701	Applications of dispersive white-light spectral interferometry in optics. 2006,	
1700	Calibration of the ZnSe pre-disperser on ESO's cryogenic IR echelle spectrograph (CRIRES): comparison of the first results from CRIRES and the laboratory data from CHARMS. <b>2006</b> ,	
1699	Immersion Factor of In-Water Radiance Sensors: Assessment for a Class of Radiometers. <b>2006</b> , 23, 302-313	19
1698	Phase calibration for attenuating phase-shift masks. <b>2006</b> ,	
1697	Antireflective Effects on a Soda-Lime Glass Induced by Ar+ Implantation. <b>2006</b> , 67, 39-42	11
1696	Variation in optical constants between photocathodes. <b>2006</b> , 564, 439-450	13
1695	Smoothing effect in the broadband laser through a dispersive wedge. <b>2006</b> , 265, 106-110	10
1694	Structural and optical properties of thermally evaporated thin films. <b>2006</b> , 38, 146-151	12

Optical filaments and optical bullets in dispersive nonlinear media. <b>2006</b> , 27, 185-203	3
1692 Establishment of Illuminance Scale at UME with an Accurately Calibrated Radiometer. <b>2006</b> , 13, 326-337	7
Time-resolved two-color interferometric photoemission of image-potential states on Cu(100). <b>2006</b> , 85, 345-350	12
1690 Interface characterization of molecular-monolayer/SiO2 based molecular junctions. <b>2006</b> , 50, 1088-1096	17
Optical multibeamforming network based on WDM and dispersion fiber in receive mode. <b>2006</b> , 54, 402-4	11 27
1688 Immersion factors for the RAMSES series of hyper-spectral underwater radiometers. <b>2006</b> , 8, 252-258	17
Near-IR imaging system for measuring temperatures in a low-NOx combustor. <b>2006</b> , 77, 026103	3
1686 Optical fibers. <b>2006</b> , 57-158	5
Infrared durable protective/antireflection coatings with high performance on Ge and Si substrates. <b>2006</b> ,	1
1684 Temperature-dependent absolute refractive index measurements of synthetic fused silica. <b>2006</b> ,	83
Improved Inverse Method for Radiative Characteristics of Closed-Cell Absorbing Porous Media. <b>2006</b> , 20, 871-883	33
Accurate Ellipsometric Measurement of Refractive Index and Thickness of Ultrathin Oxide Film. <b>2006</b> , 153, F277	15
1681 Finite size effects in Brillouin scattering from silica glass. <b>2006</b> , 74,	23
$_{1680}$ Linear and nonlinear optical response of concentric metallic nanoshells. <b>2006</b> , 2, 31-54	1
Determination of Particle Size and Number Density of Opaque Colloidal Mixtures Using Diffuse Photon Density Waves and Two-Wavelength Light Sources. <b>2007</b> , 46, 2953-2961	5
1678 Radiative Properties of Patterned Wafers With Nanoscale Linewidth. <b>2007</b> , 129, 79-90	43
Multi-photon high-excitation-energy approach to fibre grating inscription. <b>2007</b> , 18, R1-R29	55
Analytic determination of n, pand d of an absorbing film from polarimetric data in the thin-film limit. <b>2007</b> , 101, 033109	14

1675	A method for the determination of the optical constants ( n and k ) of thin films with large optical inhomogeneities. $2007$ , 54, 1453-1465	2
1674	Determination of stress-optical and thermal-optical coefficients of Nb2O5 thin film material. <b>2007</b> , 101, 043513	12
1673	New interferometric technique to measure the length (thickness) of opaque objects using a commercial interferometer. <b>2007</b> ,	
1672	Indirect optical thickness monitoring with stationary test-slides for precision optical coatings. 2007,	
1671	Broadband supercontinuum generation by bridging two separate supercontinua pumped at two different IR wavelengths. <b>2007</b> ,	
1670	Specular and diffuse reflectance of silicon photodiodes. 2007,	
1669	Photonic crystal fibers and fiber lasers (Invited). <b>2007</b> , 24, 1661	75
1668	Refractometry of organosilica microspheres. <b>2007</b> , 46, 1554-61	7
1667	Optical constants of silica glass from extreme ultraviolet to far infrared at near room temperature. <b>2007</b> , 46, 8118-33	596
1666	Impact of Transversal Defects on Confinement Loss of an All-Solid 2-D Photonic-Bandgap Fiber. <b>2007</b> , 25, 3589-3596	17
1665	Refractive index and density changes in silica glass by halogen doping. <b>2007</b> , 353, 568-572	13
1664	Temperature Effects on Prism-Based Surface Plasmon Resonance Sensor. <b>2007</b> , 24, 3081-3084	26
1663	Origin of Differing Reactivities of Aliphatic Chains on HBi(111) and Oxide Surfaces with Metal. <b>2007</b> , 111, 9384-9392	32
1662	Relationship between refractive index and density of synthetic silica glasses. <b>2007</b> , 101, 123533	20
1661	Fiber-optic-based Corrosion Sensor using OTDR. 2007,	6
1660	The Comparison Between Experiment and Calculation of the Chirp-Controlled Raman Self-Frequency Shift in a Photonic Crystal Fiber. <b>2007</b> , 19, 1292-1294	8
1659	Regioselectively Ordered Silica Nanotubes by Molecular Templating. <b>2007</b> , 19, 984-987	44
1658	Optical properties of erbium oxide thin films deposited by electron beam evaporation. <b>2007</b> , 515, 2885-2890	24

## (2008-2007)

measurements of femtosecond pulses. <b>2007</b> , 275, 354-358	7
Reflection-type confocal refractive index profile measurement method for optical waveguides: Effects of a broadband light source and multireflected lights. <b>2007</b> , 277, 74-79	1
Experimental measurements of the radiation characteristics of Anabaena variabilis ATCC 29413-U and Rhodobacter sphaeroides ATCC 49419. <b>2007</b> , 32, 4772-4785	43
Angular tuning of defect modes spectrum in the one-dimensional photonic crystal with liquid-crystal layer. <b>2007</b> , 24, 297-302	14
Colored films produced by electron beam deposition from nanometric TiO2 and Al2O3 pigment powders obtained by modified polymeric precursor method. <b>2007</b> , 75, 693-700	6
Smoothing the side lobes of a focused pattern by spectral dispersion in the broadband laser. <b>2007</b> , 118, 594-598	3
1651 Complete analysis of photonic crystal fibers by full-vectorial 2D-FDTD method. <b>2008</b> , 40, 991-1003	3
1650 Numerical analysis of the spectral response of an NSOM measurement. <b>2008</b> , 93, 47-54	
1649 Temperature sensing capacity of fiber Bragg grating at liquid nitrogen temperature. <b>2008</b> , 1, 223-225	
1648 Directional selectivity and ultra-light-trapping in solar cells. <b>2008</b> , 205, 2831-2843	
20 <del>1</del> 0 - 11 - 11 - 11 - 11 - 11 - 11 - 11 -	51
Effect of solvent composition on transparency and surface hardness of poly(methyl methacrylate)-silica nanocomposites provided on polycarbonate. <b>2008</b> , 109, 1498-1504	51
Effect of solvent composition on transparency and surface hardness of poly(methyl	
Effect of solvent composition on transparency and surface hardness of poly(methyl methacrylate)-silica nanocomposites provided on polycarbonate. <b>2008</b> , 109, 1498-1504  Interfacial modification of silica surfaces through Esocyanatopropyl triethoxy silane mine	5
Effect of solvent composition on transparency and surface hardness of poly(methyl methacrylate)-silica nanocomposites provided on polycarbonate. 2008, 109, 1498-1504  Interfacial modification of silica surfaces through Esocyanatopropyl triethoxy silane mine coupling reactions. 2008, 254, 1789-1796	5
Effect of solvent composition on transparency and surface hardness of poly(methyl methacrylate)-silica nanocomposites provided on polycarbonate. 2008, 109, 1498-1504  Interfacial modification of silica surfaces through Esocyanatopropyl triethoxy silane mine coupling reactions. 2008, 254, 1789-1796  Conical emission by femtosecond pulses with different spectral bandwidths. 2008, 281, 4780-4783	5 16 6
Effect of solvent composition on transparency and surface hardness of poly(methyl methacrylate)-silica nanocomposites provided on polycarbonate. 2008, 109, 1498-1504  Interfacial modification of silica surfaces through Esocyanatopropyl triethoxy silane mine coupling reactions. 2008, 254, 1789-1796  Conical emission by femtosecond pulses with different spectral bandwidths. 2008, 281, 4780-4783  Measurement of the optical conductivity of graphene. 2008, 101, 196405  One-dimensional photonic crystals with a planar oriented nematic layer: Temperature and angular	5 16 6 1190
Effect of solvent composition on transparency and surface hardness of poly(methyl methacrylate)-silica nanocomposites provided on polycarbonate. 2008, 109, 1498-1504  Interfacial modification of silica surfaces through Esocyanatopropyl triethoxy silaneEmine coupling reactions. 2008, 254, 1789-1796  Conical emission by femtosecond pulses with different spectral bandwidths. 2008, 281, 4780-4783  Measurement of the optical conductivity of graphene. 2008, 101, 196405  One-dimensional photonic crystals with a planar oriented nematic layer: Temperature and angular dependence of the spectra of defect modes. 2008, 106, 388-398	5 16 6 1190 29

1639	. <b>2008</b> , 26, 1854-1861	35
1638	. <b>2008</b> , 26, 1980-1985	31
1637	Effect of dispersion on the spectrum of partially coherent beams. 2008, 25, 2122-8	1
1636	Design of single-polarization elliptical-hole core circular-hole holey fibers with zero dispersion at 155 fh. <b>2008</b> , 25, 1690	12
1635	Analysis of tunneling times in absorptive and dispersive media. <b>2008</b> , 25, 1800	13
1634	Measurement of Refractive Index of Solid Medium by Critical Angle Method When Air Gap is Present. <b>2008</b> , 12, 210-214	5
1633	Increasing the blue-shift of a supercontinuum by modifying the fiber glass composition. <b>2008</b> , 16, 21076-86	26
1632	Gain Enhancement in Cladding-Pumped Silicon Raman Amplifiers. <b>2008</b> , 44, 692-704	18
1631	Local structure, optical and magnetic studies of Ni nanostructures embedded in a SiO2matrix by ion implantation. <b>2008</b> , 20, 285211	15
1630	Spectral anomalies of pulsed Hermitelaussian beams focused by a dispersive aperture lens. <b>2008</b> , 55, 947-957	
1629	Tuning the dispersion and single/multi-modeness in a hole-assisted fiber: A finite-element study. <b>2008</b> ,	
1628	Design of nanofilters for optical nanocircuits. <b>2008</b> , 77,	42
1627	Reducing photodiode reflectance by Brewster-angle operation. <b>2008</b> , 45, 11-15	14
1626	Uncertainty analysis on the absolute thickness of a cavity using a commercial wavelength scanning interferometer. <b>2008</b> ,	2
1625	Tuning the dispersion and single/multi-modeness of a hole-assisted fiber by the hole geometrical parameters. <b>2008</b> , 10, 115002	
1624	Theoretical study of microfiber resonator devices exploiting a phase shift. <b>2008</b> , 10, 025303	23
1623	Properties of Zero Dispersion Wavelengths in Silica Strands and Photonic Crystal Fibres. <b>2008</b> , 25, 993-995	3
1622	Multi-Object Infrared Camera and Spectrograph (MOIRCS) for the Subaru Telescope* I. Imaging. <b>2008</b> , 60, 1347-1362	96

1621	Inelastic light scattering by longitudinal acoustic phonons in thin silicon layers: From membranes to silicon-on-insulator structures. <b>2008</b> , 77,	43
1620	Spatiotemporal quasisolitons and resonant radiation in arrays of silicon-on-insulator photonic wires. <b>2008</b> , 78,	30
1619	Theoretical Characterization of a Commercial Large Mode Area - Endlessly Single Mode Photonic Crystal Fiber. <b>2008</b> ,	
1618	Hypersound damping in vitreous silica measured by picosecond acoustics. 2008, 77,	63
1617	Multipoint fiber-optic-based corrosion sensor. 2008,	
1616	Investigating properties of surfaces and thin films using microsphere whispering-gallery modes. <b>2008</b> ,	4
1615	Modeling of dwell time and group delay in dispersive and absorptive media. 2009, T135, 014040	1
1614	Solitary Waves of the Regularized Short Pulse and Ostrovsky Equations. <b>2009</b> , 41, 2088-2106	30
1613	Chirped biphotons and their compression in optical fibers. <b>2009</b> , 103, 193602	30
1612	Envelope localized waves of the conical type in linear normally dispersive media. 2009, 79,	9
1611	Prism refractive index measurement at INRiM. <b>2009</b> , 20, 095305	8
1610	Brewster angle reflection measurements of Hg density and laser deflection (Schlieren) measurements of Hg density gradients in an ultra-high pressure arc lamp. <b>2009</b> , 18, 025010	1
1610 1609		65
	measurements of Hg density gradients in an ultra-high pressure arc lamp. <b>2009</b> , 18, 025010  Microstructured and Photonic Bandgap Fibers for Applications in the Resonant Bio- and Chemical	
1609 1608	measurements of Hg density gradients in an ultra-high pressure arc lamp. 2009, 18, 025010  Microstructured and Photonic Bandgap Fibers for Applications in the Resonant Bio- and Chemical Sensors. 2009, 2009, 1-20  Spatial calibration of structured illumination fluorescence microscopy using capillary tissue	65
1609 1608 1607	measurements of Hg density gradients in an ultra-high pressure arc lamp. 2009, 18, 025010  Microstructured and Photonic Bandgap Fibers for Applications in the Resonant Bio- and Chemical Sensors. 2009, 2009, 1-20  Spatial calibration of structured illumination fluorescence microscopy using capillary tissue phantoms. 2009, 72, 85-92	65
1609 1608 1607	measurements of Hg density gradients in an ultra-high pressure arc lamp. 2009, 18, 025010  Microstructured and Photonic Bandgap Fibers for Applications in the Resonant Bio- and Chemical Sensors. 2009, 2009, 1-20  Spatial calibration of structured illumination fluorescence microscopy using capillary tissue phantoms. 2009, 72, 85-92  Thermal characteristics of a fiber Fabry-Perot etalon made of highly birefringent fiber. 2009, 16, 555-557	65

1603	Particle nature of light waves in dielectric media. <b>2009</b> , 404, 3880-3885	4
1602	Optical properties of ion-implanted silicon and separation by implantation of oxygen silicon-on-insulator substrates in the infrared: Study of B+ and P2+ implantation doping. <b>2009</b> , 517, 4307-4317	, 1
1601	Guided Wave Analysis of Hollow Optical Fiber for Mode-Coupling Device Applications. <b>2009</b> , 27, 4919-4926	20
1600	Variation of Ionic Strength Reveals the Interfacial Water Structure at a Charged Mineral Surface. <b>2009</b> , 113, 15364-15372	122
1599	Effect of hydroxyl impurity on temperature coefficient of refractive index of synthetic silica glasses. <b>2009</b> , 355, 2216-2219	3
1598	Observation of an electric-field-induced band gap in bilayer graphene by infrared spectroscopy. <b>2009</b> , 102, 256405	485
1597	Characterization of Silica Nanowires for Optical Sensing. <b>2009</b> , 27, 5537-5542	15
1596	Polarization-dependent effects in point-by-point fiber Bragg gratings enable simple, linearly polarized fiber lasers. <b>2009</b> , 17, 6082-95	53
1595	High efficiency excitation of plasmonic waveguides with vertically integrated resonant bowtie apertures. <b>2009</b> , 17, 8036-45	18
1594	Plasmonic data storage medium with metallic nano-aperture array embedded in dielectric material. <b>2009</b> , 17, 20203-10	26
1593	Preservation of the carrier envelope phase during cross-polarized wave generation. 2009, 17, 22358-65	10
1592	Broadband plasmon waveguide resonance spectroscopy for probing biological thin films. <b>2009</b> , 63, 1062-7	12
1591	Measurement of chromatic dispersion of microstructured polymer fibers by white-light spectral interferometry. <b>2009</b> ,	2
1590	Temperature-Shifted White-Light Interferometry for Equalization of a Fiber Coupler to Near-Zero Path Length Difference. <b>2009</b> , 21, 944-946	1
1589	Design a new PCF whose zero dispersion wavelength of 800nm is insensitive to its fiber core diameter. <b>2009</b> ,	
1588	Simultaneous measurement of substrate temperature and thin-film thickness on SiO2/Si wafer using optical-fiber-type low-coherence interferometry. <b>2009</b> , 105, 013110	16
1587	Theoretical Analysis and Preparation of Tapered Suspended Core Microstructure Fibers. 2009, 3, 233-249	4
1586	Overview on Solid Core Photonic BandGap Fibers. <b>2009</b> , 28, 27-50	15

1585	Nanoscale bowtie aperture as high efficiency light coupler with plasmonic waveguide. 2009,	
1584	Hydroxyl-concentration distribution near the binding interface formed by heating contacted flat silica glass surfaces at high temperature. <b>2009</b> , 117, 211-213	3
1583	Design of photonic crystal fiber long-period grating refractive index sensor. 2009,	
1582	Radiative Transfer in Two-Phase Dispersed Materials. <b>2010</b> , 187-234	
1581	Theoretical study on the multimodeness of a commercial endlessly single-mode PCF. <b>2010</b> , 283, 4649-4654	11
1580	Combustion chemical vapour deposition of Al2O3 films: Effect of temperature on structure, morphology and adhesion. <b>2010</b> , 205, 1838-1842	14
1579	First clinical application of a liquid-core light guide connected to an Er:YAG laser for oral treatment of leukoplakia. <b>2010</b> , 25, 669-73	6
1578	Study of the properties and structure of nanosize membranes for acousto-optic devices. <b>2010</b> , 51, 68-72	
1577	Control of Optical Performance in Infrared Region for Vanadium Dioxide Films Layered by Amorphous Silicon. <b>2010</b> , 31, 1964-1971	7
1576	Optical Temperature Measurement Method for Glowing Microcomponents. <b>2010</b> , 31, 1762-1770	
1575	Photonic generation of microwave signals by exploiting fiber birefringence effect in single-longitudinal-mode distributed Bragg reflector fiber lazer. <b>2010</b> , 52, 535-540	
1574	Microstructural characterization of thin SiOx films obtained by physical vapor deposition. <b>2010</b> , 174, 132-136	20
1573	Optical constants and thermocoloration of pulsed laser deposited molybdenum oxide thin films. <b>2010</b> , 283, 2857-2862	32
1572	Reflectance of surfactant-templated mesoporous silica thin films: Simulations versus experiments. <b>2010</b> , 518, 2134-2140	18
1571	Thin film removal mechanisms in ns-laser processing of photovoltaic materials. <b>2010</b> , 518, 2897-2904	118
1570	Dispersion controlled highly nonlinear fibers for all-optical processing at telecoms wavelengths. <b>2010</b> , 16, 378-391	37
1569	Introduction. <b>2010</b> , 1-13	2
1568	Comparative study of long-period gratings written in a boron co-doped fiber by an electric arc and UV irradiation. <b>2010</b> , 21, 025309	26

1567 The influence of aberrations in third harmonic gener	ration microscopy. <b>2010</b> , 12, 084009	4
1566 Refractive index of Lithosil and Suprasil 312 at cryoc	genic temperature. <b>2010</b> , 47, 175-178	1
An effect of Scattering by absorption bbserved in ne <b>2010</b> , 107, 083106	ear-infrared properties of nanoporous silica.	22
1564 Precision frequency measurements with interferom	etric weak values. <b>2010</b> , 82,	112
1563 Autoresonant four-wave mixing in optical fibers. <b>20</b> °	<b>10</b> , 82,	12
Mechanism of hollow-core-fiber infrared-superconti 81,	nuum compression with bulk material. <b>2010</b> ,	34
1561 Three-dimensional mapping of multiple filament arr	ays. <b>2010</b> , 81,	14
1560 Ultra-fast all-optical integrated differentiators in Bro	agg gratings. <b>2010,</b>	O
1559 Thermo-optical switches. <b>2010</b> , 61-96		2
Optimal design of broadband photonic crystal fibre sensing. <b>2010</b> ,	long-period gratings for evanescent absorption	
1557 Periodic arrays of ridge apertures as a high efficienc	y coupler for photovoltaic applications. <b>2010</b> ,	
$_{1556}$ Design of an optically invisible metamaterial fibre. <b>2</b>	010,	
1555 Optical birefringence in uniaxially compressed aerog	gels. <b>2010</b> , 12, 103016	9
Thermal expansion coefficients and composition of 2010, 43, 335104	sputter-deposited silicon oxynitride thin films.	1
Approach the angular sensitivity limit in surface plas and large resonant angle. <b>2010</b> , 49, 054403	smon resonance sensors with low index prism	21
1552 Extraordinary transmission from high-gain nanoaper	ture antennas. <b>2010</b> , 96, 211116	18
Ultradense, deep subwavelength nanowire array pho 2010, 10, 4429-34	otovoltaics as engineered optical thin films.	12
Interferometric measurement of the temperature d application to fused silica. <b>2010</b> , 49, 678-82	ependence of an index of refraction:	10

1549	Optical temperature measurements of silicon microbridge emitters. <b>2010</b> , 49, 1489-93	2
1548	Deformation-free form error measurement of thin, plane-parallel optics floated on a heavy liquid. <b>2010</b> , 49, 1849-58	6
1547	Ten-element photodetector for optical power and attenuation measurements. 2010, 49, 3774-9	3
1546	Random lasing in ballistic and diffusiveregimes for macroporous silica-based systems with tunable scattering strength. <b>2010</b> , 18, 12153-60	27
1545	Weaving the invisible thread: design of an optically invisible metamaterial fibre. <b>2010</b> , 18, 18095-105	15
1544	In situ monitoring of the formation of nanoscale polyelectrolyte coatings on optical fibers using Surface Plasmon Resonances. <b>2010</b> , 18, 20409-21	11
1543	Design of vertical Ge quantum well asymmetric Fabry-Perot modulator without DBR. <b>2010</b> , 18, 23576-83	1
1542	Design of a highly-birefringent microstructured photonic crystal fiber for pressure monitoring. <b>2010</b> , 18, 25657-64	43
1541	Sub-50 nm patterning by immersion interference lithography using a Littrow prism as a Lloyd's interferometer. <b>2010</b> , 35, 3450-2	34
1540	Generation of Lossy Mode Resonances With Absorbing Thin-Films. <b>2010</b> ,	24
1540 1539	Generation of Lossy Mode Resonances With Absorbing Thin-Films. 2010,  Transmission of p- and s-polarized light through a prism and the condition of minimum deviation. 2010, 27, 2085-90	3
1539	Transmission of p- and s-polarized light through a prism and the condition of minimum deviation.	
1539	Transmission of p- and s-polarized light through a prism and the condition of minimum deviation. <b>2010</b> , 27, 2085-90	3
1539 1538	Transmission of p- and s-polarized light through a prism and the condition of minimum deviation.  2010, 27, 2085-90  Spectral restoration for femtosecond spectral interferometry with attosecond accuracy. 2010, 27, 1104  Transparent hydrophobic durable low moisture permeation poly(fluoroimide acrylate)/SiO2	3
1539 1538 1537	Transmission of p- and s-polarized light through a prism and the condition of minimum deviation.  2010, 27, 2085-90  Spectral restoration for femtosecond spectral interferometry with attosecond accuracy. 2010, 27, 1104  Transparent hydrophobic durable low moisture permeation poly(fluoroimide acrylate)/SiO2 nanocomposite from solventless photocurable resin system. 2010, 20, 3084  Evanescent wave-initiated photopolymerisation as a new way to create monolithic open-tubular	3 16 15
1539 1538 1537 1536	Transmission of p- and s-polarized light through a prism and the condition of minimum deviation. 2010, 27, 2085-90  Spectral restoration for femtosecond spectral interferometry with attosecond accuracy. 2010, 27, 1104  Transparent hydrophobic durable low moisture permeation poly(fluoroimide acrylate)/SiO2 nanocomposite from solventless photocurable resin system. 2010, 20, 3084  Evanescent wave-initiated photopolymerisation as a new way to create monolithic open-tubular capillary columns: use as enzymatic microreactor for on-line protein digestion. 2010, 135, 477-81  Simulation of a surface plasmon resonance based on photonic crystal fiber temperature sensor.	3 16 15 29
1539 1538 1537 1536	Transmission of p- and s-polarized light through a prism and the condition of minimum deviation.  2010, 27, 2085-90  Spectral restoration for femtosecond spectral interferometry with attosecond accuracy. 2010, 27, 1104  Transparent hydrophobic durable low moisture permeation poly(fluoroimide acrylate)/SiO2 nanocomposite from solventless photocurable resin system. 2010, 20, 3084  Evanescent wave-initiated photopolymerisation as a new way to create monolithic open-tubular capillary columns: use as enzymatic microreactor for on-line protein digestion. 2010, 135, 477-81  Simulation of a surface plasmon resonance based on photonic crystal fiber temperature sensor. 2011,  Tuning of the surface plasmon resonance in TiO2/Au thin films grown by magnetron sputtering:	3 16 15 29

1531	An azimuthally polarizing photonic crystal fibre with a central gold nanowire. <b>2011</b> , 13, 063016	26
1530	Dispersion-compensation improvement for dual-concentric-core photonic crystal fibers. 2011,	
1529	Green luminescence of InGaN nanowires grown on silicon substrates by molecular beam epitaxy. <b>2011</b> , 109, 084336	46
1528	Ultra-flattened chromatic dispersion control for circular photonic crystal fibers. <b>2011</b> , 13, 055405	22
1527	Experimental study of the effect of external electric fields on interfacial dynamics of colloidal particles. <b>2011</b> , 27, 11481-8	31
1526	Optical characterization of nanostructured silver thin films studied by spectroscopic ellipsometry. <b>2011</b> ,	
1525	Simultaneous Measurement of the Core Diameter and the Numerical Aperture in Dual-Mode Step-Index Optical Fibers. <b>2011</b> , 29, 3834-3837	4
1524	Propagation of broadband gaussian Schell-model beams in the apertured fractional Fourier transformation systems. <b>2011</b> , 28, 976-82	4
1523	Refractive index measured by laser beam displacement at 월1064 nm for solvents and deuterated solvents. <b>2011</b> , 50, 4091-8	15
1522	Simulating human photoreceptor optics using a liquid-filled photonic crystal fiber. <b>2011</b> , 2, 543-51	9
1521	Enhancement of chemical sensing capability in a photonic crystal fiber with a hollow high index ring defect at the center. <b>2011</b> , 19, 1921-9	55
1520	Spectral characterization of biological aerosol particles using two-wavelength excited laser-induced fluorescence and elastic scattering measurements. <b>2011</b> , 19, 6191-208	58
1519	Highly sensitive and simple method for refractive index sensing of liquids in microstructured optical fibers using four-wave mixing. <b>2011</b> , 19, 10471-84	61
1518	Refractometric sensing with fluorescent-core microcapillaries. <b>2011</b> , 19, 21540-51	35
1517	Evolution of modes in a metal-coated nano-fiber. <b>2011</b> , 19, 25206-21	14
1516	Femtosecond surface plasmon pulse propagation. <b>2011</b> , 36, 250-2	37
1515	Low-loss silica-on-silicon waveguides. <b>2011</b> , 36, 3729-31	17
1514	Effect of annealing on pulsed laser deposited zirconium oxide thin films. <b>2011</b> , 509, 9536-9541	17

1513	Optical properties of fluorine-substituted zinc bismuth phosphate glasses. <b>2011</b> , 357, 1188-1192	17
1512	Mass and bond density measurements for PECVD a-SiCx:H thin films using Fourier transform-infrared spectroscopy. <b>2011</b> , 357, 3602-3615	45
1511	Fiber-integrated diamond-based single photon source. <b>2011</b> , 11, 198-202	105
1510	Conservation of the photon number in the generalized nonlinear Schrdinger equation in axially varying optical fibers. <b>2011</b> , 84,	10
1509	Modeling of a fiber-optic sensor based on surface plasmon resonance including the dispersion of the analyte. <b>2011</b> ,	1
1508	Dispersion optimization of photonic crystal fiber long-period gratings for a high-sensitivity refractive index sensing. <b>2011</b> ,	
1507	Broadening Adjustable Range on Post-Fabrication Resonance Wavelength Trimming of Long-Period Fiber Gratings and the Mechanisms of Resonance Wavelength Shifts. <b>2011</b> , E94-C, 641-647	4
1506	Influence of hydrogen annealing on the properties of hafnium oxide thin films. <b>2011</b> , 126, 515-523	40
1505	Selective Intermixing of InGaAs/GaAs Quantum Dot Infrared Photodetectors. <b>2011</b> , 47, 577-590	7
1504	A combined transient thermal model for laser hyperthermia of tumors with embedded gold nanoshells. <b>2011</b> , 54, 5459-5469	86
1503	Fabrication of Sealed μ-Channels Through a Fast and Reliable Photopolymerization Process. <b>2011</b> , 296, 666-676	7
1502	Morphological analysis of physically reconstructed capillary hybrid silica monoliths and correlation with separation efficiency. <b>2011</b> , 1218, 5187-94	51
1501	Xanthan/chitosan gold chip for metal enhanced protein biomarker detection. 2011, 26, 2559-65	8
1500	Physical reconstruction of packed beds and their morphological analysis: core-shell packings as an example. <b>2011</b> , 1218, 1849-60	74
1499	Investigation of intermodal interference of LP01 and LP11 modes in the liquid-core optical fiber for temperature measurements. <b>2011</b> , 122, 707-710	12
1498	Luminescence enhancement of Y2O3:Eu3+ and Y2SiO5:Ce3+,Tb3+ core particles with SiO2 shells. <b>2011</b> , 176, 436-441	43
1497	Thickness measurement of colloidal opal crystal growth by Bragg reflection. 2011, 360, 331-4	2
1496	Spectroscopic ellipsometry studies on hydrogenated amorphous silicon thin films deposited using DC saddle field plasma enhanced chemical vapor deposition system. <b>2011</b> , 519, 2863-2866	10

1495 Direct modeling of external quantum efficiency of silicon trap detectors. <b>2011</b> ,	2
Multilongitudinal-mode fiber laser temperature sensor and its applications in the mea temperature dependence of fiber birefringence. <b>2011</b> ,	surement of
1493 Fiber optic probe hydrophone for the study of acoustic cavitation in water. <b>2011</b> , 82, 0	37
1492 Subterahertz hypersound attenuation in silica glass studied via picosecond acoustics. 2	<b>2011</b> , 83, 29
Formation mechanisms of precursors of radiation-induced color centers during fabrica optical fiber preform. <b>2011</b> , 109, 083103	ation of silica 8
Narrow-band acoustic attenuation measurements in vitreous silica at frequencies betw 400 GHz. <b>2011</b> , 98, 211908	ween 20 and 36
1489 Advance in thermo-optical switches: principles, materials, design, and device structure	e. <b>2011</b> , 50, 071112 66
1488 Optical Properties. <b>2011</b> , 587-663	2
1487 Micromachined array-type Mirau interferometer for parallel inspection of MEMS. <b>2011</b>	1, 21, 065005 25
1486 Phase measurement in nondegenerate three-wave mixing spectroscopy. <b>2011</b> , 134, 04	14712 27
Optical method for measuring thermal accommodation coefficients using a whispering microresonator. <b>2011</b> , 135, 084313	g-gallery 25
$_{1484}$ Axial laser beam cleaning of tiny particles on narrow slot sidewalls. <b>2012</b> , 45, 365106	5
Axial Resolution of the Laser Affected Voxel of the Ultra-Short Pulse Laser Modification the Transparent Media. <b>2012</b> , 433-440, 5741-5745	on inside of
Simulation of surface plasmon fiber-optic sensor including the effect of oxide overlays change. <b>2012</b> ,	er thickness
1481 Optical self-sensing of impact damage in composites using E-glass cloth. <b>2012</b> , 21, 045	5021 9
Ultra-deep subwavelength periodic patterning through multilayered metamaterial mid ${f 2012},$	crocavity.
Group index determination by pulse delay measurements and dispersion study in the z dispersion region of fused silica. <b>2012</b> , 29, 2797	zero
1478 Spectral and temporal holograms with nonlinear optics. <b>2012</b> , 37, 3591-3	9

1477	Optical properties of in-vitro biomineralised silica. <b>2012</b> , 2, 607	18
1476	Dispersion control in square lattice photonic crystal fiber using hollow ring defects. <b>2012</b> , 20, 5281-90	7
1475	Photon management with core-shell nanowire structures. <b>2012</b> , 20 Suppl 2, A255-64	3
1474	Low loss silica hollow core fibers for 3-4 h spectral region. <b>2012</b> , 20, 11153-8	231
1473	Entangled photon generation using four-wave mixing in azimuthally symmetric microresonators. <b>2012</b> , 20, 21977-91	20
1472	Serpentine low loss trapezoidal silica waveguides on silicon. <b>2012</b> , 20, 22298-307	5
1471	Polarisation-resolved near-field mapping of a coupled gold nanowire array. 2012, 20, 28409-17	26
1470	Simultaneous wavenumber measurement and coherence detection using temporal phase unwrapping. <b>2012</b> , 51, 558-67	13
1469	Dispersion ultrastrong compensating fiber based on a liquid-filled hybrid structure of dual-concentric core and depressed-clad photonic crystal fiber. <b>2012</b> , 29, 2021	21
1468	Measurements of the refractometric characteristics of optical materials in the 248B000-nm spectral region. <b>2012</b> , 79, 112	1
1467	Self-organizing second-order nonlinear susceptibility in NLO-chromophore-doped amorphous ferroelectric poly-(cyano phenylene sulfide) polymers [Invited]. <b>2012</b> , 2, 2	2
1466	Full-vectorial modeling of femtosecond pulses for laser inscription of photonic structures. <b>2012</b> , 29, 1208	15
1465	Modified Roberts-Langenbeck test for measuring thickness and refractive index variation of silicon wafers. <b>2012</b> , 20, 20078-89	21
1464	Long-period grating and its cascaded counterpart in photonic crystal fiber for gas phase measurement. <b>2012</b> , 20, 20951-61	15
1463	Transfer-matrix method based on a discrete coupling model for analyzing uniform and nonuniform codirectional fiber grating couplers. <b>2012</b> , 51, 2367-72	6
1462	Optical microcavities with a thiol-functionalized gold nanoparticle polymer thin film coating. <b>2012</b> , 100, 013305	10
1461	Efficiency enhancement of InGaN multi-quantum-well solar cells via light-harvesting SiO2 nano-honeycombs. <b>2012</b> , 100, 013105	20
1460	. <b>2012</b> , 12, 237-245	13

1459	Phase matching for surface plasmon enhanced second harmonic generation in a gold grating slab. <b>2012</b> , 100, 181107	11
1458	Dispersion properties of liquid-core photonic crystal fibers. <b>2012</b> , 51, 5259-65	18
1457	In Situ Investigations of SEI Layer Growth on Electrode Materials for Lithium-Ion Batteries Using Spectroscopic Ellipsometry. <b>2012</b> , 159, A198-A207	72
1456	Circular dichroism from chiral nanomaterial fabricated by on-edge lithography. <b>2012</b> , 24, OP321-5	58
1455	Influence of Post Growth Annealing on the Optical Properties of Gallium Nitride Films Grown by Pulsed Laser Deposition. <b>2012</b> , 1432, 59	
1454	Design of turn-around-point long-period gratings in Ge-doped photonic crystal fibers for evanescent sensing. <b>2012</b> ,	1
1453	Metal oxide layer influence on the sensitivity of SPR fiber optic sensor. <b>2012</b> ,	2
1452	Nonlinear light propagation in photonic crystal fibers infiltrated with liquid crystalline materials. <b>2012</b> ,	
1451	Gold-coated optical fiber-micro-tapers for sensor applications based on the surface plasmon resonance effect. <b>2012</b> ,	
1450	. <b>2012</b> , 30, 2289-2298	37
,,,	. 2012, 30, 2289-2298  Spectroscopy of stop bands of globular photonic crystals filled with water. 2012, 39, 311-319	2
,,,		
1449	Spectroscopy of stop bands of globular photonic crystals filled with water. <b>2012</b> , 39, 311-319  Time-of-flight photon spectroscopy: a simple scheme to monitor simultaneously spectral and	2
1449	Spectroscopy of stop bands of globular photonic crystals filled with water. <b>2012</b> , 39, 311-319  Time-of-flight photon spectroscopy: a simple scheme to monitor simultaneously spectral and temporal fluctuations of emission on single nanoparticles. <b>2012</b> , 6, 10512-23  Lightpath Topology Design for Wavelength-Routed Optical Networks in the Presence of Four-Wave Mixing. <b>2012</b> , 4, 314	2
1449 1448 1447	Spectroscopy of stop bands of globular photonic crystals filled with water. <b>2012</b> , 39, 311-319  Time-of-flight photon spectroscopy: a simple scheme to monitor simultaneously spectral and temporal fluctuations of emission on single nanoparticles. <b>2012</b> , 6, 10512-23  Lightpath Topology Design for Wavelength-Routed Optical Networks in the Presence of Four-Wave Mixing. <b>2012</b> , 4, 314  Wavelength tuning of multimode interference bandpass filters by mechanical bending: experiment and theory in comparison. <b>2012</b> , 108, 117-124  Evanescent wave optical trapping and transport of micro- and nanoparticles on tapered optical	<ul><li>2</li><li>9</li><li>7</li></ul>
1449 1448 1447 1446	Spectroscopy of stop bands of globular photonic crystals filled with water. 2012, 39, 311-319  Time-of-flight photon spectroscopy: a simple scheme to monitor simultaneously spectral and temporal fluctuations of emission on single nanoparticles. 2012, 6, 10512-23  Lightpath Topology Design for Wavelength-Routed Optical Networks in the Presence of Four-Wave Mixing. 2012, 4, 314  Wavelength tuning of multimode interference bandpass filters by mechanical bending: experiment and theory in comparison. 2012, 108, 117-124  Evanescent wave optical trapping and transport of micro- and nanoparticles on tapered optical	2 9 7
1449 1448 1447 1446	Spectroscopy of stop bands of globular photonic crystals filled with water. 2012, 39, 311-319  Time-of-flight photon spectroscopy: a simple scheme to monitor simultaneously spectral and temporal fluctuations of emission on single nanoparticles. 2012, 6, 10512-23  Lightpath Topology Design for Wavelength-Routed Optical Networks in the Presence of Four-Wave Mixing. 2012, 4, 314  Wavelength tuning of multimode interference bandpass filters by mechanical bending: experiment and theory in comparison. 2012, 108, 117-124  Evanescent wave optical trapping and transport of micro- and nanoparticles on tapered optical fibers. 2012, 113, 2512-2520	2 9 7 13 38

## (2012-2012)

1441	Mid-infrared optical properties of thin films of aluminum oxide, titanium dioxide, silicon dioxide, aluminum nitride, and silicon nitride. <b>2012</b> , 51, 6789-98	504
1440	Spectroscopy of stop bands in artificial opals filled with an alcohol solution of potassium iodide. <b>2012</b> , 113, 271-274	4
1439	Immobilization of streptavidin on 4HBiC for biosensor development. <b>2012</b> , 258, 6056-6063	82
1438	Optical properties of iron oxide (Fe2O3) thin films deposited by the reactive evaporation of iron. <b>2012</b> , 521, 178-182	121
1437	Nanoparticle-mediated photothermal therapy: a comparative study of heating for different particle types. <b>2012</b> , 44, 675-84	139
1436	Near-field simulation of obliquely deposited surface-enhanced Raman scattering substrates. <b>2012</b> , 112, 113111	7
1435	Nanoplasmonic Array Enhancement of Two-Photon Absorption in a Dye Film. <b>2012</b> , 116, 17169-17173	7
1434	Preparation and characterization of poly(L-histidine)/poly(L-glutamic acid) multilayer on silicon with nanometer-sized surface structures. <b>2012</b> , 386, 252-9	6
1433	A new design of low-loss and ultra-flat zero dispersion photonic crystal fiber using hollow ring defect. <b>2012</b> , 285, 4082-4087	16
1432	Optical constants of vacuum annealed radio frequency (RF) magnetron sputtered zinc oxide thin films. <b>2012</b> , 285, 4405-4412	11
1431	Semi-analytical analysis of lithium niobate photonic wires. <b>2012</b> , 285, 4347-4352	10
1430	Long-period gratings in photonic crystal fibers operating near the phase-matching turning point for evanescent chemical and biochemical sensing. <b>2012</b> ,	2
1429	SimultaneousIn situMeasurement of Silicon Substrate Temperature and Silicon Dioxide Film Thickness during Plasma Etching of Silicon Dioxide Using Low-Coherence Interferometry. <b>2012</b> , 51, 046201	
1428	Vibrational Sum Frequency Spectroscopy Studies at Solid/Liquid Interfaces: Influence of the Experimental Geometry in the Spectral Shape and Enhancement. <b>2012</b> , 116, 22893-22903	48
1427	Determination of the Failure Stresses for Fluid-filled Microcapsules that Rupture Near the Elastic Regime. <b>2012</b> , 52, 1435-1445	5
1426	Instrumentation for dual-probe scanning near-field optical microscopy. <b>2012</b> , 83, 083709	16
1425	A giant red shift and enhancement of the light confinement in a planar array of dielectric bars. <b>2012</b> , 14, 035103	46
1424	Fundamentals of Optical Fibers. <b>2012</b> , 10-75	

XAFS Measurement System in the Soft X-ray Region for Various Sample Conditions and Multipurpose Measurements. **2012**,

1422	Improvement of the detection system in the soft X-ray absorption spectroscopy. <b>2012</b> , 44, 784-788	14
1421	Towards electrical detection of plasmons in all-silicon pin-diodes. <b>2012</b> , 249, 773-777	1
1420	Dispersion characteristics of water- and gold-infiltrated opal photonic crystals. <b>2012</b> , 48, 361-367	10
1419	Transparent, superhydrophobic, and wear-resistant coatings on glass and polymer substrates using SiO2, ZnO, and ITO nanoparticles. <b>2012</b> , 28, 11391-9	220
1418	Nonreciprocal frequency doubling of electromagnetic waves through double resonance and Bragg reflection in photonic crystals. <b>2012</b> , 12, 214-218	
1417	Process investigations of optical trap assisted direct-write microsphere near-field nanostructuring. <b>2012</b> , 61, 207-210	8
1416	Infrared emission spectroscopy of CO2 at high temperature. Part I: Experimental setup and source characterization. <b>2012</b> , 113, 1-13	24
1415	Synthesis of nanocrystalline LaF3 doped silica glasses by hydrofluoric acid catalyzed solgel process. <b>2012</b> , 177, 510-514	6
1414	LUXSim: A component-centric approach to low-background simulations. <b>2012</b> , 675, 63-77	29
1413	Polarization maintaining highly nonlinear photonic crystal fiber for supercontinuum generation at 1.55h. <b>2012</b> , 44, 1261-1269	15
1412	Tailoring supercontinuum generation using highly nonlinear photonic crystal fiber. <b>2012</b> , 44, 1889-1896	13
1411	Simultaneous Measurement of Strain and Temperature by Using a Micro-Tapered Fiber Grating. <b>2012</b> , 30, 1156-1160	62
1410	Preparation and characterization of a large mode area liquid-filled photonic crystal fiber: transition from isolated to coupled spatial modes. <b>2012</b> , 106, 521-527	14
1409	Optical properties of palladium nanoparticles under exposure of hydrogen and inert gas prepared by dewetting synthesis of thin-sputtered layers. <b>2013</b> , 15, 1	13
1408	A reflective photonic crystal fiber temperature sensor probe based on infiltration with liquid mixtures. <b>2013</b> , 13, 7916-25	22
1407	Design of turn-around-point long-period gratings in a photonic crystal fiber for refractometry of gases. <b>2013</b> , 182, 16-24	22
1406	High-sensitivity high-resolution refractometry with twin turn-around-point long-period gratings in a photonic crystal fiber. <b>2013</b> ,	

1405 Two octave spanning supercontinuum generation in hexagonal spiral photonic crystal fiber. **2013**,

1404	Positive and negative focal shifts of an apertured supercontinuum laser with rectangular spectrum. <b>2013</b> , 298-299, 34-36	3
1403	Improvement of light-harvesting efficiency in dye-sensitized solar cells using silica beads embedded in a TiO2nanoporous structure. <b>2013</b> , 46, 024006	19
1402	Temperature dependent optical properties of silver from spectroscopic ellipsometry and density functional theory calculations. <b>2013</b> , 114, 033515	21
1401	Optical Fiber Micro-Taper with Circular Symmetric Gold Coating for Sensor Applications Based on Surface Plasmon Resonance. <b>2013</b> , 8, 545-554	21
1400	Second-order nonlinear optical susceptibilities of nonelectrically poled DR1-PMMA guest-host polymers. <b>2013</b> , 117, 14857-64	9
1399	Antireflective coatings based on amorphous submicron silica particles for silicate glass: Preparation, morphology of surface, optical properties. <b>2013</b> , 8, 756-764	О
1398	Fiber-based pulse stretcher for narrowband terahertz pulse generation with a chirped-pulse beating method. <b>2013</b> , 103, 151118	2
1397	Photocontrolled adsorption of polyelectrolyte molecules on a silicon substrate. <b>2013</b> , 29, 16058-65	14
1396	A precise method for analyzing Bessel-like beams generated by broadband waves. <b>2013</b> , 52, 87-90	5
1395	Temperature recovery of opaque bodies by thermal radiation spectrum: the use of relative emissivity to select the optimal spectral range. <b>2013</b> , 20, 631-646	6
1394	Detector and dispersive delay calibration issues in broadband 2D electronic spectroscopy. <b>2013</b> , 30, 1770	20
1393	Highly nonlinear layered spiral microstructured optical fiber. <b>2013</b> , 11, 226-233	3
1392	Design Optimization of Transmission of Si/SiO2 and Ge/SiO2 Multilayer Coatings. <b>2013</b> , 87-90	
1391	Spectral and angular light-scattering from silica fractal aggregates. <b>2013</b> , 131, 160-165	9
1390	Dispersion compensation photonic crystal fibers with ultra-high dispersion coefficient and extremely low loss. <b>2013</b> ,	
1389	Temperature changes of the optical properties of (SiO2) n , (GaAs) m , and (SiO2) n (GaAs) m nanoparticles: Computer experiment. <b>2013</b> , 51, 97-105	6
1388	Quantum beats in the polarization response of a dielectric to intense few-cycle laser pulses. <b>2013</b> , 15, 013006	46

1387	Characterization of LPGs via Correlation Analysis of an Analytical Solution With Observed Transmission Spectra. <b>2013</b> , 31, 3014-3020	2
1386	Dispersion-flattened supercontinuum light source design at center wavelength for high resolution optical coherence tomography in ophthalmology. <b>2013</b> , 48, 235-240	3
1385	Ultra high sensitivity chemical photonic sensing by Machilehnder interferometer enhanced Vernier-effect. <b>2013</b> , 176, 994-1007	50
1384	Arsenic chalcogenide filled photonic crystal fibers. <b>2013</b> , 377, 231-235	2
1383	Evaluation of optical properties and thermal performances of different greenhouse covering materials. <b>2013</b> , 96, 21-32	34
1382	MgO reflectance data for Monte Carlo simulation of LaBr3:Ce scintillation crystals. <b>2013</b> , 701, 44-53	1
1381	Study of cavitation phenomenon using different fuels in a transparent nozzle by hydraulic characterization and visualization. <b>2013</b> , 44, 235-244	57
1380	Effect of Annealing on the Optical Properties of GaN Films Grown by Pulsed Laser Deposition. <b>2013</b> , 29, 752-756	9
1379	Introduction. <b>2013</b> , 1-25	2
1378	Effect of SiO2 coating in bolometric Ge light detectors for rare event searches. <b>2013</b> , 709, 22-28	13
1377	Broadband wide-angle dispersion measurements: instrumental setup, alignment, and pitfalls. <b>2013</b> , 84, 033107	5
1376	Self-guided propagation of ultrashort laser pulses in the anomalous dispersion region of transparent solids: a new regime of filamentation. <b>2013</b> , 110, 115003	89
1375	Blueshifted continuum peaks from filamentation in the anomalous dispersion regime. 2013, 87,	46
1374	Adjustable structural, optical and dielectric characteristics in solgel PMMABiO2 hybrid films. <b>2013</b> , 362, 124-135	54
1373	Coupling of sunlight into optical fibres and spectral dependence for solar energy applications. <b>2013</b> , 93, 235-243	26
1372	Optical dispersion in synthetic opal matrices filled with europium-oxide-doped silica sols. <b>2013</b> , 49, 685-691	11
1371	Gas-dependent bandgap and electrical conductivity of Cu2O thin films. 2013, 108, 230-234	30
1370	Generation of Step-Tunable Microwave Signal Using a Multiwavelength Brillouin Fiber Laser. <b>2013</b> , 25, 220-223	13

1369	Rapid and Sensitive Polarization Measurement for Characterizing Protein Adsorption at the Solid[liquid Interface. <b>2013</b> , 117, 1796-1803	7
1368	Temperature stabilization of Yb-doped fiber mode-locked oscillator for long-term stable passive two-color synchronization. <b>2013</b> ,	
1367	Optical absorption analysis and optimization of gold nanoshells. <b>2013</b> , 52, 1325-9	27
1366	Theoretical model of the influence of oxide overlayer thickness on the performance of a surface plasmon fibre-optic sensor. <b>2013</b> , 24, 025105	20
1365	Temperature effects in chromatic confocal distance sensors. 2013,	2
1364	A subwavelength core microstructured optical fiber temperature sensor based on infiltration with chloroform. <b>2013</b> ,	
1363	Absorption efficiency enhancement in inorganic and organic thin film solar cells via plasmonic honeycomb nanoantenna arrays. <b>2013</b> , 38, 3119-22	6
1362	How long wavelengths can one extract from silica-core fibers?. <b>2013</b> , 38, 4518-21	30
1361	Maintaining a stationary laser footprint during angular scan in internal-reflection experiments. <b>2013</b> , 52, 7669-74	7
1360	All-optical tunable slow light achievement in photonic crystal coupled-cavity waveguides. <b>2013</b> , 52, 6497-505	16
1360 1359	All-optical tunable slow light achievement in photonic crystal coupled-cavity waveguides. <b>2013</b> , 52, 6497-505  Effect of number density on optimal design of gold nanoshells for plasmonic photothermal therapy. <b>2013</b> , 4, 15-31	<ul><li>16</li><li>39</li></ul>
1359	Effect of number density on optimal design of gold nanoshells for plasmonic photothermal	
1359	Effect of number density on optimal design of gold nanoshells for plasmonic photothermal therapy. <b>2013</b> , 4, 15-31	39
1359 1358	Effect of number density on optimal design of gold nanoshells for plasmonic photothermal therapy. <b>2013</b> , 4, 15-31  Measurement of the Raman gain coefficient via inverse Raman scattering. <b>2013</b> , 30, 2930  Capturing a reflective cross-sectional image of an optical fiber with partially coherent laser light to	39
1359 1358 1357	Effect of number density on optimal design of gold nanoshells for plasmonic photothermal therapy. 2013, 4, 15-31  Measurement of the Raman gain coefficient via inverse Raman scattering. 2013, 30, 2930  Capturing a reflective cross-sectional image of an optical fiber with partially coherent laser light to measure the refractive index profile of a multimode optical fiber. 2013, 21, 2408-13	<ul><li>39</li><li>4</li><li>6</li></ul>
1359 1358 1357 1356	Effect of number density on optimal design of gold nanoshells for plasmonic photothermal therapy. 2013, 4, 15-31  Measurement of the Raman gain coefficient via inverse Raman scattering. 2013, 30, 2930  Capturing a reflective cross-sectional image of an optical fiber with partially coherent laser light to measure the refractive index profile of a multimode optical fiber. 2013, 21, 2408-13  The fiber fusefrom a curious effect to a critical issue: a 25th year retrospective. 2013, 21, 6422-41	<ul><li>39</li><li>4</li><li>6</li><li>60</li></ul>
1359 1358 1357 1356 1355	Effect of number density on optimal design of gold nanoshells for plasmonic photothermal therapy. 2013, 4, 15-31  Measurement of the Raman gain coefficient via inverse Raman scattering. 2013, 30, 2930  Capturing a reflective cross-sectional image of an optical fiber with partially coherent laser light to measure the refractive index profile of a multimode optical fiber. 2013, 21, 2408-13  The fiber fuse—from a curious effect to a critical issue: a 25th year retrospective. 2013, 21, 6422-41  Optical control of scattering, absorption and lineshape in nanoparticles. 2013, 21, 20322-33  Cylindrical beam propagation modelling of perturbed whispering-gallery mode microcavities. 2013,	<ul><li>39</li><li>4</li><li>6</li><li>60</li><li>8</li></ul>

1351	Twin-resonance-coupling and high sensitivity sensing characteristics of a selectively fluid-filled microstructured optical fiber. <b>2013</b> , 21, 30911-7	49
1350	Simulated vibrational sum frequency generation from a multilayer thin film system with two active interfaces. <b>2013</b> , 138, 154708	31
1349	Insights in the light trapping effect in silicon solar cells with backside diffraction gratings. 2013, 3, 034595	10
1348	Plasmon focusing in short gold sphere nanochains for surface-enhanced Raman scattering. <b>2013</b> , 52, 8809-16	6
1347	Cosine error for a class of hyperspectral irradiance sensors. <b>2013</b> , 50, 187-199	13
1346	Center Wavelength Adoption Techniques for Supercontinuum Generating Highly Nonlinear Noncircular Core Photonic Crystal Fiber. <b>2013</b> , 52, 052502	5
1345	Fine-tuning of whispering gallery modes in on-chip silica microdisk resonators within a full spectral range. <b>2013</b> , 102, 041104	13
1344	Optical constants and spatial uniformity of thermally grown oxide layer of custom, induced-junction, silicon photodiodes for a predictable quantum efficient detector. <b>2013</b> , 113, 243509	6
1343	Kelvin force microscopy characterization of charging effect in thin a-SiOxNy:H layers deposited in pulsed plasma enhanced chemical vapor deposition process by tuning the Silicon-environment. <b>2013</b> , 113, 204102	20
1342	KrF- and ArF-excimer-laser-induced absorption in silica glasses produced by melting synthetic silica powder. <b>2013</b> , 114, 014902	7
1341	Refractive index determination of SiO_2 layer in the UV/Vis/NIR range: spectrophotometric reverse engineering on single and bi-layer designs. <b>2013</b> , 8,	128
1340	The Use of Index-Matched Beads in Optical Particle Counters. <b>2014</b> , 119, 674-82	15
1339	Fabrication and applications of periodic nanostructures formed by interfering femtosecond laser proccessing. <b>2014</b> ,	
1338	Enhanced nanoparticle detection with liquid droplet resonators. <b>2014</b> , 223, 1971-1988	11
1337	Temperature dependence of the refractive index of optical fibers. <b>2014</b> , 23, 034201	8
1336	Light source design using Kagome-lattice hollow core photonic crystal fibers. <b>2014</b> , 21, 490-495	11
1335	Reactive HiPIMS deposition of SiO2/Ta2O5 optical interference filters. <b>2014</b> , 116, 213302	34
1334	Polymer waveguide Fabry-Perot resonator for high-frequency ultrasound detection. <b>2014</b> , 61, 2132-8	10

1333	Temperature sensing in seawater based on microfiber knot resonator. <b>2014</b> , 14, 18515-25	54
1332	Color high resolution full-field optical coherence microscopy for contrast-enhanced imaging. 2014,	
1331	The GRAVITY metrology system: modeling a metrology in optical fibers. <b>2014</b> ,	O
1330	Design of an Optical Trapping Device Based on an Ultra-High Q/V Resonant Structure. <b>2014</b> , 6, 1-16	24
1329	Near-field analysis of CdSe quantum dot conjugated core-shell nanoparticle. 2014,	
1328	On the light trapping mechanism in silicon solar cells with backside diffraction gratings. <b>2014</b> ,	
1327	Damage-free single-mode transmission of deep-UV light in hollow-core PCF. <b>2014</b> , 22, 15388-96	35
1326	Surface scattering of core-shell particles with anisotropic shell. <b>2014</b> , 31, 162-71	4
1325	Second-harmonic generation enhancement in the presence of Tamm plasmon-polaritons. <b>2014</b> , 39, 6895-8	24
1324	Three-band, 1.9-th axial resolution full-field optical coherence microscopy over a 530-1700 nm wavelength range using a single camera. <b>2014</b> , 39, 1374-7	6
1323	Parametric formulation of the dielectric function of palladium and palladium hydride thin films. <b>2014</b> , 53, 5294-306	8
1322	Long-term stable passive synchronization between two-color mode-locked lasers with the aid of temperature stabilization. <b>2014</b> , 22, 4091-7	12
1321	Liquid core photonic crystal fiber with low-refractive-index liquids for optofluidic applications. <b>2014</b> , 22, 17320-30	19
1320	Flexible tool for simulating the bulk optical properties of polydisperse spherical particles in an absorbing host: experimental validation. <b>2014</b> , 22, 20223-38	22
1319	Thin sample refractive index by transmission spectroscopy. <b>2014</b> , 22, 28537-52	11
1318	Interferometric measurement of the temperature coefficient of the refractive index dn/dT and the coefficient of thermal expansion of Pr:YLF laser crystals. <b>2014</b> , 22, 30683-96	4
1317	Variations in optical coherence tomography resolution and uniformity: a multi-system performance comparison. <b>2014</b> , 5, 2066-81	15
1316	Liquid crystal assisted optical fibres. <b>2014</b> , 22, 262-73	16

1315	A semi-analytical model for the approximation of plasmonic bands in arrays of metal wires in photonic crystal fibers. <b>2014</b> , 22, 11741-53	10
1314	Generalized full-vector multi-mode matching analysis of whispering gallery microcavities. <b>2014</b> , 22, 13507-14	12
1313	Integrated polarizers based on tapered highly birefringent photonic crystal fibers. <b>2014</b> , 22, 17769-75	3
1312	Microfluidic assistant beat-frequency interferometer based on a single-hole-infiltrated dual-mode microstructured optical fiber. <b>2014</b> , 22, 25224-32	3
1311	Polarization splitter based on dual-core photonic crystal fiber. <b>2014</b> , 22, 30461-6	60
1310	Extinction properties of ultrapure water down to deep ultraviolet wavelengths. <b>2014</b> , 4, 1932	12
1309	General approach for the sensitivity analysis and optimization of integrated optical evanescent-wave sensors. <b>2014</b> , 31, 851	5
1308	Characterization of coplanar poled electro optic polymer films for Si-photonic devices with multiphoton microscopy. <b>2014</b> , 104, 161109	2
1307	Group Delay in THz Spectroscopy with Ultra-Wideband Log-Spiral Antennae. <b>2014</b> , 35, 918-931	9
1306	Elimination of bandwidth effect in attenuation measurement with picosecond ultrasonics. <b>2014</b> , 53, 086602	3
1305	Control of Microphase Separation of Polystyrene-Silica Nanocomposites by Using Perhydropolysilazane and Partially Epoxidized Poly(styrene-block-butadiene-block-styrene). <b>2014</b> , 51, 362-368	1
1304	Ultrashort optical waveguide excitations in uniaxial silica fibers: elastic collision scenarios. <b>2014</b> , 90, 063203	10
1303	Model of a double-sided surface plasmon resonance fiber-optic sensor. <b>2014</b> ,	
1302	Study on dielectric function models for surface plasmon resonance structure. <b>2014</b> , 2014, 503749	14
1301	Efficient phase-matched third harmonic generation from mid-IR to near-IR regions in a double asymmetric plasmonic slot waveguide. <b>2014</b> ,	
1300	Z-scan studies of nonlinear optical properties of colloidal gold nanorods and nanoshells. <b>2014</b> , 9, 093797	5
1299	Optical properties of C-Pd films prepared on silica substrate studied by UV-VIS-NIR spectroscopy. <b>2014</b> ,	1
1298	Analysis of Nanoparticle-Based Surface Plasmon Resonance Fiber Optic Sensor. <b>2014</b> , 605, 131-134	

Analysis of phase interrogation of SPR fiber optic sensors with characteristics tailored by the 1297 application of different metal-dielectric overlays. 2014, Polycrystalline indium films in the percolation threshold regime: time correlation between electric 1296 2 conduction and optical properties with film morphology. 2014, 1, 016302 An investigation into second harmonic generation by Si-rich SiNxthin films deposited by RF 1295 24 sputtering over a wide range of Si concentrations. 2014, 47, 215101 Exploration of higher-order mode coupling in long-period gratings for sensitive monitoring of 1294 polyelectrolyte self-assembly at nanoscale. 2014, Stack of PECVD silicon nitride nano-films on optical fiber end-face for refractive index sensing. 1293 1 2014. Short-length fiber laser oscillation in 4-mm Nd-doped silica fiber fabricated by zeolite method. 10 2014, 328, 121-123 Thermal and optical properties of hyperbranched fluorinated polyimide/mesoporous SiO2 1291 22 nanocomposites exhibiting high transparency and reduced thermo-optical coefficients. 2014, 55, 2848-2855 1290 A transparent aqueous-saturated sand surrogate for use in physical modeling. 2014, 9, 187-206 60 Effect of 3-Aminopropyltriethoxysilane on polycarbonate based waterborne polyurethane 1289 31 transparent coatings. 2014, 77, 1073-1078 1288 Europium superluminescence in optically transparent photonic crystals. 2014, 50, 150-157 4 Theoretical analysis of transverse mode conversion using transient long-period gratings induced by 1287 9 ultrashort pulses in optical fibers. 2014, 115, 225-235 Nonlinear refractive indices of nonlinear liquids: wavelength dependence and influence of retarded 1286 26 response. **2014**, 117, 803-816 PMMABiO2 hybrid films as gate dielectric for ZnO based thin-film transistors. 2014, 146, 380-388 35 Enhanced Faraday rotation via resonant tunnelling in tri-layers containing magneto-optical metals. 12 2014, 47, 025002 Second-order nonlinear optical susceptibilities in nonelectrically poled guestBost polymers with 1283 2 tricyanofuran chromophores. **2014**, 53, 01AD09 Synthesis and evaluation of thermoplastic polyurethanes as thermo-optic waveguide materials. 1282 2014, 46, 349-354 1281 Transformation of Optical Radiation by Two-Layered Nanoparticles with Metallic Shells. 2014, 81, 862-865 1280 CFD characterization of monolithic reactors for kinetic studies. 2014, 92, 1570-1578

Demonstration of Color Separation with 2IKDP Wedge in High Power Laser Facilities. **2014**, 31, 014203

Oxidation of copper nanoparticles in water monitored in situ by localized surface plasmon resonance spectroscopy. <b>2014</b> , 4, 20659	10
Research on the polarization and temperature characteristics of subwavelength aluminum gratings. <b>2014</b> , 16, 105711	3
1276 Light source design using hollow core photonic crystal fibers. <b>2014</b> ,	O
Shell-thickness-dependent nonlinear optical properties of colloidal gold nanoshells. <b>2014</b> , 2, 7239-7246	16
Plasmonic dye-sensitized solar cells incorporated with Au-TiOIhanostructures with tailored configurations. <b>2014</b> , 6, 1823-32	94
Highly transparent, bright green, solgel-derived monolithic silica-(Tb,Ce)PO4 glass-ceramic phosphors. <b>2014</b> , 4, 26692-26696	8
1272 Reflection spectra of synthetic opal at liquid-nitrogen temperature. <b>2014</b> , 50, 1007-1011	1
1271 Ultrafast Plasmonics on Gold Nanowires: Confinement, Dispersion, and Pulse Propagation. <b>2014</b> , 1, 1173	3-1180 12
Magnetoliposomes based on nickel/silica core/shell nanoparticles: Synthesis and characterization. <b>2014</b> , 148, 978-987	10
1269 Hybrid photonic-plasmonic microcavities for Q/V ratio enhancement. <b>2014</b> ,	1
1268 Self-assembly of long chain fatty acids: effect of a methyl branch. <b>2014</b> , 16, 17869-82	7
Quantum imaging with undetected photons. <b>2014</b> , 512, 409-12	292
1266 Underwater-transparent nanodendritic coatings for directly monitoring cancer cells. <b>2014</b> , 3, 332-7	30
Plasmonic bar-coupled dots-on-pillar cavity antenna with dual resonances for infrared absorption and sensing: performance and nanoimprint fabrication. <b>2014</b> , 8, 2618-24	25
1264 Exciton binding energy and nonhydrogenic Rydberg series in monolayer WS(2). <b>2014</b> , 113, 076802	1358
Metalpolymer nano-composite films with ordered vertically aligned metal cylinders for sub-wavelength imaging. <b>2014</b> , 116, 893-900	3
Improvements in filtered Rayleigh scattering measurements using FabryPerot etalons for spectral filtering of pulsed, 532-nm Nd:YAG output. <b>2014</b> , 116, 681-698	17

1261	Computer study of the Raman spectra and infrared optical properties of gallium nitride and gallium arsenic nanoparticles with SiO2 core and shell. <b>2014</b> , 16, 1	2
1260	Filamentation of a phase-modulated pulse under conditions of normal, anomalous and zero group velocity dispersion. <b>2014</b> , 44, 577-584	3
1259	Disentangling electrons and lattice nonlinear optical response in metal-dielectric Bragg filters. <b>2014</b> , 89,	12
1258	Radiation characteristics and optical properties of filamentous cyanobacterium Anabaena cylindrica. <b>2014</b> , 31, 836-45	13
1257	Analysis of Phase Interrogated SPR Fiber Optic Sensors With Bimetallic Layers. <b>2014</b> , 14, 3662-3668	25
1256	Experimental demonstration of sharp Fano resonance in optical metamaterials composed of asymmetric double bars. <b>2014</b> , 39, 4057-60	44
1255	Analytical modeling of the radial pn junction nanowire solar cells. <b>2014</b> , 116, 024308	13
1254	Quantitative measurement of fluorescence brightness of single molecules. <b>2014</b> , 2, 035003	17
1253	Design of a new photonic/plasmonic microcavity allowing a strong light-matter interaction. <b>2014</b> ,	3
1252	The role of microstructure on the optical performance of neutron irradiated dielectric mirrors. <b>2014</b> , 445, 281-290	9
1251	Structural and optical properties of dysprosium oxide thin films. <b>2014</b> , 591, 234-239	4
1250	Optimal design of gold nanoshells for optical imaging and photothermal therapy. <b>2014</b> , 125, 3702-3706	7
1249	Monitoring layer-by-layer assembly of polyelectrolyte multi-layers using high-order cladding mode in long-period fiber gratings. <b>2014</b> , 196, 475-479	9
1248	Enhanced ZnTe infiltration in porous silicon by Isothermal Close Space Sublimation. <b>2014</b> , 188, 93-98	3
1247	Nanostructured antireflective bilayers: Optical design and preparation. <b>2014</b> , 145, 176-185	1
1246	Optimal dimensions of gold nanoshells for light backscattering and absorption based applications. <b>2014</b> , 146, 468-474	7
1245	Suppression of stimulated Brillouin scattering in integrated chalcogenide waveguides. <b>2014</b> , 31, 178	1
1244	Recovery of permittivity and depth from near-field data as a step toward infrared nanotomography. <b>2014</b> , 8, 6911-21	73

1243	Large area, low cost anti-reflective coating for solar glasses. <b>2014</b> , 128, 283-288	35
1242	Cosolvent-Free Sol <b>G</b> el Synthesis and Optical Characterization of Silica Glasses Containing LaF3 and (La,Er)F3 Nanocrystals. <b>2014</b> , 87, 765-772	3
1241	Light bullets from Mid-IR femtosecond filament in air. <b>2014</b> , 541, 012071	5
1240	Noble-Metal-Free Sunlight Harvesting Meta-surface for Water Evaporation. 2014,	
1239	Nonlinear Group IV photonics based on silicon and germanium: from near-infrared to mid-infrared. <b>2014</b> , 3, 247-268	138
1238	Influence of Refractive Index in Particle Sizing by Light Extinction Spectrum. <b>2015</b> , 102, 315-321	1
1237	Optimizing Plasmonically Enhanced Upconversion. <b>2015</b> , 77, 478-486	7
1236	A plastic scintillator-based activity monitor for tritiated water in the GBq/Irange. <b>2015</b> , 798, 24-29	4
1235	Metal-dielectric-metal based narrow band absorber for sensing applications. <b>2015</b> , 23, 29842-7	102
1234	Quantitative characterization of energy absorption in femtosecond laser micro-modification of fused silica. <b>2015</b> , 23, 32541-7	10
1233	Transmission optical coherence tomography based measurement of optical material properties. <b>2015</b> , 23, 33550-63	4
1232	Resonant isotropic optical magnetism of plasmonic nanoclusters in visible light. <b>2015</b> , 92,	34
1231	Generation and excitation of different orbital angular momentum states in a tunable microstructure optical fiber. <b>2015</b> , 23, 33741-52	17
1230	Observation of excitonic resonances in the second harmonic spectrum of MoS2. <b>2015</b> , 92,	39
1229	Chiral cavity ring down polarimetry: Chirality and magnetometry measurements using signal reversals. <b>2015</b> , 143, 104202	27
1228	Sub-10 nm near-field localization by plasmonic metal nanoaperture arrays with ultrashort light pulses. <b>2015</b> , 5, 17584	7
1227	The dynamics of femtosecond pulsed laser removal of 20 nm Ni films from an interface. <b>2015</b> , 107, 124101	11
1226	Advanced lab on Fresnel equations. <b>2015</b> , 83, 935-941	3

1225	Enhanced quality factor of Fano resonance in optical metamaterials by manipulating configuration of unit cells. <b>2015</b> , 107, 211108	21
1224	Temperature behavior of sound velocity of fluorine-doped vitreous silica thin films studied by picosecond ultrasonics. <b>2015</b> , 118, 014307	10
1223	Scattering suppression in epsilon-near-zero plasmonic fractal shells. <b>2015</b> , 5, 2491	1
1222	Deriving polarization properties of desert-reflected solar spectra with PARASOL data. <b>2015</b> , 15, 7725-7734	7
1221	Enhancement in the excitonic spontaneous emission rates for Si nanocrystal multi-layers covered with thin films of Au, Ag, and Al. <b>2015</b> , 26, 435701	
1220	Supercontinuum generation in bandgap engineered, back-end CMOS compatible silicon rich nitride waveguides. <b>2015</b> , 9, 498-506	65
1219	Chemical-assisted femtosecond laser writing of optical resonator arrays. <b>2015</b> , 9, 656-665	6
1218	Pattern formation on silicon by laser-initiated liquid-assisted colloidal lithography. <b>2015</b> , 26, 455303	5
1217	Visibility of atomically-thin layered materials buried in silicon dioxide. <b>2015</b> , 26, 455701	5
1216	Supercontinuum Generation With Photonic Crystal Fibers and Its Application in Nano-imaging. <b>2015</b>	2
1215	Fabrication of anti-reflection coating layers for silicon solar cells by liquid phase deposition. <b>2015</b> , 14, 279-290	О
1214	Design Procedure and Fabrication of Reproducible Silicon Vernier Devices for High-Performance Refractive Index Sensing. <b>2015</b> , 15, 13548-67	9
1213	Up-conversion enhancement in Er3+ doped TiO2 through plasmonic coupling: Experiments and finite-element modeling. <b>2015</b> , 106, 053101	17
1212	Battling absorptive losses by plasmon Exciton coupling in multimeric nanostructures. 2015, 5, 53245-53254	12
1211	Introduction and Background Information. <b>2015</b> , 1-9	
1210	Development of a deep-sea laser-induced breakdown spectrometer for in situ multi-element chemical analysis. <b>2015</b> , 95, 20-36	108
1209	Control of the average light transmission in one-dimensional photonic structures by tuning the random layer thickness distribution. <b>2015</b> , 46, 450-453	8
1208	High Resolution NIR TFBG-Assisted Biochemical Sensors. <b>2015</b> , 33, 3363-3373	31

1207 Optimisation of polymer optical fibre based interferometric sensors. 2015,

1206	Design of single mode single polarization large mode area photonic crystal fiber. <b>2015</b> ,	
1205	Third-harmonic generation susceptibility spectroscopy in free fatty acids. <b>2015</b> , 20, 095013	8
1204	Design of SiOx slab optical waveguides. <b>2015</b> ,	
1203	Integrated liquid-filled directional coupler for temperature sensing. 2015,	
1202	Phase interrogated plasmonic optical fiber optrode with bimetallic layers. <b>2015</b> ,	
1201	Magnetic response at visible and near-infrared frequencies from black phosphorus sheet arrays. <b>2015</b> , 23, 30667-80	4
1200	Validation of quantitative attenuation and backscattering coefficient measurements by optical coherence tomography in the concentration-dependent and multiple scattering regime. <b>2015</b> , 20, 121314	45
1199	Real-time measurement of temperature variation during nanosecond pulsed-laser-induced contamination deposition. <b>2015</b> , 54, 10579-85	4
1198	Bulk damage and absorption in fused silica due to high-power laser applications. <b>2015</b> ,	4
1197	Nonlinear photoluminescence spectrum of single gold nanostructures. <b>2015</b> , 9, 894-900	40
1196	Band gap splitting and average transmission lowering in ordered and disordered one-dimensional photonic structures composed by more than two materials with the same optical thickness. <b>2015</b> , 338, 523-527	11
1195	Efficient phase-matched third harmonic generation in a metal-clad plasmonic double-slot waveguide. <b>2015</b> , 17, 025506	6
1194	Temperature control of light transmission using mixed system of silica hollow particles with nanoparticle shell and organic components. <b>2015</b> , 7, 1107-13	3
1193	Wavelength-Tunable Dispersion Compensating Photonic Crystal Fibers Suitable for Conventional/Coarse Wavelength Division Multiplexing Systems. <b>2015</b> , 33, 2240-2245	11
1192	Implications of sample aging on the formation of internally etched silica coated gold nanoparticles. <b>2015</b> , 5, 3774-3780	9
1191	Design optimization of Si optical window for 4.2 h wavelength. <b>2015</b> , 118, 923-929	
1190	Theoretical Study of Phase-Interrogated Surface Plasmon Resonance Based on Optical Fiber Sensors with Metallic and Oxide Layers. <b>2015</b> , 10, 979-987	10

## (2015-2015)

1189	A robust smart window: reversibly switching from high transparency to angle-independent structural color display. <b>2015</b> , 27, 2489-95	292
1188	Surface Plasmon Resonance Sensors. <b>2015</b> ,	10
1187	Backscattering Properties of Gold Nanoshells: Quantitative Analysis and Optimization for Biological Imaging. <b>2015</b> , 102, 1511-1519	5
1186	One-Dimensional Chirality: Strong Optical Activity in Epsilon-Near-Zero Metamaterials. <b>2015</b> , 115, 057401	36
1185	Optimizing magneto-optical effects in the ferromagnetic semiconductor GaMnAs. 2015, 395, 340-344	10
1184	Focal switch of broadband laser in a dispersion dual-focus system. <b>2015</b> , 352, 14-18	1
1183	Opal-matrix nanocomposites containing metallic nanoparticles. <b>2015</b> , 51, 840-847	O
1182	Intensity Distributions of a Supercontinuum Laser in an Apertured Dispersion Lens. <b>2015</b> , 32, 034201	
1181	Theoretical investigation of a dispersion compensating photonic crystal fiber with ultra-high dispersion coefficient and extremely low confinement loss. <b>2015</b> , 16, 1-8	14
1180	Electrostriction enhancement in metamaterials. <b>2015</b> , 91,	16
1179	Modeling of Solar Cell Efficiency Improvement Using Pyramid Grating in Single Junction Silicon Solar Cell. <b>2015</b> , 61-67	4
1178	Quantum state tomography of orbital angular momentum photonic qubits via a projection-based technique. <b>2015</b> , 17, 033037	14
1177	Realization of Optical Power Scale Based on Cryogenic Radiometry and Trap Detectors. <b>2015</b> , 64, 1702-1708	5
1176	Nonlinear Interference and Tailorable Third-Harmonic Generation from Dielectric Oligomers. <b>2015</b> , 2, 578-582	99
1175	Metal oxide one dimensional photonic crystals made by RF sputtering and spin coating. <b>2015</b> , 41, 8655-8659	21
1174	Sequestration of cerium(III) bromide into mesoporous silica. <b>2015</b> , 211, 158-161	1
1173	Analysis of the light trapping effect on the performance of silicon-based solar cells: absorption enhancement. <b>2015</b> , 54, 3591	34
1172	Second-harmonic frequency-resolved optical gating covering two and a half optical octaves using a single spectrometer. <b>2015</b> , 119, 339-345	4

Quality-factor enhancement of Fano resonance in asymmetric-double-bar metamaterials by alternately arranging inversed unit cells in the optical region. **2015**,

1170	Fiber-optic refractive index sensor based on surface plasmon resonance. <b>2015</b> ,	
1169	Dielectric Resonator Nanoantenna Coupled to Metallic Coplanar Waveguide. 2015, 7, 1-7	7
1168	Realizing high photovoltaic efficiency with parallel multijunction solar cells based on spectrum-splitting and -concentrating diffractive optical element. <b>2015</b> , 24, 054201	O
1167	Optical isolation via one-dimensional magneto-photonic crystals containing nonlinear defect layer. <b>2015</b> , 352, 91-95	6
1166	Bio-Inspired Structural Colors Produced via Self-Assembly of Synthetic Melanin Nanoparticles. <b>2015</b> , 9, 5454-60	200
1165	Spatially Mapping Energy Transfer from Single Plasmonic Particles to Semiconductor Substrates via STEM/EELS. <b>2015</b> , 15, 3465-71	66
1164	Quantitative phase microscopy via optimized inversion of the phase optical transfer function. <b>2015</b> , 54, 8566-79	27
1163	Dielectric-loaded surface plasmon polariton crossing waveguides using multimode interference. <b>2015</b> , 40, 2269-72	10
1162	Dispersion compensation in three-photon fluorescence microscopy at 1,700 nm. <b>2015</b> , 6, 1392-7	30
1161	Fabrication and characterization of periodically patterned silica fiber structures for enhanced second-order nonlinearity. <b>2015</b> , 23, 8113-27	7
1160	Towards integration of a liquid-filled fiber capillary for supercontinuum generation in the 1.2-2.4 fb range. <b>2015</b> , 23, 8281-9	47
1159	High birefringence photonic crystal fiber with high nonlinearity and low confinement loss. <b>2015</b> , 23, 8329-37	89
1158	Nanoslit-microcavity-based narrow band absorber for sensing applications. <b>2015</b> , 23, 20715-20	104
1157	Enhanced transmission modulation based on dielectric metasurfaces loaded with graphene. <b>2015</b> , 23, 23787-97	71
1156	Direct observation of patterned self-assembled monolayers and bilayers on silica-on-silicon surfaces. <b>2015</b> , 5, 149	1
1155	Optimising apodized grating couplers in a pure SOI platform to -0.5 dB coupling efficiency. <b>2015</b> , 23, 16289-304	58
1154	Velocity of the mass center motion and duration evolution of pulses of a small number of oscillations in dispersive optical media. <b>2015</b> , 119, 485-496	2

1153	. <b>2015</b> , 33, 4478-4487	2
1152	Facile solvothermal synthesis of high refractive index ZrO2 spheres: estimation of the enhanced light extraction efficiency. <b>2015</b> , 5, 81915-81919	8
1151	Design of a family of ring-core fibers for OAM transmission studies. <b>2015</b> , 23, 10553-63	95
1150	Curvature-induced geometric momenta: the origin of waveguide dispersion of surface plasmons on metallic wires. <b>2015</b> , 23, 12174-88	26
1149	Full loss compensation in hybrid plasmonic waveguides under electrical pumping. <b>2015</b> , 23, 19358-75	18
1148	Determination of the effective index and thickness of biomolecular layer by Fano resonances in gold nanogrid array. <b>2015</b> , 23, 21596-606	9
1147	Lens-free inline holographic microscopy with numerical correction of layers with different refractive index. <b>2015</b> , 40, 752-5	2
1146	Highly Sensitive Temperature Sensor Based on a Polymer-Coated Microfiber Interferometer. <b>2015</b> , 27, 2591-2594	47
1145	Measurement of Lateral and Interfacial Thermal Conductivity of Single- and Bilayer MoS2 and MoSe2 Using Refined Optothermal Raman Technique. <b>2015</b> , 7, 25923-9	195
1144	Fundamentals of Optical Fiber Sensing Schemes Based on Coherent Optical Time Domain Reflectometry: Signal Model Under Static Fiber Conditions. <b>2015</b> , 33, 3660-3671	59
1143	Extraordinary reflection and transmission with direction dependent wavelength selectivity based on parity-time-symmetric multilayers. <b>2015</b> , 117, 023104	28
1142	Experimental evidence for an optical interference model for vibrational sum frequency generation on multilayer organic thin film systems. I. Electric dipole approximation. <b>2015</b> , 142, 024703	16
1141	Optical and transport properties of dense liquid silica. <b>2015</b> , 22, 062706	19
1140	Multiple-input multiple-output based high density on-chip optical interconnect. 2015,	
1139	Dispersion Compensation in Three-Photon Fluorescence Microscopy at 1,700 nm for in vivo Imaging. <b>2015</b> ,	
1138	Theoretical and experimental investigations on the temperature dependence of the refractive index of amorphous silica. <b>2015</b> , 429, 198-201	10
1137	Antiresonant guiding in a poly(methyl-methacrylate) hollow-core optical fiber. 2015, 17, 105603	2
1136	On-chip phase measurement for microparticles trapped on a waveguide. <b>2015</b> , 15, 3918-24	7

1135	Visible supercontinuum radiation of light bullets in the femtosecond filamentation of IR pulses in fused silica. <b>2015</b> , 45, 401-407	19
1134	Effects of sample dispersion on ultrafast laser focusing. <b>2015</b> , 32, 1272	6
1133	Protein biosensing with fluorescent microcapillaries. <b>2015</b> , 23, 2577-90	26
1132	Comparison of microfacet BRDF model elements to diffraction BRDF model elements. 2015,	2
1131	Aerogel Cherenkov detectors in colliding beam experiments. <b>2015</b> , 58, 503-511	11
1130	Photonic band gap in 1D multilayers made by alternating SiO2 or PMMA with MoS2 or WS2 monolayers. <b>2015</b> , 48, 267-270	7
1129	Shape effects of GeSbTe nanodots on the near-field interaction with a silver triangle antenna. <b>2015</b> , 54, 042002	
1128		2
1127	Deep-ultraviolet transparent monolithic solgel derived silicaREPO4 (RE = Y, Lallu except Pm) glass-ceramics: characterization of the crystal structure and ultraviolet absorption edge, and application to narrow-band UVB phosphors. <b>2015</b> , 3, 9894-9901	14
1126	The quantitative effect of silica nanoparticles on optical properties of thin solid silica UV-cured films. <b>2015</b> , 279, 25-31	4
1125	Highly efficient solid-state distributed feedback dye laser based on polymer-filled nanoporous glass composite excited by a diode-pumped solid-state Nd:LSB microlaser. <b>2015</b> , 54, 7962-72	10
1124	TiO2 Nanoparticle/SiO2 Composite Back Reflector for Solar Cells. <b>2015</b> , 77, 242-247	4
1123	Fabrication of metallic hole array metamaterials with 760nm and 1930nm lattice constant by interfering femtosecond laser processing. <b>2015</b> , 17, 10-14	2
1122	Surface nanostructures for fluorescence probing of supported lipid bilayers on reflective substrates. <b>2015</b> , 7, 18020-4	2
1121	Imaginary rest mass of a photon in a dispersive medium. <b>2015</b> , 126, 5304-5306	11
1120	Novel techniques for high precision refractive index measurements, and application to assessing neutron damage and dose in crystals. <b>2015</b> , 784, 198-201	1
1119	Dispersion properties of liquid crystal core photonic crystal fibers calculated by a multipole method modified for anisotropic inclusions. <b>2015</b> , 338, 123-127	7
1118	A laboratorial prototype of a weight measuring system using optical fiber Bragg grating sensors embedded in silicone rubber. <b>2015</b> , 61, 58-66	12

1117	Monitoring the dominance of higher-order chromatic dispersion with spectral interferometry using the stationary phase point method. <b>2015</b> , 338, 292-299	4
1116	Dual-concentric-core photonic crystal fibers with two layers of outer ring core. <b>2015</b> , 47, 1721-1729	
1115	A Simple Method for the Evaluation of the Pulse Width of an Ultraviolet Femtosecond Laser Used in Two-Photon Ionization Mass Spectrometry. <b>2016</b> , 6, 136	1
1114	Characteristics of Highly Birefringent Photonic Crystal Fiber with Defected Core and Equilateral Pentagon Architecture. <b>2016</b> , 2016, 1-8	5
1113	Black phosphorus-based one-dimensional photonic crystals and microcavities. <b>2016</b> , 55, 9288-9292	8
1112	Effect of Anderson localization on light emission from gold nanoparticle aggregates. <b>2016</b> , 7, 2013-2022	10
1111	The Application of Cryogenic Laser Physics to the Development of High Average Power Ultra-Short Pulse Lasers. <b>2016</b> , 6, 23	14
1110	Vernier-like super resolution with guided correlated photon pairs. <b>2016</b> , 24, 300-7	
1109	Singularimetry of local phase gradients using vortex lattices and in-line holography. <b>2016</b> , 24, 2259-72	3
1108	Thermochromic modulation of surface plasmon polaritons in vanadium dioxide nanocomposites. <b>2016</b> , 24, 17321-31	17
1107	Asymmetric band gap shift in electrically addressed blue phase photonic crystal fibers. <b>2016</b> , 24, 22718-22729	11
1106	Dispersion of nondegenerate nonlinear refraction in semiconductors. <b>2016</b> , 24, 24907-24920	13
1105	Substrate surface patterning by optical near field modulation around colloidal particles immersed in a liquid. <b>2016</b> , 24, 27340-27351	3
1104	In-line optofluidic refractive index sensing in a side-channel photonic crystal fiber. <b>2016</b> , 24, 27674-27682	33
1103	Robust design procedure for dielectric resonator metasurface lens array. <b>2016</b> , 24, 29153-29169	4
1102	Broadband optical waveguide couplers with arbitrary coupling ratios designed using a genetic algorithm. <b>2016</b> , 24, 30547-30561	19
1101	Coupling of nitrogen-vacancy centers in a nanodiamond to a silver nanocube. <b>2016</b> , 6, 3394	9
1100	Tuning the Optoelectronic Properties of ZnO:Al by Addition of Silica for Light Trapping in High-Efficiency Crystalline Si Solar Cells. <b>2016</b> , 3, 1500462	13

1099	An Assessment of the Applicability of Particle Light Scattering Theories to Birefringent Polycrystalline Ceramics. <b>2016</b> , 99, 551-556	7
1098	Soft Surfaces for the Reversible Control of Thin-Film Microstructure and Optical Reflectance. <b>2016</b> , 28, 2595-600	33
1097	Low-Noise 3-D Avalanche Photodiodes. <b>2016</b> , 8, 1-10	2
1096	Cylindrical Bragg waveguide based temperature sensors. <b>2016</b> ,	2
1095	Polarisation independent silicon-on-insulator slot waveguides. <b>2016</b> , 6, 37760	7
1094	Multiple-beam laser patterning on aluminum oxide, zirconium oxide, and hydroxyapatite ceramic materials using a microlens array. <b>2016</b> , 28, 042003	4
1093	Broadband dispersion compensating photonic crystal fiber with a high compensation ratio. 2016,	2
1092	Numerical study of usefulness of parabolic index profile for the design of erbium doped fiber lasers and amplifiers. <b>2016</b> ,	
1091	A Diagnostic Technique for Particle Characterization Using Laser Light Extinction. 2016, 138,	О
1090	Generation of laser-induced periodic surface structures on transparent material-fused silica. <b>2016</b> , 108, 181607	16
1089	Optical properties of a four-layer waveguiding nanocomposite structure in near-IR regime. <b>2016</b> , 48, 1	2
1088	Repulsion of polarized particles near a magneto-optical metamaterial. <b>2016</b> , 94,	8
1087	Thermalization and Bose-Einstein condensation of quantum light in bulk nonlinear media. <b>2016</b> , 115, 24002	14
1086	Plasmonically enhanced upconversion of 1500 nm light via trivalent Er in a TiO2 matrix. <b>2016</b> , 109, 263102	18
1085	Phonon-polariton meta-atoms for far infrared range. <b>2016</b> , 24, 96-102	2
1084	Enhancement of solar cells parameters by periodic nanocylinders. <b>2016</b> , 37, 064004	5
1083	Interferometric Motion Detection in Atomic Layer 2D Nanostructures: Visualizing Signal Transduction Efficiency and Optimization Pathways. <b>2016</b> , 6, 28923	11
1082	Complex photonic structure based on magneto-optic waveguide and photonic crystal. 2016,	

## (2016-2016)

1081	Second and third harmonic generation in few-layer gallium telluride characterized by multiphoton microscopy. <b>2016</b> , 108, 073103	41
1080	Fiber optic monitoring of lithium-ion batteries: A novel tool to understand the lithiation of batteries. <b>2016</b> ,	7
1079	Enhancement of the transverse magneto-optical Kerr effect via resonant tunneling in trilayers containing magneto-optical metals. <b>2016</b> , 109, 033106	8
1078	Analysis of the optical and thermal properties of transparent insulating materials containing gas bubbles. <b>2016</b> , 100, 468-477	8
1077	Excitation efficiency of a side-pumped fiberized fluorescent dye microcapillary. <b>2016</b> , 28, 28-37	
1076	Cryogenic nanosecond and picosecond high average and peak power (HAPP) pump lasers for ultrafast applications. <b>2016</b> , 4,	9
1075	Retroreflective Janus Microparticle as a Nonspectroscopic Optical Immunosensing Probe. <b>2016</b> , 8, 10767-74	33
1074	Generation of carrier-envelope phase-stable mid-infrared pulses via dual-wavelength optical parametric amplification. <b>2016</b> , 24, 8660-5	32
1073	Mid-infrared surface plasmon polariton chemical sensing on fiber-coupled ITO coated glass. <b>2016</b> , 41, 2493-6	20
1072	Broadband second-harmonic phase-matching in dispersion engineered slot waveguides. <b>2016</b> , 24, 773-86	12
1071	Metal-insulator-metal waveguides for particle trapping and separation. <b>2016</b> , 16, 2302-8	10
1070	Arc-Induced Long-Period Fiber Gratings in the Dispersion Turning Points. <b>2016</b> , 34, 4584-4590	31
1069	Giant sensitivity of optical fiber sensors by means of lossy mode resonance. <b>2016</b> , 232, 660-665	62
1068	Highly-efficient and angle-independent zero-order half waveplate at broad visible wavelength based on Au nanofin array embedded in dielectric. <b>2016</b> , 24, 7966-76	11
1067	Additional peak appearing in the one-photon luminescence of single gold nanorods. <b>2016</b> , 41, 1325-8	4
1066	Design of ultra-short polarization beam splitter based on liquid-filled photonic crystal fiber. <b>2016</b> , 48, 1	8
1065	Supercontinuum generation in a multi-plate medium. <b>2016</b> , 24, 7224-31	31
1064	Enhancement of second-harmonic generation in nonlinear nanolaminate metamaterials by nanophotonic resonances. <b>2016</b> , 24, 9651-9	10

1063	Ultrafast Coherent Raman Scattering at Plasmonic Nanojunctions. <b>2016</b> , 120, 20943-20953	38
1062	Design of a high-performance optical tweezer for nanoparticle trapping. <b>2016</b> , 122, 1	8
1061	A chemical approach to control the refractive index of solgel matrices for liquid-crystal dispersion devices. <b>2016</b> , 78, 411-421	4
1060	A broadband tapered nanocavity for efficient nonclassical light emission. <b>2016</b> , 24, 20904-24	16
1059	Interaction Between Light and Photosynthetic Microorganisms. <b>2016</b> , 48, 107-149	5
1058	Effect of distance-dependent plasmonic coupling between gold nanorods and silicon substrate on second harmonic generation. <b>2016</b> ,	
1057	Bloch-like surface waves in Fibonacci quasi-crystals and Thue-Morse aperiodic dielectric multilayers. <b>2016</b> ,	1
1056	Development of an opto-electronic fiber device with multiple nano-probes. <b>2016</b> , 27, 445204	
1055	Four-layer nanocomposite structure as an effective optical waveguide switcher for near-IR regime. <b>2016</b> , 49, 435103	20
1054	Sensitivity Characteristics of Multimode-Interference Optical-Fiber Temperature-Sensor With Solid Cladding Material. <b>2016</b> , 16, 8921-8927	12
1053	Lithography-Free Fabrication of Silica Nanocylinders with Suspended Gold Nanorings for LSPR-Based Sensing. <b>2016</b> , 12, 6745-6752	21
1052	A Novel Method Based on Digital Image Processing Technique and Finite Element Method for Rapidly Modeling Optical Properties of Actual Microstructured Optical Fibers. <b>2016</b> , 8, 1-14	4
1051	Influence of optical angular momentum on filamentation of 800 nm femtosecond laser pulses in fused silica. <b>2016</b> ,	
1050	Measurement of refractive index dispersion of a fused silica plate using Fabry-Perot interference. <b>2016</b> , 55, 6285-91	13
1049	Air and dielectric bands photonic crystal microringresonator for refractive index sensing. <b>2016</b> , 41, 3655-8	19
1048	Hyperspectral volumetric coherent anti-Stokes Raman scattering microscopy: quantitative volume determination and NaCl as non-resonant standard. <b>2016</b> , 47, 1167-1173	15
1047	Supercontinuum generation using a selectively water-filled photonic crystal fiber for enhancement in the visible spectral region. <b>2016</b> , 55, 072501	2
1046	Imaging of in vitro parenteral drug precipitation. <b>2016</b> , 512, 219-223	2

1045	Scaling limit of silicon nano-wire waveguides. <b>2016</b> ,	1
1044	Near-field levitated quantum optomechanics with nanodiamonds. <b>2016</b> , 94,	13
1043	Optical properties of V-groove silicon nitride trench waveguides. <b>2016</b> , 33, 1851-9	2
1042	A novel polarization splitter based on octagonal dualcore photonic crystal fiber. <b>2016</b> , 12, 257-260	3
1041	Broadband efficient directional coupling to short-range plasmons: towards hybrid fiber nanotips. <b>2016</b> , 24, 7507-24	18
1040	Large-mode-area single-polarization single-mode photonic crystal fiber: design and analysis. <b>2016</b> , 55, 4995-5000	21
1039	Dispersion engineering of a As2Se3-based strip/slot hybrid waveguide for mid-infrared broadband wavelength conversion. <b>2016</b> , 30, 1650336	7
1038	Complex waveguide based on a magneto-optic layer and a dielectric photonic crystal. <b>2016</b> , 100, 45-56	4
1037	Lab-on-Fiber Plasmonic Probes for Ultrasound Detection: A Comparative Study. <b>2016</b> , 34, 5189-5198	11
1036	Brilliant Structurally Colored Films with Invariable Stop-Band and Enhanced Mechanical Robustness Inspired by the Cobbled Road. <b>2016</b> , 8, 22585-92	20
1035	Imprinting high-gradient topographical structures onto optical surfaces using magnetorheological finishing: manufacturing corrective optical elements for high-power laser applications. <b>2016</b> , 55, 5240-8	8
1034	Foundry-compatible SOI waveguides with a graphene top layer for wideband wavelength conversion. <b>2016</b> ,	3
1033	Resonance effects in the Raman scattering of monolayer and few-layer MoSe2. <b>2016</b> , 93,	77
1032	Broadband beamsplitter for high intensity laser applications in the infra-red spectral range. <b>2016</b> , 24, 16752-9	7
1031	Transfer matrix approach for the Kerr and Faraday rotation in layered nanostructures. <b>2016</b> , 28, 375802	13
1030	Form birefringence induced in multicomponent glass by femtosecond laser direct writing. <b>2016</b> , 41, 2739-42	18
1029	Analysis of a plasmonic based optical fiber optrode with phase interrogation. <b>2016</b> , 6, 221-233	6
1028	Angular characteristics of a multimode fibre surface plasmon resonance sensor under wavelength interrogation. <b>2016</b> , 49, 025401	3

1027	Excitation of Bloch-like surface waves in quasi-crystals and aperiodic dielectric multilayers. <b>2016</b> , 41, 2915-8	14
1026	Flat-Top Supercontinuum and Tunable Femtosecond Fiber Laser Sources at 1.92.5 fb. <b>2016</b> , 34, 4847-4855	13
1025	Long-Term Stabilization of an Actively Mode-Locked Er-Doped Fiber-Ring Laser via Dynamic Intracavity Loss Feedback. <b>2016</b> , 34, 3959-3965	1
1024	Optical Fiber Coupler With a Hollow Core Fiber for Magnetic Fluid Detection. <b>2016</b> , 34, 5220-5225	5
1023	Plasmonic-multimode-interference-based logic circuit with simple phase adjustment. <b>2016</b> , 6, 24546	30
1022	Chapter 13 Technological Extensions of Full-Field Optical Coherence Microscopy for Multicontrast Imaging. <b>2016</b> , 467-518	
1021	Magneto-optical plasmonic heterostructure with ultranarrow resonance for sensing applications. <b>2016</b> , 6, 28077	86
1020	Label-free detection of real-time DNA amplification using a nanofluidic diffraction grating. <b>2016</b> , 6, 31642	16
1019	Spaser and Optical Amplification Conditions in Gold-Coated Active Nanoparticles. <b>2016</b> , 120, 24941-24949	14
1018	Accurate modeling of high-repetition rate ultrashort pulse amplification in optical fibers. <b>2016</b> , 6, 34742	16
1017	Third-order spontaneous parametric down-conversion in a ring microcavity. <b>2016</b> , 13, 115204	9
1016	Highly efficient modulation of FRET in an orthogonally arranged BODIPY-DTE dyad. <b>2016</b> , 6, 28638	12
1015	Scaling multimode fibre IM/DD transmission capacity through spatial-spectral multiplexing. <b>2016</b> ,	
1014	Generation of spectrally stable 6.5-fs visible pulses via filamentation in krypton. <b>2016</b> , 4,	8
1013	Ultrabroadband Chirped Mirror design based on FDTD method. 2016,	
1012	Dispersion characteristics of nanometer-scaled silicon nitride suspended membrane waveguides. <b>2016</b> , 37, 114007	
1011	Investigation of 18-channel CWDM arrayed waveguide grating with silica-based waveguide. <b>2016</b> , 55, 087110	4
1010	Design of a polymer-filled silicon nitride strip/slot asymmetric hybrid waveguide for realizing both flat dispersion and athermal operation. <b>2016</b> , 55, 4827-32	2

1009 A Novel Electronically-Controlled Optical Switch. **2016**, 22, 177-184

1008	Performance analysis of polymer optical fibre based Fabry-Perot sensor formed by two uniform Bragg gratings. <b>2016</b> ,	1
1007	Comparison of self-written waveguide techniques and bulk index matching for low-loss polymer waveguide interconnects. <b>2016</b> ,	1
1006	Theoretical investigation into the optimized design of a durable OFSPR hydrogen sensor based on a PdY alloy. <b>2016</b> ,	
1005	Lasing of whispering gallery modes in optofluidic microcapillaries. <b>2016</b> , 24, 12466-77	18
1004	High-sensitivity and tunable refractive index sensor based on dual-core photonic crystal fiber. <b>2016</b> , 33, 1330	24
1003	Nonlinear optical model for strip plasmonic waveguides. <b>2016</b> , 33, 1341	6
1002	Demonstration of sharp multiple Fano resonances in optical metamaterials. <b>2016</b> , 24, 9332-9	28
1001	A refractive-index biosensor based on directional coupling of silica waveguides. <b>2016</b> , 127, 4019-4023	4
1000	Annealing Effects on Structure and Optical Properties of Diamond-Like Carbon Films Containing Silver. <b>2016</b> , 11, 146	30
999	A Technique to Match the Refractive Index of Different Diesel Fuels with the Refractive Index of Transparent Materials to Improve the Experimental Visualization. <b>2016</b> , 40, 261-269	7
998	The efficiencies of resonant and nonresonant multiphoton ionization in the femtosecond region. <b>2016</b> , 141, 5274-80	17
997	Digital Plasmonic Absorption Modulator Exploiting Epsilon-Near-Zero in Transparent Conducting Oxides. <b>2016</b> , 8, 1-13	41
996	Cladding modes in photonic crystal fiber: characteristics and sensitivity to surrounding refractive index. <b>2016</b> , 55, 017106	4
995	Optical microfiber-loaded surface plasmonic TE-pass polarizer. <b>2016</b> , 78, 101-105	7
994	Ultralow-Loss CMOS Copper Plasmonic Waveguides. <b>2016</b> , 16, 362-6	64
993	Enhanced photovoltaic performance of ultrathin Si solar cells via semiconductor nanocrystal sensitization: energy transfer vs. optical coupling effects. <b>2016</b> , 8, 5873-83	10
992	Inorganic Fillers for Dental Resin Composites: Present and Future. <b>2016</b> , 2, 1-11	86

Near-field localization by two dimensional metallic nano-post arrays with ultrashort light pulses. **2016**,

990	. <b>2016</b> , 34, 1990-1996	27
989	Rapid fabrication of angle-independent structurally colored films with a superhydrophobic property. <b>2016</b> , 130, 202-208	29
988	Femtosecond pulse shaping by ultrathin plasmonic metasurfaces. <b>2016</b> , 33, A1	16
987	Swept source digital holographic phase microscopy. <b>2016</b> , 41, 665-8	13
986	Third Harmonic Generation With the Effect of Nonlinear Loss. <b>2016</b> , 34, 1274-1280	5
985	Magneto-optical switching of Bloch surface waves in magnetophotonic crystals. <b>2016</b> , 415, 82-86	8
984	Thioxanthone in apolar solvents: ultrafast internal conversion precedes fast intersystem crossing. <b>2016</b> , 18, 6637-47	41
983	Higher refractive index and lower wavelength dispersion of SiO2 glass by structural ordering evolution via densification at a higher temperature. <b>2016</b> , 6, 19144-19149	7
982	Design of single-polarization single-mode coupler based on dual-core photonic crystal fiber. <b>2016</b> , 55, 027101	2
981	Lasing in robust cesium lead halide perovskite nanowires. <b>2016</b> , 113, 1993-8	551
980	Broadband azimuthal polarization conversion using gold nanowire enhanced step-index fiber. <b>2016</b> , 41, 448-51	16
979	Multiple-Input Multiple-Output Enabled Large Bandwidth Density On-Chip Optical Interconnect. <b>2016</b> , 34, 2969-2974	2
978	Dispersion in silica microbubble resonators. <b>2016</b> , 41, 1257-60	19
977	Repulsion of polarised particles from anisotropic materials with a near-zero permittivity component. <b>2016</b> , 5, e16022	19
976	Broadband dispersion-engineered microresonator on a chip. <b>2016</b> , 10, 316-320	64
975	Three-Dimensional Beam Propagation Modelling of Nanostructured Whispering-Gallery Microcavities. <b>2016</b> , 1-1	1
974	Method for producing angled optical fiber tips in the laboratory. <b>2016</b> , 55, 026120	7

## (2017-2016)

973	The effect of optical dispersion on magneto-optical responses of single-cavity and dual-cavity magnetophotonic crystals at near infrared wavelengths. <b>2016</b> , 70, 1	4
972	Third-harmonic generation at the interfaces of a cuvette filled with selected organic solvents. <b>2016</b> , 55, 595-602	2
971	Etched LPFGs in Reflective Configuration for Sensitivity and Attenuation Band Depth Increase. <b>2016</b> , 28, 1077-1080	4
970	Spectral characteristic of Goos⊞Echen effect in a plasmonic waveguide. <b>2016</b> , 127, 1952-1956	1
969	Prospective effect in dispersion properties of photonic crystal fibers by selective water-filling of holes. <b>2016</b> , 55, 491-7	2
968	The study of burst pulses envelope in Ytterbium-doped fiber amplifier modulating by pulsed pump source. <b>2016</b> , 360, 83-88	
967	Tailoring of nearly zero flattened dispersion photonic crystal fibers. <b>2016</b> , 361, 104-109	14
966	Short-length polarization splitter based on dual-core photonic crystal fiber with hexagonal lattice. <b>2016</b> , 363, 80-84	27
965	Membrane-based purification of proteins from nanoparticle dispersions: Influences of membrane type and ultrafiltration conditions. <b>2016</b> , 158, 171-182	22
964	Dispersion properties of transverse anisotropic liquid crystal core photonic crystal fibers. <b>2016</b> , 364, 1-8	8
963	Diagnostic of Surface Plasmons Resonances in Nanosized Gold Films by Modulation Polarization Spectroscopy. <b>2016</b> , 11, 557-563	6
962	Opportunities for Wideband Wavelength Conversion in Foundry-Compatible Silicon Waveguides Covered With Graphene. <b>2016</b> , 22, 347-359	16
961	Optimizing the figure of merit of gold nanoshell-based refractive index sensing. <b>2016</b> , 127, 250-253	8
960	Rigorous design of an ultra-high Q/V photonic/plasmonic cavity to be used in biosensing applications. <b>2016</b> , 77, 151-161	26
959	Monodisperse silica-filled composite restoratives mechanical and light transmission properties. <b>2017</b> , 33, 280-287	34
958	Visible Light, Wide-Angle Graded Metasurface for Back Reflection. <b>2017</b> , 4, 228-235	54
957	Linear and nonlinear optical behavior of epsilon near zero metamaterials: opportunities and challenges. <b>2017</b> ,	2
956	A monolithic micro-optical interferometer deep etched into fused silica. <b>2017</b> , 174, 40-45	11

955	Coherent ultra-violet to near-infrared generation in silica ridge waveguides. <b>2017</b> , 8, 13922	50
954	Influence of grafting on the glass transition temperature of PS thin films. 2017, 40, 11	8
953	Production of photonic nanojets by using pupil-masked 3D dielectric cuboid. <b>2017</b> , 50, 175102	25
952	Active directional switching of surface plasmon polaritons using a phase transition material. <b>2017</b> , 7, 43723	29
951	Correlational analysis of Eu3+ charge transfer state using La effective charge in La-based mixed-anion host compounds. <b>2017</b> , 56, 032601	2
950	Systematic design of highly birefringent photonic crystal fibers. <b>2017</b> , 123, 1	8
949	Temperature-driven switchable-beam Yagi-Uda antenna using VO2 semiconductor-metal phase transitions. <b>2017</b> , 392, 109-113	6
948	Simple and Complex Metafluids and Metastructures with Sharp Spectral Features in a Broad Extinction Spectrum: ParticleParticle Interactions and Testing the Limits of the Beer[lambert Law. <b>2017</b> , 121, 2987-2997	8
947	Refractory material based frequency selective emitters/absorbers for high efficiency and thermal stable thermophotovoltaics. <b>2017</b> , 163, 98-104	24
946	Structural and emission properties of Tb-doped nitrogen-rich silicon oxynitride films. <b>2017</b> , 28, 115710	15
946	Structural and emission properties of Tb-doped nitrogen-rich silicon oxynitride films. 2017, 28, 115710  Influence of double- and triple-layer antireflection coatings on the formation of photocurrents in multijunction IIIIV solar cells. 2017, 51, 88-92	15
	Influence of double- and triple-layer antireflection coatings on the formation of photocurrents in	
945	Influence of double- and triple-layer antireflection coatings on the formation of photocurrents in multijunction IIII solar cells. <b>2017</b> , 51, 88-92  Optical fiber 1205 waveguide coupler covered with hydrophobic zeolite film for vapor sensing.	1
945	Influence of double- and triple-layer antireflection coatings on the formation of photocurrents in multijunction IIIIV solar cells. 2017, 51, 88-92  Optical fiber Ta2O5 waveguide coupler covered with hydrophobic zeolite film for vapor sensing. 2017, 248, 359-366  Improved light output power of GaN-based ultraviolet light-emitting diode using a mesh-type	1
945 944 943	Influence of double- and triple-layer antireflection coatings on the formation of photocurrents in multijunction IIIIV solar cells. 2017, 51, 88-92  Optical fiber a2O5 waveguide coupler covered with hydrophobic zeolite film for vapor sensing. 2017, 248, 359-366  Improved light output power of GaN-based ultraviolet light-emitting diode using a mesh-type GaN/SiO2/Al omnidirectional reflector. 2017, 214, 1600789  Random laser emission from a Rhodamine B-doped GPTS/TEOS-derived organic/silica monolithic	1 6 2
<ul><li>945</li><li>944</li><li>943</li><li>942</li></ul>	Influence of double- and triple-layer antireflection coatings on the formation of photocurrents in multijunction IIIIV solar cells. 2017, 51, 88-92  Optical fiber 1205 waveguide coupler covered with hydrophobic zeolite film for vapor sensing. 2017, 248, 359-366  Improved light output power of GaN-based ultraviolet light-emitting diode using a mesh-type GaN/SiO2/Al omnidirectional reflector. 2017, 214, 1600789  Random laser emission from a Rhodamine B-doped GPTS/TEOS-derived organic/silica monolithic xerogel. 2017, 14, 065801  Optical Characteristics of Strontium Titanate Films Formed by Sol-Gel Method on Quartz	1 6 2 13
<ul><li>945</li><li>944</li><li>943</li><li>942</li><li>941</li></ul>	Influence of double- and triple-layer antireflection coatings on the formation of photocurrents in multijunction IIIIV solar cells. 2017, 51, 88-92  Optical fiberIIa2O5 waveguide coupler covered with hydrophobic zeolite film for vapor sensing. 2017, 248, 359-366  Improved light output power of GaN-based ultraviolet light-emitting diode using a mesh-type GaN/SiO2/Al omnidirectional reflector. 2017, 214, 1600789  Random laser emission from a Rhodamine B-doped GPTS/TEOS-derived organic/silica monolithic xerogel. 2017, 14, 065801  Optical Characteristics of Strontium Titanate Films Formed by Sol-Gel Method on Quartz Substrates. 2017, 84, 132-135  Large area manufacturing of plasmonic colour filters using substrate conformal imprint	1 6 2 13

937	Enhanced photoresponsivity in organic field effect transistors by silver nanoparticles. <b>2017</b> , 46, 270-275	5
936	Stress Sensitivity Analysis of Optical Fiber Bragg Grating-Based Fabry Pfot Interferometric Sensors. <b>2017</b> , 35, 2654-2659	25
935	Slow light generation using SBS in a liquid-core photonic crystal fiber. <b>2017</b> , 64, 632-638	2
934	Ultraviolet Raman Wide-Field Hyperspectral Imaging Spectrometer for Standoff Trace Explosive Detection. <b>2017</b> , 71, 173-185	17
933	. 2017,	0
932	Numerical Study of Novel Ratiometric Sensors Based on Plasmon-Exciton Coupling. <b>2017</b> , 71, 2377-2384	6
931	UV-SPR biosensor for biomolecular interaction studies. <b>2017</b> ,	
930	General rules for incorporating noble metal nanoparticles in organic solar cells. 2017,	
929	W/Cu thin film infrared reflector for TiNxOy based selective solar absorber with high thermal stability. <b>2017</b> , 121, 203101	6
928	Design, fabrication and characterization of TiO 2 -SiO 2 multilayer with tailored color glazing for thermal solar collectors. <b>2017</b> , 130, 275-284	17
927	Magneto-optical switching in microcavities based on a TGG defect sandwiched between periodic and disordered one-dimensional photonic structures. <b>2017</b> , 142, 249-255	6
926	Design of high-temperature solar-selective coatings for application in solar collectors. <b>2017</b> , 170, 102-113	21
925	Fluorescence and Scattering Dual-Mode Multiplexed Imaging with GoldBilver Alloy Core Silica Shell Nanoparticles. <b>2017</b> , 121, 8944-8951	9
924	Dispersion-enhanced third-harmonic microscopy. <b>2017</b> , 393, 289-293	3
923	Characterizing the differential mode group delay and modal dispersion of long few-mode fiber based on electrical spectral interferometry. <b>2017</b> , 56, 036110	
922	Transition from Optical Bound States in the Continuum to Leaky Resonances: Role of Substrate and Roughness. <b>2017</b> , 4, 723-727	132
921	A user-friendly guide to the optimum ultraviolet photolithographic exposure and greyscale dose of SU-8 photoresist on common MEMS, microsystems, and microelectronics coatings and materials. <b>2017</b> , 9, 2495-2504	7
920	. <b>2017</b> , 9, 1-11	13

919	Transparent Long-Pass Filter with Short-Wavelength Scattering Based on Morpho Butterfly Nanostructures. <b>2017</b> , 4, 741-745	12
918	Infrared Plasmonics with Conductive Ternary Nitrides. <b>2017</b> , 9, 10825-10834	34
917	Magneto-ellipsometry as a powerful technique for investigating magneto-optical structures properties. <b>2017</b> , 440, 153-156	3
916	Tailoring of broadband dispersion-compensating photonic crystal fibre. <b>2017</b> , 64, 1134-1145	1
915	A true fiber optic refractometer. <b>2017</b> , 11, 1600157	41
914	Hybrid-Mode-Assisted Long-Distance Excitation of Short-Range Surface Plasmons in a Nanotip-Enhanced Step-Index Fiber. <b>2017</b> , 17, 631-637	20
913	Theoretical investigation into the optimisation of an optical fibre surface plasmon resonance hydrogen sensor based on a PdY alloy. <b>2017</b> , 28, 015104	4
912	Second-Harmonic Enhancement with Mie Resonances in Perovskite Nanoparticles. <b>2017</b> , 4, 76-84	64
911	Volume relaxation of quenched silica at room temperature monitored by whispering gallery mode resonance wavelength. <b>2017</b> , 476, 52-59	3
910	Polarization filter based on plasmonic photonic crystal fiber with asymmetry around Au-coated and liquid-filled air holes. <b>2017</b> , 149, 162-168	10
909	Near-Electric-Field Tuned Plasmonic Au@SiO2and Ag@SiO2Nanoparticles for Efficient Utilization in Luminescence Enhancement and Surface-Enhanced Spectroscopy. <b>2017</b> , 121, 23062-23071	24
908	A regional, size-dependent, and causal effective medium model for Asian and Saharan mineral dust refractive index spectra. <b>2017</b> , 114, 327-341	16
907	Enhancement of light emission and internal quantum efficiency in orange and red regions for regularly arrayed InGaN/GaN nanocolumns due to surface plasmon coupling. <b>2017</b> , 111, 133110	5
906	Direct exciton emission from atomically thin transition metal dichalcogenide heterostructures near the lifetime limit. <b>2017</b> , 7, 12383	84
905	Topology optimized gold nanostrips for enhanced near-infrared photon upconversion. 2017, 111, 133102	10
904	The Surface of Ice Is Like Supercooled Liquid Water. <b>2017</b> , 129, 15746-15750	17
903	Polarization-independent asymmetric light transmission in all-dielectric photonic structures. <b>2017</b> , 73, 484-488	1
902	Sharp convex gold grooves for fluorescence enhancement in micro/nano fluidic biosensing. <b>2017</b> , 5, 8839-88-	444

## (2017-2017)

901	Enhancement and interplay of first- and second-order spatial dispersion in metamaterials with moderate-permittivity inclusions. <b>2017</b> , 96,	5
900	Arbitrary manipulation of amplitude and phase of a set of highly discrete coherent spectra. <b>2017</b> , 95,	4
899	Holographic characterization of colloidal particles in turbid media. <b>2017</b> , 111, 153702	18
898	Angle-selective all-dielectric HuygensImetasurfaces. <b>2017</b> , 50, 434002	36
897	Ultra-narrow band perfect absorbers based on Fano resonance in MIM metamaterials. 2017, 405, 216-221	44
896	Leidenfrost drops cooling surfaces: theory and interferometric measurement. <b>2017</b> , 827, 614-639	23
895	Polarization exchange of optical eigenmode pair in twisted-nematic Fabry-Pfot resonator. <b>2017</b> , 96, 022711	5
894	Enhancing Organic Semiconductor-Surface Plasmon Polariton Coupling with Molecular Orientation. <b>2017</b> , 17, 6151-6156	10
893	Strain and thermal conductivity in ultrathin suspended silicon nanowires. 2017, 96,	20
892	Method of determining dispersion dependence of refractive index of nanospheres building opals. <b>2017</b> , 73, 437-440	7
891	Klein tunneling near the Dirac points in metal-dielectric multilayer metamaterials. 2017, 7, 9678	1
890	The Surface of Ice Is Like Supercooled Liquid Water. <b>2017</b> , 56, 15540-15544	16
889	Highly sensitive in-line microfluidic sensor based on microfiber-assisted Machidehnder interferometer for glucose sensing. <b>2017</b> , 19, 115803	7
888	Development of Particle Streak Velocimetry with a Cold Flow Supersonic Nozzle. 2017,	1
887	A dielectric-encapsulated 2D photonic crystal based solar thermophotovoltaic power generator. <b>2017</b> , 125, 1253-1259	10
886	Influence of the core size on light propagation in photonic liquid crystal fibers. <b>2017</b> , 25, 198-204	1
885	Low-Temperature Atmospheric Pressure Plasma-Enhanced CVD of Nanocomposite Coatings Molybdenum Disulfide (Filler)Bilicon Oxide (Matrix) 12017, 4, 1700241	13
884	Surface plasmon polariton nanocavity with ultrasmall mode volume. <b>2017</b> , 50, 315102	

883	Analytical modelization of a fiber optic-based surface plasmon resonance sensor. 2017, 402, 618-623	7
882	Harnessing Surface Wrinkling@racking Patterns for Tunable Optical Transmittance. <b>2017</b> , 5, 1700425	49
881	Liquid-filled dispersion-flattened photonic crystal fiber. 2017,	
880	Separating the pH-Dependent Behavior of Water in the Stern and Diffuse Layers with Varying Salt Concentration. <b>2017</b> , 121, 20229-20241	59
879	Genetic algorithm optimization of grating coupled near-field interference lithography systems at extreme numerical apertures. <b>2017</b> , 19, 095003	10
878	Leaky Bloch-like surface waves in the radiation-continuum for sensitivity enhanced biosensors via azimuthal interrogation. <b>2017</b> , 7, 3233	23
877	Highly efficient multicolor multifocus microscopy by optimal design of diffraction binary gratings. <b>2017</b> , 7, 5284	12
876	Neutron reflectometry yields distance-dependent structures of nanometric polymer brushes interacting across water. <b>2017</b> , 13, 5767-5777	14
875	Spectral properties of an UV fused silica within 0.8 to 5 µm at elevated temperatures. <b>2017</b> , 85, 293-299	14
874	Enhance photocatalysis of TiO2 and ZnO ceramics by addition of fused silica as a UV guiding medium. <b>2017</b> , 43, 15237-15245	5
873	Light intensity field enhancement (LIFE) induced localized edge abrasion of silica-coated silver nanoprisms. <b>2017</b> , 9, 15356-15361	4
872	Effect of low NiO doping on anomalous light scattering in zinc aluminosilicate glass-ceramics. <b>2017</b> , 473, 152-169	9
871	Comment on "Defocusing complex short-pulse equation and its multi-dark-soliton solution". <b>2017</b> , 96, 026201	2
870	Soliton-like behavior in fast two-pulse collisions in weakly perturbed linear physical systems. <b>2017</b> , 71, 1	6
869	Effect of heat treatment on the nanoporosity of silica PECVD films elucidated by low-energy positron annihilation and ellipsometric porosimetry. <b>2017</b> , 122, 185304	5
868	Nonlinear photoionization of transparent solids: A nonperturbative theory obeying selection rules. <b>2017</b> , 96,	12
867	Rigorous Coupled Wave Analysis for Plasmonic Nanoparticles. <b>2017</b> , 866, 341-344	
866	Fast Surface-Plasmon-Mediated Electro-Optics of a Liquid Crystal on a Metal Grating. <b>2017</b> , 8,	19

865	Tunneling and Origin of Large Access Resistance in Layered-Crystal Organic Transistors. <b>2017</b> , 8,	35
864	Plasmonic photonic crystal fiber polarization filter with asymmetry around Au-coated and liquid-filled air holes. <b>2017</b> , 49, 1	5
863	Hybrid photonic-crystal fiber. <b>2017</b> , 89,	123
862	Effect of Temperature on the Organization of Acetonitrile at the Silica/Liquid Interface. <b>2017</b> , 121, 26432-26	437
861	OCT Amplitude and Speckle Statistics of Discrete Random Media. <b>2017</b> , 7, 14873	24
860	Study of the electric field enhancement in resonant metasurfaces. <b>2017</b> , 19, 125104	7
859	Development of Embedded Fiber-Optic Evanescent Wave Sensors for Optical Characterization of Graphite Anodes in Lithium-Ion Batteries. <b>2017</b> , 9, 41284-41290	21
858	Fiber Optic Sensor for Real-Time Sensing of Silica Scale Formation in Geothermal Water. <b>2017</b> , 7, 3387	16
857	Polarized surface-enhanced Raman spectroscopy of suspended carbon nanotubes by Pt-Re nanoantennas. <b>2017</b> , 96,	4
856	Effect of photonic crystal stop-band on photoluminescence of aBi1⊠Cx:H. <b>2017</b> , 95,	10
855	Measurement of different types of optical loss using high-precision laser photometer. 2017, 28, 065007	
854	Phase-interrogated SPR sensing structures based on tapered and tip optrode optical fiber configurations with bimetallic layers. <b>2017</b> , 28, 095203	3
853	Optical properties of periodic, quasi-periodic, and disordered one-dimensional photonic structures. <b>2017</b> , 72, 403-421	81
852	High-Quality Ultrathin Gold Layers with an APTMS Adhesion for Optimal Performance of Surface Plasmon Polariton-Based Devices. <b>2017</b> , 9, 25049-25056	34
851	Parasitic Photon-Pair Suppression via Photonic Stop-Band Engineering. <b>2017</b> , 118, 073603	9
850	Hybrid-Waveguide Ring Resonator for Biochemical Sensing. <b>2017</b> , 17, 4781-4790	24
849	High precision laser photometer for laser optics. 2017,	
848	A blueprint for a simultaneous test of quantum mechanics and general relativity in a space-based quantum optics experiment. <b>2017</b> , 4,	7

847	Wavelength and Phase Detection Based SMS Fiber Sensors Optimized With Etching and Nanodeposition. <b>2017</b> , 35, 3743-3749	26
846	Design of a Single-Polarization Single-Mode Photonic Crystal Fiber Filter Based on Surface Plasmon Resonance. <b>2017</b> , 12, 1325-1330	24
845	An inexpensive high-temperature optical fiber thermometer. <b>2017</b> , 187, 358-363	2
844	Influence of substrate and film thickness on polymer LIPSS formation. <b>2017</b> , 394, 125-131	22
843	Ultra-short polarization beam splitter based on dual core photonic crystal fiber. 2017, 64, 445-450	9
842	Numerical analysis of photonic crystal fiber based hemoglobin sensor. <b>2017</b> , 130, 825-829	3
841	Comparison of finite element and transfer matrix methods for numerical investigation of surface plasmon waveguides. <b>2017</b> , 382, 132-137	20
840	Double telecom band thermo-optic switch based on dual-line filled photonic liquid crystal fibres. <b>2017</b> , 44, 479-483	12
839	Influence of Dielectric Coating on Performance of Surface Plasmon Resonance Sensor. <b>2017</b> , 12, 1121-1130	19
838	Cascaded ring resonator and Mach-Zehnder interferometer with a Sagnac loop for Vernier-effect refractive index sensing. <b>2017</b> , 240, 76-89	24
837	Optical sensors based on lossy-mode resonances. <b>2017</b> , 240, 174-185	113
836	Plasmonic Effects in Tin Disulfide Nanostructured Thin Films Obtained by the Close-Spaced Vacuum Sublimation. <b>2017</b> , 12, 1213-1220	5
835	Numerical simulation of coherent visible-to-near-infrared supercontinuum generation in the CHCl3-filled photonic crystal fiber with 1.06 h pump pulses. <b>2017</b> , 88, 215-221	9
834	Effect of the reflection by the silicon aggregates on the photoluminescence from silicon nitride film embedded silicon nanocrystals. <b>2017</b> , 68, 334-338	2
833	Relationships between the optical and Raman behavior of van Hove singularity in twisted bi- and fewlayer graphenes and environmental effects. <b>2017</b> , 111, 238-247	8
832	A new structure of photonic crystal fiber with high sensitivity, high nonlinearity, high birefringence and low confinement loss for liquid analyte sensing applications. <b>2017</b> , 12, 8-14	33
831	Solutions for Modal Squeeze in Dual-Concentric Core Photonic Crystal Fibers. <b>2017</b> , 29, 849-852	1
830	Photonic crystal fibre polarization filter with round lattice based on surface plasmon resonance. <b>2017</b> , 64, 205-209	2

829	Cascading Second-Order Microring Resonators for a Box-Like Filter Response. 2017, 35, 5347-5360	19
828	Low-power bistability in graphene-comprising 3D photonic resonant circuits. <b>2017</b> , 122, 233101	9
827	Surface Plasmon Polariton Resonance of Gold, Silver, and Copper Studied in the Kretschmann Geometry: Dependence on Wavelength, Angle of Incidence, and Film Thickness. <b>2017</b> , 86, 124721	20
826	Microstructure fiber with extremely high nonlinearity for supercontinuum generation. 2017,	1
825	Effect of Dopant Diffusion on the Long-Term Stability of Fabry <b>P</b> flot Optical Fiber Sensors. <b>2017</b> , 35, 5317-5323	9
824	Glucose sensor realized with photonic crystal fiber-based Sagnac interferometer. <b>2017</b> , 405, 143-146	22
823	Lambertian and photonic light trapping analysis with thickness for GaAs solar cells based on 2D periodic pattern. <b>2017</b> , 11, 217-224	8
822	Astigmatism-corrected echelle spectrometer using an off-the-shelf cylindrical lens. <b>2017</b> , 56, 7861-7868	15
821	Noninvasive characterization of optical fibers. <b>2017</b> , 42, 4946-4949	4
820	Versatile dispersion characteristics of water solution of glycerine in selective filling of holes in photonic crystal fibers. <b>2017</b> , 56, 2927-2936	3
819	Vectorial control of nonlinear emission via chiral butterfly nanoantennas: generation of pure high order nonlinear vortex beams. <b>2017</b> , 25, 2569-2582	15
818	Analysis and manipulation of the induced changes in the state of polarization by mirror scanners. <b>2017</b> , 56, 4513-4521	
817	Enhancing ultraviolet spontaneous emission with a designed quantum vacuum. <b>2017</b> , 25, 4162-4179	3
816	Monolithic optical link in silicon-on-insulator CMOS technology. <b>2017</b> , 25, 5440-5456	19
815	Digital waveguide adiabatic passage part 1: theory. <b>2017</b> , 25, 5466-5479	1
814	Fast and full range measurements of ellipsometric parameters using a 45° dual-drive symmetric photoelastic modulator. <b>2017</b> , 25, 5725-5733	11
813	Method to simulate and analyse induced stresses for laser crystal packaging technologies. <b>2017</b> , 25, 5927-59-	——— 4 <b>0</b> 6
812	Unified theory of whispering gallery multilayer microspheres with single dipole or active layer sources. <b>2017</b> , 25, 6192-6214	11

811	Corrugation-assisted metal-coated angled fiber facet for wavelength-dependent off-axis directional beaming. <b>2017</b> , 25, 8366-8385	9
810	Synthesis, fabrication and characterization of a highly-dispersive mirrors for the 2 μm spectral range. <b>2017</b> , 25, 10234-10240	8
809	Optimization in nanocoated D-shaped optical fiber sensors. <b>2017</b> , 25, 10743-10756	35
808	Low-crosstalk orbital angular momentum fiber coupler design. <b>2017</b> , 25, 11200-11209	10
807	Control of gain/absorption in tunable hyperbolic metamaterials. <b>2017</b> , 25, 13153-13162	16
806	Compensation-free broadband entangled photon pair sources. <b>2017</b> , 25, 22667-22678	14
805	Benchmarking of software tools for the characterization of nanoparticles. <b>2017</b> , 25, 26760-26780	11
804	Real-time robust direct and indirect photon separation with polarization imaging. 2017, 25, 29432	3
803	Polarization-resolved characterization of plasmon waves supported by an anisotropic metasurface. <b>2017</b> , 25, 32631	17
802	Design, fabrication and characterization of a hybrid metal-dielectric nanoantenna with a single nanocrystal for directional single photon emission. <b>2017</b> , 7, 834	9
801	Analysis of nanogap-induced spectral blue-shifts of plasmons on fiber-integrated gold, silver and copper nanowires. <b>2017</b> , 7, 1486	7
800	Origin of third harmonic generation in plasmonic nanoantennas. <b>2017</b> , 7, 1575	12
799	Harnessing nonlinearities near material absorption resonances for reducing losses in plasmonic modulators. <b>2017</b> , 7, 2168	36
798	Gain optimization, bleaching, and e-beam structuring of IR-140 doped PMMA and integration with plasmonic waveguides. <b>2017</b> , 7, 3963	6
797	Modal interference in optical nanofibers for sub-Angstrom radius sensitivity. 2017, 4, 157	17
796	Liquid modified photonic crystal fiber for simultaneous temperature and strain measurement. <b>2017</b> , 5, 129	36
795	D-shaped photonic crystal fiber refractive index sensor based on surface plasmon resonance. <b>2017</b> , 56, 6988-6992	73
794	Measurement of thickness profiles of glass plates by analyzing Haidinger fringes. <b>2017</b> , 56, 1855-1860	3

793	High power cladding light stripper using segmented corrosion method: theoretical and experimental studies. <b>2017</b> , 25, 8760-8776	12
792	Temperature-calibrated high-precision refractometer using a tilted fiber Bragg grating. <b>2017</b> , 25, 25910-2591	827
791	Metallic Fresnel zone plate implemented on an optical fiber facet for super-variable focusing of light. <b>2017</b> , 25, 30290-30303	24
790	Mid-wave infrared narrow bandwidth guided mode resonance notch filter. <b>2017</b> , 42, 223-226	21
7 <sup>8</sup> 9	High-sensitivity integrated devices based on surface plasmon resonance for sensing applications. <b>2017</b> , 5, 654	37
788	Tunable femtosecond near-IR source by pumping an OPA directly with a 90 MHz Yb:fiber source. <b>2017</b> , 56, 3104-3108	1
787	From parabolic-trough to metasurface-concentrator: assessing focusing in the wave-optics limit. <b>2017</b> , 42, 1520-1523	8
786	Comparative analysis of anti-reflection coatings on solar PV cells through TiO2 and SiO2 nanoparticles. <b>2021</b> , ahead-of-print,	1
7 <sup>8</sup> 5	Crossings in photonic crystal fiber with hybrid core and design of broadband dispersion compensating photonic crystal fiber. <b>2021</b> , 63, 102485	3
7 <sup>8</sup> 4	Design and Characterization of Q-Enhanced Silicon Nitride Racetrack Micro-Resonators. <b>2021</b> , 39, 2917-2923	2
783	Recent advances in ultraviolet nanophotonics: from plasmonics and metamaterials to metasurfaces. <b>2021</b> , 10, 2283-2308	10
782	Dielectric function of vanadium oxide thin films by thermal annealing. <b>2021</b> , 60, 4477-4484	O
781	New-Generation Liquid Crystal Materials for Application in Infrared Region. 2021, 14,	3
7 <sup>8</sup> 0	Design, fabrication and assessment of an optomechanical sensor for pressure and vibration detection using flexible glass multilayers. <b>2021</b> , 115, 111023	5
779	Solar Pumping of Fiber Lasers with Solid-State Luminescent Concentrators: Design Optimization by Ray Tracing. <b>2021</b> , 9, 2100479	1
778	The expression for calculating mode effective indices of hollow-core anti-resonant fibers in non-resonant wavelength regions. <b>2021</b> , 53, 1	
777	Angular selection of transmitted light and enhanced spontaneous emission in grating-coupled hyperbolic metamaterials. <b>2021</b> , 29, 21458-21472	3
776	Nonparaxial Mie Theory of Image Formation in Optical Microscopes and Characterization of Colloidal Particles. <b>2021</b> , 15,	1

775	A universal robust bottom-up approach to engineer Greta-oto-inspired anti-reflective structure. <b>2021</b> , 2, 100479	4
774	Experimental methods for laboratory measurements of helium spectral line broadening in white dwarf photospheres. <b>2021</b> , 28, 062902	O
773	LayerPCM: An implicit scheme for dielectric screening from layered substrates. <b>2021</b> , 154, 224114	3
772	GV mll on-chip particle accelerator driven by few-cycle femtosecond laser pulse. 2021, 23, 063031	2
771	Electrostatically Tuned Optical Filters Based on Hybrid Plasmonic-Dielectric Thin Films for Hyperspectral Imaging. <b>2021</b> , 12,	0
770	Optimization of the operational parameters of ultrashort laser pulses for high self-compression with simplified thin-film compressor technique. 1	
769	Optimization of Fiber Bragg Gratings Inscribed in Thin Films Deposited on D-Shaped Optical Fibers. <b>2021</b> , 21,	2
768	Numerical Analysis of Protection Method of Metallic Sub-Wavelength Concentric Arrays for Radially Polarized Light Selection and Its Applications. <b>2021</b> , 21,	O
767	Analysis of Kerr comb generation in silicon microresonators under the influence of two-photon absorption and fast free-carrier dynamics. <b>2021</b> , 103,	2
766	Investigation of a diode-pumped Ti:sapphirelaser modelocked using carbon nanotubes.	
765	Optical Fibers. <b>2021</b> , 21-65	
764	Eigenmode symmetry assignment of triangular-lattice photonic crystal slabs and their Dirac cones materialized by effective degeneracy in the mid-infrared region. <b>2021</b> , 29, 19486-19494	1
763	High-accuracy room temperature planar absolute radiometer based on vertically aligned carbon nanotubes. <b>2021</b> , 29, 22533-22552	5
762	Direct laser writing of depressed-cladding waveguides in extremely low expansion lithium aluminosilicate glass-ceramics. <b>2021</b> , 138, 106846	1
762 761		2
	aluminosilicate glass-ceramics. <b>2021</b> , 138, 106846  Optimization of light scattering enhancement by gold nanoparticles in fused silica optical fiber.	
761	aluminosilicate glass-ceramics. <b>2021</b> , 138, 106846  Optimization of light scattering enhancement by gold nanoparticles in fused silica optical fiber. <b>2021</b> , 29, 19450-19464	2

757 Graphene-gold nanowires-graphene sensitized optical fiber sensor. **2021**,

756	Optical manipulation of a dielectric particle along polygonal closed-loop geometries within a single water droplet. <b>2021</b> , 11, 12690	O
755	Optical trap for an atom around the midpoint between two coupled identical parallel optical nanofibers. <b>2021</b> , 103,	2
754	Measuring the structure and equation of state of polyethylene terephthalate at megabar pressures. <b>2021</b> , 11, 12883	4
753	Energy flux optimization in 1D multiperiodic four-component photonic crystals. <b>2021</b> , 489, 126875	1
752	Design of a Surface Plasmon Resonance Temperature Sensor with Multi-Wavebands Based on Conjoined-Tubular Anti-Resonance Fiber. <b>2021</b> , 8, 231	2
75 <sup>1</sup>	First-Principles Calculation of the Optical Rotatory Power of Periodic Systems: Application on EQuartz, Tartaric Acid Crystal, and Chiral (n,m)-Carbon Nanotubes. <b>2021</b> , 17, 4063-4076	2
750	. 2021,	
749	Optical Power Scale Realization by Laser Calorimeter after 45 Years of Operation. <b>2021</b> , 126,	1
748	Probing the screening of the Casimir interaction with optical tweezers. <b>2021</b> , 3,	O
747	Direct-write microsphere photolithography of hierarchical infrared metasurfaces. <b>2021</b> , 60, 7122-7130	
746	Dual-Channel Surface Plasmon Resonance <b>B</b> ased Photonic Crystal Fiber Sensor with Metal-Ta2O5 Coating at Near-infrared Wavelength. 1	2
745	Ultra-wide sensing range plasmonic refractive index sensor based on a two-dimensional circular-hole grating engraved on a gold film. <b>2021</b> , 26, 104396	12
744	Dependence of the refractive index on density, temperature, and the wavelength of the incident light. <b>2021</b> , 94, 1	1
743	Turn Around Point Long Period Fiber Gratings With Coupling to Asymmetric Cladding Modes Fabricated by a Femtosecond Laser and Coated With Titanium Dioxide. <b>2021</b> , 39, 4784-4793	3
742	Photonic Crystal Fiber-Based Reconfigurable Biosensor Using Phase Change Material. <b>2021</b> , 20, 338-344	8
741	Instability of residual stress of crystalline and glass oxide thin films prepared by sol-gel method. <b>2021</b> , 130, 035305	1
740	Surface plasmon resonance is possible in an optical fiber tapered to a point. <b>2021</b> , 39, 043206	

739	Distributed Feedback Laser Based on Tunable Photonic Hypercrystal. <b>2021</b> , 14,	8
738	Generation of Radially Polarized Single Photons with Plasmonic Bullseye Antennas. <b>2021</b> , 8, 2190-2196	3
737	Phenylboronic acid functionalized helical long period grating for glucose sensing. <b>2021</b> , 64, 102557	2
736	Simultaneous Determination of Refractive Index and Thickness of Submicron Optical Polymer Films from Transmission Spectra. <b>2021</b> , 13,	5
735	High-Throughput Wafer-Scale Wrinkle Patterning: a Single-Step Fabrication Process and Applications for Tunable Optical Transmittance. <b>2021</b> , 3, 3200-3206	0
734	Non-zero dispersion-shifted ring fiber for the orbital angular momentum mode. <b>2021</b> , 29, 25428-25438	1
733	Light trapping transparent electrodes with a wide-angle response. <b>2021</b> , 29, 24989-24999	1
732	Near-unity third-harmonic circular dichroism driven by a quasibound state in the continuum in asymmetric silicon metasurfaces. <b>2021</b> , 104,	13
731	Polarization-dependent refractive index analysis for nanoporous microcavities by ray tracing of a propagating electromagnetic field. <b>2021</b> , 11, 2924	2
730	Full Explicit Numerical Modeling in Time-Domain for Nonlinear Electromagnetics Simulations in Ultrafast Laser Nanostructuring. <b>2021</b> , 11, 7429	O
729	Effects of chemical potential and cavity thickness on defective mode sensitivity for a cancer cell in a biosensor formed using a photonic crystal. <b>2021</b> , 240, 166823	1
728	The Role of Substrate on Thermal Evolution of Ag/TiO Nanogranular Thin Films. <b>2021</b> , 11,	2
727	Nonreciprocal photonic spin Hall effect of magnetic Weyl semimetals. <b>2021</b> , 119, 081103	0
726	Coherent dynamics of Floquet-Bloch states in monolayer WS2 reveals fast adiabatic switching. <b>2021</b> , 104,	1
725	Polarization-insensitive optical modulators based on single ENZ-graphene layers. 2021,	
724	Wavefront Control with Nanohole Array-Based Out-of-Plane Metasurfaces. <b>2021</b> , 4, 8699-8705	3
723	Design of a large bandwidth 2 ½ interferometric switching cell based on a sub-wavelength grating. <b>2021</b> , 23, 085801	6
722	Thin silicon via crack-assisted layer exfoliation for photoelectrochemical water splitting. <b>2021</b> , 24, 102921	2

721	Theory of molecular emission power spectra. II. Angle, frequency, and distance dependence of electromagnetic environment factor of a molecular emitter in plasmonic environments. <b>2021</b> , 155, 074101	1
720	Theoretical Analysis of On-Chip Vertical Hybrid Plasmonic Nanograting. 1	О
719	Active Electromagnetically Induced Transparency Effect in Graphene-Dielectric Hybrid Metamaterial and Its High-Performance Sensor Application. <b>2021</b> , 11,	2
718	Extraordinary enhancement of the transverse magneto-optical Kerr effect with high-refractive-index nanostructures. <b>2021</b> ,	
717	Multifunctional and reconfigurable graphene/liquid crystal-assisted asymmetrical Fabry-Pfot cavity for reflected light control. <b>2021</b> , 29, 27816-27829	1
716	Real-Time Visualization of the Cleaning of Ceria Particles from Silicon Dioxide Films Using PVA Brush Scrubbing. <b>2021</b> , 10, 084004	3
715	Coupling system with concave and positive legative angular cone lenses group for the Cassegrain receiving antenna system. <b>2021</b> , 493, 127029	2
714	In-Line Mach-Zehnder Interferometers Based on a Capillary Hollow-Core Fiber Using Vernier Effect for a Highly Sensitive Temperature Sensor. <b>2021</b> , 21,	3
713	Large optical and structural enhancement by designing VOx nanostructures for smart windows applications. <b>2021</b> , 270, 115216	1
712	Compact 1 IN power splitters with arbitrary power ratio for integrated multimode photonics. <b>2021</b> , 23, 095802	1
711	Tunable Q-switched Tm/Ho-codoped fiber laser based on a thermo-optically controlled multimode interference fiber structure. <b>2021</b> , 18, 095103	
710	Enhancing SiN Waveguide Nonlinearity with Heterogeneous Integration of Few-Layer WS. <b>2021</b> , 8, 2713-2721	3
709	Design of an all-fiber mode power splitter for mode-division-multiplexing transmission. <b>2021</b> , 60, 8480-8484	
708	Quantitative in situ measurement of optical force along a strand of cleaved silica optical fiber induced by the light guided therewithin. <b>2021</b> , 9, 2016	2
707	A High-adhesion Binding Strategy for Silica Nanoparticle-based Superhydrophobic Coatings <b>2021</b> , 625,	6
706	Study of ultrathin-film amorphous silicon solar cell performance using photonic and plasmonic nanostructure.	2
705	Refraction of space-time wave packets: II. experiments at normal incidence. <b>2021</b> , 38, 1450-1461	4
704	Microstructured antireflective encapsulant on concentrator solar cells.	O

703	Prediction of Self-Assembled Dewetted Nanostructures for Photonics Applications via a Continuum-Mechanics Framework. <b>2021</b> , 16,	
702	Refractive index modulation in magnetophoresis of bioreaction induced self-assembled magnetic fluid. <b>2021</b> , 46, 4658-4661	2
701	A large birefringence and high nonlinearity liquid crystal photonic crystal fiber with low confinement loss. <b>2021</b> , 65, 102610	3
700	Experimental validation of the fundamental mode approximation for stacked metasurfaces and its application to the treatment of arbitrary period ratios. <b>2021</b> , 6, 096109	
699	Influence of thermal cycling on the optical and the electrical properties of atmospheric pressure chemical vapor deposited tin oxide films grown using water and methanol vapors as oxidizers. <b>2021</b> , 734, 138841	1
698	Optimization Design of SNS Sensor Structural Parameters for Battery Expansion Monitoring. <b>2021</b> , 9,	
697	Performance optimization of bi-metallic surface plasmon resonance based sensors with silicon layer using poynting vector analysis. <b>2021</b> , 53, 1	1
696	Sub-Kelvin Feedback Cooling and Heating Dynamics of an Optically Levitated Librator. <b>2021</b> , 127, 123605	3
695	In-Volume Laser Direct Writing of Silicon@hallenges and Opportunities. 2100140	7
694	Fundamental Limits to the Refractive Index of Transparent Optical Materials. <b>2021</b> , 33, e2103946	8
693	Optical method for simultaneous thickness measurements of two layers with a significant thickness difference. <b>2021</b> , 29, 31615-31631	2
692	Rigorous coupled-wave analysis of a multi-layered plasmonic integrated refractive index sensor. <b>2021</b> , 29, 36201-36210	2
691	Measurement of dynamic wetting using phase-shifting imaging ellipsometer: comparison of pure solvent and nanoparticle suspension on film thickness profile, apparent contact angle, and precursor film length. <b>2021</b> , 62, 1	
690	Design guidelines for collimating or focusing graded-index fiber tips. <b>2021</b> , 29, 29982-29995	1
689	Resonance behavior of diffraction on encapsulated guided-mode grating of subwavelength thickness. <b>2021</b> , 46, 100953	
688	Origin of spontaneous wave mixing processes in multimode GRIN fibers. <b>2021</b> , 29, 30822-30833	O
687	Inverse Design of Equivalent-Graded-Index Photonic-Crystal Fiber Based on Empirical Dispersion Formula. <b>2021</b> , 39, 5598-5603	4
686	Defect mode modulation for a protein solution cavity surrounded by graphene and nanocomposite layers. <b>2021</b> , 242, 167161	1

685	Hybrid nanowires for phase-matching of third-harmonic generation in hyperbolic metamaterial. <b>2021</b> , 60, 8744-8755	1
684	Design of surface Plasmon resonance based both side polished photonic crystal fiber for highly efficient refractive index sensor. <b>2021</b> , 168062	O
683	Silver nanowire mediated random lasing in silica cladded dye doped polymer microstructure. <b>2021</b> , 504, 127466	O
682	U-grooved dual-channel plasmonic sensor for simultaneous multi-analyte detection. <b>2021</b> , 38, 3055	1
681	Review on transparent polycrystalline ceramics. 1	2
680	Extremely high sensitivity magnetic field sensing based on birefringence-induced dispersion turning point characteristics of microfiber coupler. <b>2021</b> , 29, 104743	8
679	Optical properties of silicon oxynitride films grown by plasma-enhanced chemical vapor deposition. <b>2021</b> , 736, 138887	4
678	Polarization-independent highly-efficient splitter based on the cross-shaped ridge structure. <b>2021</b> , 127499	1
677	Design and characterization of high birefringence three suspended-cores fiber with few-mode. <b>2021</b> , 244, 167473	1
676	Theoretical investigations of Tamm plasmon resonance for monitoring of isoprene traces in the exhaled breath: Towards chronic liver fibrosis disease biomarkers. <b>2021</b> , 413, 127610	5
675	Sensitivity and linearity enhanced wide-detection range surface-plasmon-resonance photonic-crystal-fiber sensor. <b>2021</b> , 29, 104707	1
674	First observation of quasifhonochromatic optical Cherenkov radiation in a dispersive medium (quartz). <b>2021</b> , 417, 127680	O
673	Analysis and measurement of the medium dispersion in the open-cavity of fiber-optic Fabry-Perot interferometer. <b>2021</b> , 331, 112892	1
672	Measuring the wedge of flat optical windows. <b>2021</b> , 498, 127257	
671	Re-analysis of single-mode conditions for thin-film lithium niobate rib waveguides. <b>2021</b> , 30, 104824	1
670	Hybrid nanowire-hyperbolic metamaterial based broadband absorber for the visible and near-infrared regions. <b>2021</b> , 189, 109701	3
669	Gradient-index solar sail and its optimal orbital control. <b>2021</b> , 119, 107103	5
668	Broad range bimodal microcavity in-line Mach-Zehnder interferometers. <b>2022</b> , 145, 107503	

667	Dual-pumped flat optical frequency comb based on normal dispersion AlGaAs on insulator waveguide: Numerical investigation. <b>2022</b> , 502, 127415	
666	Absorptive metasurface color filters based on hyperbolic metamaterials for a CMOS image sensor. <b>2021</b> , 29, 3643-3658	3
665	Probing into the double identity of Cu in bimetallic CuAg-TNTA hot-electron devices for photo-hydrogen conversion.	1
664	Enhanced Nonlinear Emission from Single Multilayered Metal <b>D</b> ielectric Nanocavities Resonating in the Near-Infrared. <b>2021</b> , 8, 512-520	10
663	High birefringence and broadband dispersion compensation photonic crystal fiber. 2021,	1
662	Numerical investigation of a real-time temperature sensor based on high-order soliton compression. <b>2021</b> , 18, 025101	4
661	. <b>2021</b> , 9, 107804-107811	1
660	An Integrated Detection Based on a Multi-Parameter Plasmonic Optical Fiber Sensor. <b>2021</b> , 21,	7
659	Optical Fibers. 24-78	3
658	Sub-Wavelength Passive Optical Isolators Using Photonic Structures Based on Weyl Semimetals. <b>2020</b> , 8, 2000100	26
,		
657	The Spectral Irradiance Monitor: Measurement Equations and Calibration. 2005, 169-204	1
6 <sub>57</sub>	The Spectral Irradiance Monitor: Measurement Equations and Calibration. 2005, 169-204  The Spectral Irradiance Monitor: Scientific Requirements, Instrument Design, and Operation Modes. 2005, 141-167	5
	The Spectral Irradiance Monitor: Scientific Requirements, Instrument Design, and Operation	
656	The Spectral Irradiance Monitor: Scientific Requirements, Instrument Design, and Operation Modes. <b>2005</b> , 141-167	5
656 655	The Spectral Irradiance Monitor: Scientific Requirements, Instrument Design, and Operation Modes. 2005, 141-167  Density and Refractive Index of Densified Silica Glass. 1992, 117-122  Electromagnetic Wave Diffraction by Periodic Planar Metamaterials with Nonlinear Constituents.	5 1
656 655 654	The Spectral Irradiance Monitor: Scientific Requirements, Instrument Design, and Operation Modes. 2005, 141-167  Density and Refractive Index of Densified Silica Glass. 1992, 117-122  Electromagnetic Wave Diffraction by Periodic Planar Metamaterials with Nonlinear Constituents. 2016, 81-98	5 1 8
656 655 654 653	The Spectral Irradiance Monitor: Scientific Requirements, Instrument Design, and Operation Modes. 2005, 141-167  Density and Refractive Index of Densified Silica Glass. 1992, 117-122  Electromagnetic Wave Diffraction by Periodic Planar Metamaterials with Nonlinear Constituents. 2016, 81-98  INTRODUCTION. 1989, 1-25	5 1 8
656 655 654 653	The Spectral Irradiance Monitor: Scientific Requirements, Instrument Design, and Operation Modes. 2005, 141-167  Density and Refractive Index of Densified Silica Glass. 1992, 117-122  Electromagnetic Wave Diffraction by Periodic Planar Metamaterials with Nonlinear Constituents. 2016, 81-98  INTRODUCTION. 1989, 1-25  INTRODUCTION. 1995, 1-27  Real-Time Spectroscopic Ellipsometry Studies of the Nucleation, Growth, and Optical Functions of	5 1 8 3

649	Introduction. <b>1999</b> , 1-12	1
648	Optical properties of Er3+ heavily doped silica glass fabricated by zeolite method. <b>2020</b> , 543, 120149	3
647	Dispersion engineering in asymmetric dual-width Si3N4 waveguide with high confinement based on super-mode theory. <b>2020</b> , 464, 125474	1
646	Rapid three-dimensional structuring of transparent SiO2 glass using interparticle photo-cross-linkable suspensions. <b>2020</b> , 1,	13
645	Determination of optical dispersion and film thickness of semiconducting disordered layers by transmission measurements: Application for chemically vapor deposited Si and SnO2 film. <b>1997</b> , 70, 246-248	20
644	Coupling between guided modes of two parallel nanofibers. <b>2020</b> , 22, 123007	3
643	Comprehensive mathematical modelling of ultra-high Q grating-assisted ring resonators. <b>2020</b> , 22, 035802	13
642	Field emission from laser-processed niobium (110) single crystals. <b>2019</b> , 22,	2
641	Quasiparticle and excitonic effects in the optical response of KNbO3. <b>2019</b> , 3,	7
640	Second-harmonic generation in single-layer monochalcogenides: A response from first-principles real-time simulations. <b>2019</b> , 3,	11
639	Increasing the Sensitivity of an Optic Level Sensor With a Wavelength and Phase Sensitive Single-Mode Multimode Single-Mode Fiber Structure. <b>2017</b> , 17, 5515-5522	11
638	Single fiber reflectance spectroscopy calibration. <b>2017</b> , 22, 1-4	9
637	High-birefringence photonic crystal fiber polarization filter with gold-coated and liquid-filled air holes based on surface plasmon resonance. <b>2018</b> , 57, 1	1
636	Designing the measurement of the atomic mass density wave of a Gaussian mass-polariton pulse in optical fibers. <b>2019</b> , 58, 1	2
635	Accelerating optics design optimizations with deep learning. <b>2019</b> , 58, 1	17
634	Picosecond laser ablation on glass using wavelength of 1064, 532, and 355 nm. <b>2020</b> , 59, 1	3
633	Simulation of the influence of line edge roughness on the performance of deep ultraviolet wire grid polarizers. <b>2017</b> ,	2
632	Controlling quantum interference using metamaterials. 2019,	2

631	Subwavelength photonic hook generated by shaped fiber tip with asymmetric terahertz radiation. <b>2020</b> ,	1
630	Luminescent Properties of Carbon Nanodots Bound to the Surface of Spherical Microresonator. <b>2020</b> , 62, 1898-1904	1
629	A general framework for pearlescent materials. <b>2020</b> , 39, 1-15	6
628	An Experimental Method for Determination of the Refractive Index of Liquid Samples Using Michelson Interferometer. <b>2016</b> , 129, 59-63	5
627	D-shaped silicon core fiber-based surface plasmon-resonance refractive index sensor in 2 $\mu$ m. <b>2020</b> , 59, 5539	6
626	High concentration factor diffractive microlenses integrated with CMOS single-photon avalanche diode detector arrays for fill-factor improvement. <b>2020</b> , 59, 4488-4498	9
625	Surface plasmon resonance temperature sensor based on a photonic crystal fiber filled with silver nanowires. <b>2020</b> , 59, 5108-5113	18
624	Precise thickness profile measurement insensitive to spatial and temporal temperature gradients on a large glass substrate. <b>2020</b> , 59, 5881-5887	6
623	High-speed fiber-based spectrometer for plasma Thomson scattering. <b>2020</b> , 59, 7045-7052	1
622	Lossy mode resonance in an etched-out optical fiber taper covered by a thin ITO layer. <b>2020</b> , 59, 9254-9258	5
621	Design for a high birefringence photonic crystal fiber with multimode and low loss. 2018, 57, 6-13	8
620	Design and analysis for a bend-resistant and large-mode-area photonic crystal fiber with hybrid	
	cladding. <b>2018</b> , 57, 3976-3982	10
619		7
619 618	Cladding. <b>2018</b> , 57, 3976-3982  Design of a hybrid chalcogenide-glass on lithium-niobate waveguide structure for	
	Cladding. 2018, 57, 3976-3982  Design of a hybrid chalcogenide-glass on lithium-niobate waveguide structure for high-performance cascaded third- and second-order optical nonlinearities. 2019, 58, D1-D6  Theoretical and experimental investigation of broadband dispersion tailoring of high-order mode in	7
618	Cladding. 2018, 57, 3976-3982  Design of a hybrid chalcogenide-glass on lithium-niobate waveguide structure for high-performance cascaded third- and second-order optical nonlinearities. 2019, 58, D1-D6  Theoretical and experimental investigation of broadband dispersion tailoring of high-order mode in the hybrid microsphere cavity. 2019, 58, 1522-1529	7
618	Design of a hybrid chalcogenide-glass on lithium-niobate waveguide structure for high-performance cascaded third- and second-order optical nonlinearities. 2019, 58, D1-D6  Theoretical and experimental investigation of broadband dispersion tailoring of high-order mode in the hybrid microsphere cavity. 2019, 58, 1522-1529  Glucose sensing by absorption spectroscopy using lensed optical fibers. 2019, 58, 2456-2462  Structure design of a conic lens pair for improving the transmission efficiency of a Cassegrain	7 1 5

## (2018-2019)

613	Absorptive angular-selective filters consisting of dielectric multilayers combined with thin absorbing layers. <b>2019</b> , 58, 9094-9104	1
612	Determination of the fundamental absorption and optical bandgap of dielectric thin films from single optical transmittance measurements. <b>2019</b> , 58, 9585-9594	6
611	Highly flexible fiber delivery of a high peak power nanosecond Nd:YAG laser beam for flexiscopic applications. <b>2021</b> , 12, 444-461	1
610	Second-harmonic generation of second-order modes in thermally poled double-anode optical fibers. <b>2017</b> , 34, 2640	1
609	Supercontinuum generation by femtosecond flat-top laser pulses in fused silica. <b>2019</b> , 36, G6	4
608	Propagation of circularly and elliptically polarized few-cycle solitons in a Kerr medium. <b>2019</b> , 36, 312	6
607	Effect of the thermally excited lower laser level in a neodymium-doped fiber. 2019, 36, 736	6
606	Design of aluminum-based nanoring arrays for realizing efficient plasmonic sensors. <b>2019</b> , 36, 786	10
605	Self-referenced plasmonic sensor with TiO2 grating on thin Au layer: simulated performance analysis in optical communication band. <b>2019</b> , 36, F25	27
604	Surface-plasmon-based photonic crystal fibers for high-bandwidth filter realization. <b>2019</b> , 36, 1574	4
603	Exposed-core localized surface plasmon resonance biosensor. <b>2019</b> , 36, 2306	36
602	Multipass-cell-based post-compression of radially and azimuthally polarized pulses to the sub-two-cycle regime. <b>2019</b> , 36, 2517	7
601	Supercontinuum generation in seven-core fibers. <b>2019</b> , 36, 2927	6
600	Array of symmetric nanohole dimers with high sensitivity for detection of changes in an STT-RAM ultrathin dielectric layer. <b>2019</b> , 36, 3090	1
599	Asymmetric light transmission based on a 1D triangular metal grating. <b>2020</b> , 37, 1428	2
598	Hyperbolic metamaterial for the Tamm plasmon polariton application. <b>2020</b> , 37, 2215	17
597	Polarization gradient cooling and trapping of charged and neutral microspheres. <b>2021</b> , 38, 60	Ο
596	Investigation of different configurations and operation regimes of fiber pulse generators based on nonlinear spectral re-shaping. <b>2018</b> , 26, 27247-27264	21

595	Dual-polarized highly sensitive plasmonic sensor in the visible to near-IR spectrum. <b>2018</b> , 26, 30347-30361	99
594	Simultaneous measurement of refractive index and temperature for prism-based surface plasmon resonance sensors. <b>2019</b> , 27, 576-589	19
593	Effective optical properties of nanoparticle-mediated surface plasmon resonance sensors. <b>2019</b> , 27, 3091-3100	2
592	Axially-offset differential interference contrast microscopy via polarization wavefront shaping. <b>2019</b> , 27, 3837-3850	5
591	Optical diagnostic methods for monitoring the poling of thin-film lithium niobate waveguides. <b>2019</b> , 27, 12025-12038	12
590	Low-loss TeO-coated SiN waveguides for application in photonic integrated circuits. <b>2019</b> , 27, 12529-12540	12
589	On the calculation of the quality factor in contemporary photonic resonant structures. <b>2019</b> , 27, 14505-14522	31
588	Correction of spectral distortion in two-dimensional electronic spectroscopy arising from the wedge-based delay line. <b>2019</b> , 27, 15474-15484	5
587	Optical microscopy for measuring tapered fibers beyond the diffraction limit. <b>2019</b> , 27, 24403-24415	2
586	Functional lasing microcapillaries for surface-specific sensing. <b>2019</b> , 27, 26967-26978	5
585	Strong circular dichroism in chiral plasmonic metasurfaces optimized by micro-genetic algorithm. <b>2019</b> , 27, 28313-28323	27
584	Thickness uniformity measurements and damage threshold tests of large-area GaAs/AlGaAs crystalline coatings for precision interferometry. <b>2019</b> , 27, 36731-36740	7
583	End-to-end topology for fiber comb based optical frequency transfer at the 10 level. <b>2019</b> , 27, 36886-36902	10
582	Generating few-cycle pulses with integrated nonlinear photonics. <b>2019</b> , 27, 37374-37382	20
581	Ultrafast nonlinear refraction measurements of infrared transmitting materials in the mid-wave infrared. <b>2019</b> , 27, 37940	8
580	Parallel spectroscopic ellipsometry for ultra-fast thin film characterization. <b>2020</b> , 28, 9288-9309	9
579	Lasing in SiN-organic hybrid (SiNOH) waveguides. <b>2020</b> , 28, 5085-5104	6
578	Shape-dependent infrared reflectance properties of CNT forest metamaterial arrays. <b>2020</b> , 28, 607-625	7

577	Mid-IR Dirac-cone dispersion relation materialized in SOI photonic crystal slabs. <b>2020</b> , 28, 4194-4203	5
576	Ultra-narrowband polarization insensitive transmission filter using a coupled dielectric-metal metasurface. <b>2020</b> , 28, 773-787	13
575	Interaction and hybridization of orthogonal Fabry-Pfot like surface plasmon modes in metal-dielectric grating structures. <b>2020</b> , 28, 3541-3551	4
574	Doublet metalens design for high numerical aperture and simultaneous correction of chromatic and monochromatic aberrations. <b>2020</b> , 28, 18059-18076	21
573	Fused silica ablation by double femtosecond laser pulses: influence of polarization state. <b>2020</b> , 28, 15189-152	0 <b>¢</b>
572	Efficient second harmonic generation in nanophotonic GaAs-on-insulator waveguides. <b>2020</b> , 28, 9521-9532	22
571	Proposal for an ultra-broadband polarization beam splitter using an anisotropy-engineered Mach-Zehnder interferometer on the x-cut lithium-niobate-on-insulator. <b>2020</b> , 28, 10899-10908	21
570	Shallow-etched thin-film lithium niobate waveguides for highly-efficient second-harmonic generation. <b>2020</b> , 28, 19669-19682	23
569	Angle-resolved reflection spectra of Dirac cones in triangular-lattice photonic crystal slabs. <b>2020</b> , 28, 21601-21615	3
568	Ultrafast intermodal third harmonic generation in a liquid core step-index fiber filled with CCl. <b>2020</b> , 28, 25037-25047	4
567	Polarization-independent high diffraction efficiency two-dimensional grating based on cylindrical hole nano arrays. <b>2020</b> , 28, 28810-28818	5
566	Design of efficient radiative emission and daytime cooling structures with SiN and SiO nanoparticle laminate films. <b>2020</b> , 28, 35784-35794	1
565	Mode-splitting in a microring resonator for self-referenced biosensing. <b>2021</b> , 29, 346-358	6
564	Nanophotonic tantala waveguides for supercontinuum generation pumped at 1560 nm. <b>2020</b> , 45, 4192-4195	7
563	Exposure-dependent refractive index of Nanoscribe IP-Dip photoresist layers. <b>2019</b> , 44, 29-32	39
562	High-Q tellurium-oxide-coated silicon nitride microring resonators. <b>2019</b> , 44, 118-121	15
561	Long-term stable supercontinuum generation and watt-level transmission in liquid-core optical fibers. <b>2019</b> , 44, 2236-2239	8
560	Pump-probe multi-species CARS in a hollow-core PCF with a 20 ppm detection limit under ambient conditions. <b>2019</b> , 44, 2486-2489	2

559	Soliton supermode transitions and total red shift suppression in multi-core fibers. <b>2019</b> , 44, 4159-4162	4
558	Biosensing applications of all-dielectric SiO2-PDMS meta-stadium grating nanocombs. <b>2020</b> , 10, 1018	14
557	Simple technique for determining the refractive index of phase-change materials using near-infrared reflectometry. <b>2020</b> , 10, 1675	7
556	Optical materials for maximal nanophotonic response [Invited]. <b>2020</b> , 10, 1561	10
555	Optical properties of VO2 thin films deposited on different glass substrates. <b>2019</b> , 9, 663	11
554	Investigation and modeling of UV band-pass-filtering white compound materials for potting or embedding in micro-optical applications. <b>2019</b> , 9, 1002	3
553	Reducing leakage current during periodic poling of ion-sliced x-cut MgO doped lithium niobate thin films. <b>2019</b> , 9, 3146	17
552	Spacelime wave packets that travel in optical materials at the speed of light in vacuum. <b>2019</b> , 6, 139	46
551	Maximum length sequence dielectric multilayer reflector. <b>2018</b> , 1, 358	4
550	Insights from a systematic study of crosstalk in adiabatic couplers. <b>2019</b> , 2, 629	3
549	Temperature sensor based on liquid-filled negative curvature optical fibers. 2019, 2, 2123	10
548	High repetition rate flat coherent optical frequency comb generation based on the normal dispersion tantalum pentoxide optical waveguide. <b>2019</b> , 2, 2704	3
547	Four-wave mixing in high-Q tellurium-oxide-coated silicon nitride microring resonators.	4
546	Planar nanophotonic structures for intensity based readout refractive index sensing applied to dissolved methane detection. <b>2020</b> , 3, 3556	1
545	Ultra-broadband nanophotonic phase shifter based on subwavelength metamaterial waveguides. <b>2020</b> , 8, 359	14
544	Two optical sensing elements for H2O and NO2 gas sensing based on the single plasmonic $\square$ photonic crystal slab. <b>2020</b> , 9, 203-208	4
543	Numerical analysis of photonic crystal fibre with high birefringence and high nonlinearity. 2020,	4
542	Controlling the plasmon resonance via epsilon-near-zero multilayer metamaterials. <b>2020</b> , 9, 3637-3644	7

541	A Nonviscous Water-Based Pore Fluid for Modeling With Transparent Soils. <b>2015</b> , 38, 20140278	10
540	Past, Present, and Future of Transparent Soils. <b>2015</b> , 38, 20150079	57
539	ONE-WAY TOPOLOGICAL STATES ALONG VAGUE BOUNDARIES IN SYNTHETIC FREQUENCY DIMENSIONS INCLUDING GROUP VELOCITY DISPERSION (INVITED). <b>2020</b> , 169, 33-43	4
538	Ultrafast supercontinuum generation in bulk condensed media. <b>2017</b> , 57,	86
537	Optical Analysis of a ZnO/Cu<sub>2</sub>O Subcell in a Silicon-Based Tandem Heterojunction Solar Cell. <b>2017</b> , 07, 57-69	16
536	WPTherml: A Python Package for the Design of Materials for Harnessing Heat. <b>2019</b> , 7,	8
535	Metallo-Dielectric Colloidal Films as SERS Substrate.	1
534	Photonic crystal fibers with high nonlinearity, large birefringence and multiple zero dispersion-wavelength. <b>2014</b> , 63, 134210	2
533	SimultaneousIn situMeasurement of Silicon Substrate Temperature and Silicon Dioxide Film Thickness during Plasma Etching of Silicon Dioxide Using Low-Coherence Interferometry. <b>2012</b> , 51, 046201	2
532	A broadband single-polarization single-mode hollow core anti-resonant optical fiber. <b>2021</b> ,	
531	Near-Surface Buried Plasmonic Nanoparticles in Glass as Novel Nonlinear Saturable Absorbers for Ultrafast Lasers. 2101664	1
530	High-Performance Laterally Oriented Nanowire Solar Cells with Ag Gratings. <b>2021</b> , 11,	1
529	Analysis of non-idealities in rhomb compensators. <b>2021</b> , 29, 36328-36352	O
528	Numerical neural network approach to simultaneous material classification and sizing of aerosolized particles. <b>2021</b> , 107982	
527	Measurement of phase refractive index directly from phase distributions detected with a spectrally resolved interferometer. <b>2021</b> , 60, 10009-10015	1
526	Extraordinary transmission of gold-capped sphere arrays in mid-infrared range. <b>2021</b> , 29, 35191-35205	O
525	Time-frequency analysis of light-bullet dynamics during femtosecond filamentation in the anomalous dispersion regime. <b>2021</b> , 104,	О
524	High-efficient subwavelength-scale optofluidic waveguides with tapered microstructured optical fibers. <b>2021</b> , 29, 38068-38081	O

523	Strong optical non-reciprocity in one-dimensional photonic crystal containing a Weyl semimetal-based defect. <b>2021</b> , 121, 111583	1
522	Unidirectional propagation based on nonreciprocal defect modes in one-dimensional magneto-optical photonic crystals. <b>2021</b> , 248, 166230	1
521	MaPBI3 and 2D hybrid organic-inorganic perovskite based microcavities employing periodic, aperiodic, and disordered photonic structures with light-induced tuning possibility. <b>2021</b> , 12, 100105	
520	Tungsten oxide films by radio-frequency magnetron sputtering for near-infrared photonics. <b>2021</b> , 12, 100093	
519	The Optical Fibre. <b>2001</b> , 21-70	
518	Abkīzungsverzeichnis, physikalische Konstanten und Materialdaten. <b>2002</b> , 1-11	1
517	Einmodenfasern. <b>2002</b> , 80-213	4
516	Thermo-optic Effects of Bragg Grating Optical Temperature Sensor. <b>2002</b> , 3, 24-30	
515	Quantitative phase characterization and compensation by multiphoton intrapulse interference phase scan (MIIPS). <b>2006</b> , 526-529	
514	Q. <b>2007</b> , 355-378	
513	Methods of Cavity-Enhanced Laser Absorption Spectroscopy Using Microresonator Whispering-Gallery Modes. <b>2009</b> , 97-121	
512	Electron Beam Lithography for the Nanofabrication of Optical Devices. <b>2009</b> , 109-126	
511	One-dimensional photonic crystals with a planar oriented nematic layer: Temperature and angular dependence of the spectra of defect modes. <b>2010</b> , 106, 388	
511		
	dependence of the spectra of defect modes. <b>2010</b> , 106, 388  Multilongitudinal-mode fiber laser temperature sensor and its applications in the measurement of	
510	dependence of the spectra of defect modes. <b>2010</b> , 106, 388  Multilongitudinal-mode fiber laser temperature sensor and its applications in the measurement of temperature dependence of fiber birefringence. <b>2011</b> ,	
510	dependence of the spectra of defect modes. 2010, 106, 388  Multilongitudinal-mode fiber laser temperature sensor and its applications in the measurement of temperature dependence of fiber birefringence. 2011,  Entangled photon generation in microresonators via accidental degeneracies. 2012,	

505	Wellenausbreitung in dielektrischen Medien. <b>2014</b> , 13-55	
504	Study of 1550 nm low loss single mode all-solid photonic bandgap fibers. <b>2014</b> , 63, 074210	Ο
503	Suppressing Chirp of THz Pulses by Using an Optical Fiber as a Pulse Stretcher for Chirped Pulse Beating. <b>2014</b> ,	
502	Silica (Fused). <b>1971</b> , 68-69	
501	Optical Sources. <b>1979</b> , 499-556	
500	Fiber Characterization. <b>1979</b> , 343-399	
499	Structural Relaxation Effects in Dry Thermal Silicon Dioxide Films on Silicon. <b>1988</b> , 159-167	0
498	Modeling of Dispersion Effects in Optical Systems. <b>1989</b> , 268-275	2
497	Distortion of Femtosecond Laser Pulses in Optical Systems and Their Applications. <b>1990</b> , 168-174	
496	Materials for Waveguide Optoelectronics. <b>1992</b> , 1-19	
495	Optical Fibers. <b>1992</b> , 113-131	
494	Kinetics of Oxidation of Silicon by Electron Cyclotron Resonance Plasmas. <b>1993</b> , 55-62	
493	Coherent transmission technologies. <b>1995</b> , 43-102	
492	Simultaneous measurement of film and substrate optical parameters from multiple sample single wavelength ellipsometric data. <b>1999</b> , 6, 285-292	1
491	Aerogel Cherenkov detectors in colliding beam experiments. <b>2015</b> , 185, 540-548	1
490	The Spectral Properties of (SiO2)n, (GaN)m, (GaAs)m, (SiO2)n(GaN)m, and (SiO2)n(GaAs)m Nanoparticles: Computer Experiment. <b>2015</b> , 1-20	
489	Temporal walk-off affecting optical Kerr gating in the sub-ps time range. 2015,	
488	The Spectral Properties of (SiO2)n, (GaN)m, (GaAs)m, (SiO2)n(GaN)m, and (SiO2)n(GaAs)m Nanoparticles: Computer Experiment. <b>2016</b> , 745-767	

The Dispersion Characteristic of the Fused Quartz and the Dispersion Compensation of the Prism 487 Pair. 2016, 06, 136-148 Fabrication and Characterization of Micro-, Nano- and Hierarchically Structured Lotus-Like Surfaces. 486 2016, 97-203 Measuring the internal temperature of dielectrics machined by the ultrashort laser pulse through 485 the black-body irradiation method. **2016**, 65, 125201 Experimental studies of two sets of four-wave mixing processes in a single-zero-dispersion 484 microstructured fiber by the same pump. 2016, 65, 214201 Chapter 3 Modeling Nonlinear Optical Phenomena in Silicon Nanocrystal Structures. 2016, 61-108 483 Chapter 1 Elements of an Optical Microring Resonator. 2016, 1-52 482 481 Mode and Loss Analysis of a Graded Si1 ☐Gex StripWaveguide. 2017, 1 A Monte Carlo approach for investigating the fabrications imperfections for high-efficiency 480 metasurface solar concentrators. 2017, Mid-IR Generation by Difference Frequency Generation in a Hybrid Plasmonic Waveguide. 2017, 479 478 Optimal indium-gallium-nitride Schottky-barrier thin-film solar cells. 2017, Low cost ellipsometer using a standard commercial polarimeter. 2017, 477 Time-domain properties of femtosecond laser diffracted by transmitting blazed gratings. 2017, 476 Surface plasmon resonance biosensor based on D-shaped photonic crystal fiber. 2018, 475 Visible/Infrared narrow-band Resonant Absorber. 2018, 474 Dielectrics and Electrooptics. 2018, 813-899 473 Fundamentals. **2018**, 13-58 472 Polarizing Gires-Tournois interferometer as intra-cavity frequency-selective element in high-power 471 lasers. 2018, One-dimensional disordered photonic structures with two or more materials. 2018, 470

469	All solid nitroaniline-silica photonic bandgap fiber. <b>2018</b> ,	
468	Assessing microlens quality based on 3D irradiance measurement at the focal spot area. 2018,	
467	Structural color tuning in 1D photonic crystals with electric field and magnetic field. 2018,	
466	Refractive index and dispersion measurement using low-coherence interferometry with broadband confocal scanning. <b>2018</b> ,	
465	Spectroscopic measurements of asteroids allow mitigation of differential color refraction effects on ground-based astrometry and orbit prediction accuracy. <b>2018</b> ,	0
464	Opto-thermal characteristics of amorphous polyimides for optical applications. <b>2018</b> , 8, 2159	3
463	Tailoring of silicon nitride waveguide with ultra-flat and ultra-wide dispersion. 2018,	
462	Experimental validation of a 2D approximation method for investigating photonic components: case study refractive index sensor. <b>2018</b> ,	
461	Simple spectral reduction algorithm used for the echelle spectrometer. <b>2018</b> , 57, 8921-8927	2
460	Demonstration of time-of-flight technique with all-optical modulation and MCT detection in SWIR/MWIR range. <b>2018</b> ,	
459	Enhancement of plasma resonance in a Hi-Bi D-shaped photonic crystal fiber SPR sensor. 2018,	
458	Reflective metasurface with a funnel shaped waveguide array for electromagnetic field enhancement. <b>2018</b> ,	
457	[h-gap \$pectroscopy: Reflected-Wave Phase and Film Characterization. 2018, 63, 957	
456	Light Harvesting and Biomass Generation. <b>2019</b> , 13-30	
455	Introduction and Background Information. <b>2019</b> , 1-9	
454	Broadband and low confinement loss photonic crystal fibers supporting 48 orbital angular momentum modes. <b>2019</b> ,	1
453	Spatially resolved cross-sectional refractive index profile of fs laser-written waveguides using a genetic algorithm. <b>2019</b> , 27, 2488-2498	4
452	Soliton Dynamics in Multi-Core Fibers: Supermode Transitions and Raman-Shift Suppression. <b>2019</b> ,	

451	Bloch surface wave excitation using a maximum length sequence grating structure. <b>2019</b> ,
450	Design of photonic crystal fiber for efficient supercontinuum generation. 2019,
449	Polarization wavefront shaping for quantitative phase contrast imaging by axially-offset differential interference contrast (ADIC) microscopy. <b>2019</b> ,
448	Passive and active whispering gallery mode microresonators in optical engineering. 2019,
447	Photoconverter with luminescent concentrator. Matrix material. <b>2019</b> , 22, 80-87
446	Simulation of single mode optical waveguide and Mach-Zehnder interferometer in deep-ultraviolet band. <b>2019</b> ,
445	RGB wavelength demultiplexer based on PCF/POF structure. <b>2019</b> ,
444	Laser beam diffraction inspection of periodic metal/oxide structures with submicron period. 2019,
443	Surface electromagnetic wave sensor utilizing a one-dimensional photonic crystal. <b>2019</b> ,
442	Low-cost fabrication of functional plasmonic fiber-optic-based sensors using microsphere photolithography. <b>2019</b> ,
441	Optical and thermal modeling of Ti-doped optothermal fiber converter for laser surgery. <b>2019</b> , 1
440	Plasma-mirror frequency-resolved optical gating using a liquid-sheet jet in ultraviolet region. <b>2019</b> , 44, 3234-3237
439	Dispersion of chromia films (eskolaite) in UV-VIS. <b>2019</b> , 70, 36-43
438	Deep neural network (DNN) surrogate models for the accelerated design of optical devices and systems. <b>2019</b> ,
437	Ni subwavelength grating/SiO2/Ag based optical magnetic field sensor with normal incident geometry. <b>2019</b> ,
436	Second-harmonic-generation enhancement in cavity resonator integrated grating filters. <b>2019</b> , 44, 5198-5201 $_4$
435	Performance improvement of refractive index sensor based on two-dimensional metal-dielectric grating. <b>2019</b> ,
434	Highly Sensitive Retro-Reflectance Fiber-Optic Sensors for Liquid-Liquid Interface Detection. <b>2019</b> ,

433	Prospects for continuous-wave molecular modulation in Raman-active microresonators. <b>2019</b> , 27, 34154-3416	<b>58</b> 0
432	Ultrafast nonlinear refraction measurements of infrared transmitting materials in the mid-wave infrared. <b>2019</b> , 27, 37940-37951	4
431	Supresili de una lilea de emisili infrarroja a 1550 nm, mediante un sistema de rejilla Bragg de fibra ptica sintonizada por tensili mecilica. <b>2020</b> , 24, 97-101	
430	Accurate measurements of phase refractive index of soft contact lenses. <b>2020</b> , 28, 10818-10835	
429	Determination of refractive index, size, and solid content of monodisperse polystyrene microsphere suspensions for the characterization of optical phantoms. <b>2020</b> , 11, 1901-1918	2
428	Dependencia de la sensibilidad en un cristal fotflico unidimensional con el figulo incidente de la radiacifi para la deteccifi de clula cancergenas. <b>2020</b> , 23, 181-195	
427	Approximation of Fabry-Plot resonances in Ag/quartz/Ag structures. 2020,	1
426	Optical properties of PlatSil SiliGlass tissue-mimicking phantoms. <b>2020</b> , 11, 3753-3768	2
425	Simulations of photothermal effects and thermodynamics induced by optical resonance in a fiber metallic Fabry-Perot cavity. <b>2020</b> , 59, 6466-6475	1
424	Single-shot multispectral birefringence mapping by supercontinuum vector beams. <b>2020</b> , 59, 7131-7138	1
423	Omnidirectional and compact transmissive chromatic polarizers based on a dielectric-metal-dielectric structure. <b>2020</b> , 28, 25073-25084	2
422	Nonlinear pulse reshaping in a typically designed silicon on insulator waveguide and its application to generate high repetition rate pulse train.	3
421	Thin Film Reflectance Model for Trap Detector. 2021,	
420	Graphene-based dual-band near-perfect absorption in Rabi splitting between topological edge and Fabry-Perot cavity modes.	2
419	References. <b>1983</b> , 597-642	
418	Dual-Side Polished SPR Biosensor with Wide Sensing Range. <b>2020</b> ,	O
417	Interface-induced field-like optical spin torque in a ferromagnet/heavy metal heterostructure. <b>2021</b> , 10, 1169-1176	2
416	Surface Enhanced Raman Scattering of Silver Nanoparticles with Slot Waveguide. <b>2020</b> ,	

Lossy Mode Resonance Sensors Based on Double ITO/TiO2 and Triple TiO2/ITO/TiO2 Thin Film Coated Single Mode Fiber Taper. **2020**, 65, 1457-1459

414	Diamond diffractive opticsEecent progress and perspectives. <b>2021</b> , 10, 19-30	O
413	Realization of a tunable fiber-based double cavity system. <b>2020</b> , 102,	3
412	Frequency-domain calculation of Smith-Purcell radiation for metallic and dielectric gratings. <b>2020</b> , 59, 11146-11155	4
411	Micro-spectroscopy of Buried Short-Range Surface Plasmon Polaritons Supported by Thin Polycrystalline Gold Films. <b>2021</b> , 16, 737-746	1
410	Characterization and application of nonlinear plastic materials for post-CPA pulse compression. <b>2020</b> , 45, 6575-6578	1
409	Non-Zero Dispersion-Shifted Ring Fiber for OAM Mode. <b>2020</b> ,	1
408	2D modeling of silicon optical PN phase shifter. <b>2020</b> , 59, 998-1007	1
407	Theoretical Implications for Surface Plasmon Resonance Based on Microstructured Optical Fiber. <b>2020</b> , 43-52	
406	Angular Dependence of Ionoluminescence for Silica Case. <b>2020</b> ,	
405	Simultaneously Detecting of Temperature and Concentration of Ethanol liquid by using Surface Plasmon Resonance. <b>2020</b> ,	
404	Broadly tunable laser based on novel metallic resonant leaky-mode diffraction grating. <b>2020</b> , 28, 4340-4346	3
403	Radiative Properties of Nanomaterials. <b>2020</b> , 497-622	
402	Non-Zero Dispersion-Shifted and Dispersion-Flatted Air-Core Ring Fiber for OAM Mode. <b>2020</b> ,	
401	Dual scanning interferometric technique for measurements of the temperature and concentration dependence of the refractive index of liquids. <b>2020</b> , 32, 015907	1
400	Enhanced extinction ratios of metasurface polarizers by surface-plasmon interference. <b>2020</b> , 37, 673	1
399	Three-dimensional laser damage positioning by a deep-learning method. <b>2020</b> , 28, 10165-10178	О
398	Transient grating in a thin gas target for characterization of extremely short optical pulses. <b>2020</b> , 45, 2231-2234	

397	Subwavelength high-performance polarizers in the deep ultraviolet region. <b>2020</b> , 28, 11652-11665	Ο
396	Resonance characteristics of transmissive optical filters based on metal/dielectric/metal structures. <b>2020</b> , 44, 219-228	2
395	A temperature sensor based on D-shape photonic crystal fiber coated with AulliO2 and AgliiO2. <b>2021</b> , 53, 1	1
394	Angle-Resolved Hollow-Core Fiber-Based Curvature Sensing Approach. <b>2021</b> , 9, 72	O
393	Sensitivity of lossy mode resonance-based optical fiber sensors as a function of the coating material refractive index. <b>2021</b> , 75, 1	3
392	Mode-Center Placement of Monolayer WS2 in a Photonic Polymer Waveguide. 2101684	1
391	Refractive index spectroscopy and material dispersion in fused silica glass. <b>2020</b> , 45, 4268-4271	3
390	Simple technique for determining the refractive index of phase-change materials using near-infrared reflectometry. <b>2020</b> , 10, 1675	
389	Analysis of material concentration in step-index fibers with alumina cores produced by means of the powder-in-tube technique. <b>2020</b> , 28, 28283-28294	
388	Plasmonic nanoarcs: a versatile platform with tunable localized surface plasmon resonances in octave intervals. <b>2020</b> , 28, 30889-30907	2
387	Black and white fused silica: modified sol-gel process combined with moth-eye structuring for highly absorbing and diffuse reflecting SiO glass. <b>2020</b> , 28, 32499-32516	1
386	Tuning the optical response in sputtered multilayered metal-dielectric thin films. <b>2020</b> , 3, 3061	
385	Transient optical properties of highly excited dielectric materials: Apparent birefringence and delayed reflectivity increase. <b>2020</b> , 2,	5
384	Design of binary-phase diffusers for a compressed sensing snapshot spectral imaging system with two cameras. <b>2020</b> , 59, 7853-7864	2
383	Predicting the refractive index of amorphous materials using the Bruggeman effective medium approximation. <b>2020</b> , 59, 8822-8827	1
382	Laser beam shaping improves the transmission efficiency of Cassegrain antenna. 2020,	
381	Slow light nanocoatings for ultrashort pulse compression. <b>2021</b> , 12, 6518	1
380	Determining the Surface Potential of Charged Aqueous Interfaces Using Nonlinear Optical Methods. <b>2021</b> , 125, 25307-25315	4

379	Lossy mode resonances in photonic crystal fibers. <b>2021</b> , 17,	O
378	Thermally Tunable Orbital Angular Momentum Mode Generator Based on Dual-Core Photonic Crystal Fibers <b>2021</b> , 11,	O
377	Precision size and refractive index analysis of weakly scattering nanoparticles in polydispersions.	1
376	Microscopical Quantification of Ion-Induced Nanodefects in Monolayer MoS2 Based on Differential Reflectance. <b>2022</b> , 9, 2101612	1
375	High resolution graphene angle sensor based on ultra-narrowband optical perfect absorption. <b>2021</b> , 29, 41206	2
374	Particle swarm optimization of polymer-embedded broadband metasurface reflectors.	1
373	Interdigitated Three-Dimensional Heterogeneous Nanocomposites for High-Performance Mechanochromic Smart Membranes. <b>2021</b> ,	4
372	High-Sensitivity Tunable Bloch Surface WavesBiosensor Using Nanocomposite Cap Layer. 2100607	1
371	Highly Dispersive Germanium-Doped Coupled Ring-Core Fiber for Vortex Modes. 2021, 1-1	2
370	A cost-effective edge coupler with high polarization selectivity for thin film lithium niobate modulators. <b>2021</b> , 1-1	3
369	Single-Material, Near-Infrared Selective Absorber Based on Refractive Index-Tunable Tamm Plasmon Structure. 2102388	0
368	Characteristics of Ultrasensitive Hexagonal-Cored Photonic Crystal Fiber for Hazardous Chemical Sensing. <b>2022</b> , 9, 38	1
367	Numerical finite-difference time-domain calculation for extreme enhancement of magneto-optical effect at ultraviolet wavelength using Ni-subwavelength grating on SiO2/Ni structure. 1	
366	Aplanatic meniscus lens corrector for Ritchey-ChrEien telescopes <b>2022</b> , 30, 6076-6089	O
365	Ultra-Short Dual-Core Photonic Crystal Fiber Polarization Beam Splitter with Round Lattice and As2S3-Filled Center Air Hole. <b>2022</b> , 9, 36	0
364	Femtosecond LIPSS on indium-tin-oxide thin films at IR wavelengths <b>2022</b> , 61, 386-391	0
363	Enhancement of Optical Coupling Efficiency of Surface Plasmon Resonance Based Sensors. <b>2022</b> , 10, 879-892	0
362	Design of an Integrated Bell-State Analyzer on a Thin-Film Lithium Niobate Platform. <b>2022</b> , 14, 1-9	О

361	Design of absorptive multilayer coatings for satellite thin-film solar cells and studying the dispersion effect on them. <b>2022</b> , 252, 168504	0
360	Heterogeneous Gas-filling in Anti-resonant Hollow Core Fibers. 2020,	
359	Sensitivity Enhancement of a bi-metallic Surface Plasmon Resonance based Sensor Using Poynting vector Analysis. <b>2021</b> ,	
358	Surface Plasmon Resonance Refractive Index Sensor Based on Photonic Crystal Fiber with Silver Film and Titanium Dioxide Film. <b>2021</b> ,	O
357	Active Compensation of Radiation Effects on Optical Fibers for Sensing Applications 2021, 21,	0
356	Geometric effects of plasmonic nanoscale heterostructures on infrared activity. 2022, 39, 651	
355	Influence of non-Hermitian mode topology on refractive index sensing with plasmonic waveguides.	0
354	Optical Janus Effect in Large Area Multilayer Plasmonic Films. 2100333	
353	Optical Fibers. <b>2022</b> , 67-168	
352	PVP-Capped Gold Nanoparticles: Thermal Nonlinear Refraction Probed by Spatial Self-Phase Modulation. 2100600	
351	Chiral Hybrid Copper(I) Halides for High Efficiency Second Harmonic Generation with a Broadband Transparency Window.	
350	Interpreting light guidance in antiresonant and photonic bandgap waveguides and fibers by light scattering: analytical model and ultra-low guidance <b>2022</b> , 30, 2768-2779	Ο
349	Powerful supercontinuum vortices generated by femtosecond vortex beams with thin plates.	2
348	Impact of Mode-Area Dispersion on Nonlinear Pulse Propagation in Gas-Filled Anti-Resonant Hollow-Core Fiber. <b>2022</b> , 9, 25	
347	Simple, efficient and accurate method toward the monitoring of ethyl butanoate traces 2022, 54, 126	Ο
346	Photon spin angular momentum driven magnetization dynamics in ferromagnet/heavy metal bilayers. <b>2022</b> , 131, 023901	Ο
345	Chiral Hybrid Copper(I) Halides for High Efficiency Second Harmonic Generation with a Broadband Transparency Window <b>2022</b> ,	12
344	Characteristic parameters of photonic nanojets of single dielectric microspheres illuminated by focused broadband radiation <b>2022</b> , 12, 173	O

343	Tailored Multi-Color Dispersive Wave Formation in Quasi-Phase-Matched Exposed Core Fibers <b>2022</b> , e2103864	2
342	Biosensor based on plasmonic Mach-Zehnder interferometer with metallic gratings. <b>2022</b> , 71, 017301	
341	Using lossy mode resonance for in situ measurement of the refractive index of a layer deposited on an optical fiber lateral surface <b>2022</b> , 47, 361-364	O
340	Dual elliptical core-based photonic crystal sensor for detection of ultra-low-level bioethanol concentration. 1	
339	Metasurface-based solar absorber with absorption prediction using machine learning. <b>2022</b> , 124, 112049	10
338	Boosting the SiN nonlinear photonic platform with transition metal dichalcogenide monolayers <b>2022</b> , 47, 734-737	
337	Reducing bend-induced loss and crosstalk in a two-mode ridge waveguide by steplike thickness structuring <b>2022</b> , 61, 1164-1170	1
336	PHz Electronic Device Design and Simulation for Waveguide-Integrated Carrier-Envelope Phase Detection. <b>2022</b> , 1-1	
335	Highly Birefringent Anti-Resonant Hollow-Core Fiber with a Bi-Thickness Fourfold Semi-Tube Structure. 2100365	2
334	Understanding Haze: Modeling Size-Resolved Mineral Aerosol from Satellite Remote Sensing. <b>2022</b> , 14, 761	O
333	Flow Regime and Reynolds Number Variation Effects on the Mixing Behavior of Parallel Flows. <b>2022</b> , 110619	0
332	Visible and near-infrared programmable multi-level diffractive lenses with phase change material SbS <b>2022</b> , 30, 6808-6817	2
331	Integrated photonics enables continuous-beam electron phase modulation 2021, 600, 653-658	4
330	Study of Highly Coherent Mid-Infrared Supercontinuum Generation in CMOS Compatible Si-rich SiN Tapered Waveguide. <b>2022</b> , 1-1	O
329	Environmentally Sustainable Electroplating of Selective Cobalt-Chromium Coating on Stainless Steel for Efficient Solar Collectors.	
328	All-dielectric magnetophotonic gratings for maximum TMOKE enhancement 2022,	2
327	Mie scattering from optically levitated mixed sulfuric acid-silica core-shell aerosols: observation of core-shell morphology for atmospheric science <b>2022</b> ,	1
326	Monitoring the gold nanoshell growth mechanism: stabilizing and destabilizing effects of PEG-SH molecules <b>2022</b> ,	

325	An Efficient Technique for Evaluating the Characteristics of a Polarization Converter Consisting of an Asymmetric Waveguide. <b>2022</b> , 1-1	1
324	Dispersion Effects of Materials on Dielectric Nanophotonic Devices. 2022,	
323	Agcu/Tio2 Hot-Electron Device for Solar Water Splitting: The Mechanisms Of Lspr and Time-Domain Characterization.	
322	Microstructured fiber sensor based on resonance coupling between cladding mode and surface plasmon mode for sucrose determination. <b>2022</b> , 1-1	
321	Femtosecond imaging of spatial deformation of surface plasmon polariton wave packet during resonant interaction with nanocavity. <b>2022</b> , 11, 1321-1333	О
320	Dynamic ellipsometry measurement based on a simplified phase-stable dual-comb system <b>2022</b> , 30, 7806-7820	
319	Electronic, Structural, and Mechanical Properties of SiO_{2} Glass at High Pressure Inferred from its Refractive Index <b>2022</b> , 128, 077403	2
318	Machine-Engineered Active Disorder for Digital Photonics. <b>2022</b> , 10, 2102642	Ο
317	Broadband and tunable bandgap guidance based on ring-pattern liquid-filled photonic crystal fibers <b>2022</b> , 47, 2157-2160	О
316	Efficient coupling between single mode fibers and glass chip waveguides via graded refractive index fiber tips <b>2022</b> , 30, 12294-12307	Ο
315	Textured concave anti-reflecting coating and convex back reflector to enhance the absorbance of amorphous Si solar cells. <b>2022</b> , 97, 055503	0
314	Generation of stable temporal doublet by a single-mode silicon core optical fiber. <b>2022</b> , 24, 055503	1
313	Real-time measurement of parametric influences on the refractive index and length changes in silica optical fibers <b>2022</b> , 30, 15659-15668	0
312	Efficient low threshold frequency conversion in AlGaAs-on-insulator waveguides. 2022,	Ο
311	Long Range Raman-Amplified Distributed Acoustic Sensor Based on Spontaneous Brillouin Scattering for Large Strain Sensing <b>2022</b> , 22,	
310	Design study for an efficient semiconductor quantum light source operating in the telecom C-band based on an electrically-driven circular Bragg grating <b>2022</b> , 30, 10919-10928	1
309	Analyzing Anisotropy in 2D Rhenium Disulfide Using Dichromatic Polarized Reflectance <b>2022</b> , e2108028	3
308	10kW rectangular laser beam generation with incoherent space combiner. <b>2022</b> , 169011	

307	Computational upper-limit of directional light emission in nano-LED via inverse design <b>2022</b> , 30, 9008-9020	1
306	Sub-10´fs´pulse´generation´by´post-compression for peak-power enhancement of a 100-TW Ti:Sapphire laser <b>2022</b> , 30, 8734-8741	2
305	Selective broadband absorption by mode splitting for radiative cooling 2022, 30, 14258-14273	0
304	Internal phase control of coherent fiber laser array without ambiguous phase based on double wavelength detection <b>2022</b> , 61, 3429-3434	O
303	Refractometric Detection of Adulterated Milk Based on Multimode Interference Effects 2022, 11,	
302	Time-varying orbital angular momentum in tight focusing of ultrafast pulses <b>2022</b> , 30, 13416-13433	1
301	A method to eliminate the zeroth order with low polarization-independent loss by a transmission grating. <b>2022</b> , 169049	
300	Dynamic Tomographic Phase Microscopy by Double Six-Pack Holography <b>2022</b> , 9, 1295-1303	1
299	Performance optimization of a metasurface incorporating non-volatile phase change material <b>2022</b> , 30, 12982-12994	
298	High-sensitivity refractive index sensor with cascaded dual-core photonic crystal fiber based on vernier effect. <b>2022</b> , 256, 168488	1
297	Design of Ultra-Dispersion Flattened M-type Few-Mode Fiber for Weakly-coupled Mode Division Multiplexing Transmission. <b>2022</b> , 169040	
296	Photonic nanojet of a Gaussian beam illuminated low refractive index microsphere in air: A comprehensive variation of parameters. <b>2022</b> , 282, 108121	1
295	The effect of interface roughness on spectral efficiency of thermophotovoltaics with multi-layer filters. <b>2022</b> , 257, 168663	
294	The Bresnel Equations For Diffuse radiation on Inclined photovoltaic Surfaces (FEDIS). 2022, 161, 112362	2
293	Performance of nanoimprinted and nanocoated optical label-free biosensor - nanocoating properties perspective. <b>2022</b> , 153, 107009	1
292	Hybrid additive manufacturing for the fabrication of freeform transparent silica glass components. <b>2022</b> , 54, 102727	O
291	Electric and magnetic dipole emission of Eu3+: Effect of proximity to a thin aluminum film. <b>2022</b> , 246, 118778	1
290	Fluorescence properties of ions adsorbed from aqueous solutions on fused silica and CaF2 - Test cases of Eu3+ and Tb3+. <b>2022</b> , 247, 118865	

289	High-efficiency multi-port beam control device based on periodic nanodisk arrays. 2022, 152, 108102	O
288	The Magneto-Optical Voigt Parameter from Magneto-Optical Ellipsometry Data for Multilayer Samples with Single Ferromagnetic Layer. <b>2021</b> , 63, 1485-1495	
287	Features of Light Localization by an Inhomogeneous Film. <b>2021</b> , 47, 717-720	1
286	Unveiling the Coupling of Single Metallic Nanoparticles to Whispering-Gallery Microcavities 2021,	4
285	Talbot self-imaging and two-photon interference in ring-core fibers. 2021, 104,	0
284	Continuous-wave generation of photon pairs in silica nanofibers using single-longitudinal- and multilongitudinal-mode pumps. <b>2021</b> , 104,	O
283	Design of Nanoarchitectures for Magnetoplasmonic Biosensing with Near-Zero-Transmittance Conditions. <b>2021</b> ,	2
282	A Mechanically Reliable Transparent Antifogging Coating on Polymeric Lenses. <b>2022</b> , 9, 2101864	2
281	Single-Port Coherent Perfect Loss in a Photonic Crystal Nanobeam Resonator 2021, 11,	
280	Fused silica based photonic crystal fiber with small modal area and high nonlinearity. 2021,	
279	Design, fabrication, and characterization of a low-index center and trench-assisted 7-ring-core 5-mode-group fiber for dense space-division multiplexing <b>2022</b> , 30, 650-663	1
278	Angular Interrogation-Based Self-Referenced LMR Sensor With High Sensitivity and High Figure of Merit. <b>2021</b> , 33, 1463-1466	O
277	Hybrid Plasmonic SOI Ring Resonator for Bulk and Affinity Bio - sensing Applications. 1	1
<sup>2</sup> 77	Hybrid Plasmonic SOI Ring Resonator for Bulk and Affinity Bio - sensing Applications. 1  Surface plasmon resonance based tunable D-shaped single polarization filter at the communication band. 2022, 12, 1947	1
	Surface plasmon resonance based tunable D-shaped single polarization filter at the communication	1
276	Surface plasmon resonance based tunable D-shaped single polarization filter at the communication band. <b>2022</b> , 12, 1947  Volumetric additive manufacturing of silica glass with microscale computed axial lithography <b>2022</b>	
276 275	Surface plasmon resonance based tunable D-shaped single polarization filter at the communication band. 2022, 12, 1947  Volumetric additive manufacturing of silica glass with microscale computed axial lithography 2022, 376, 308-312  In-Depth Conceptual Study of an Enhanced Plasmonic Sensing System Using Antireflective Coatings	11

271 Table\_1.DOCX. **2019**,

270	Implementing a Thin-Film Reflectance Model for Trap Detectors at the SCL. <b>2022</b> , 14, 28-32	
269	GaP Nanowire Waveguides. <b>2022</b> ,	
268	Fast long-distance transport of cold cesium atoms. <b>2022</b> , 105,	1
267	High sensitivity surface plasmon resonance sensor based on D-shaped high birefringence photonic crystal fibre. 1-8	
266	Plasmon mode manipulation based on multi-layers hyperbolic metamaterials.	2
265	Giant optical anisotropy of WS2 flakes in the visible region characterized by Au substrate assisted near-field optical microscopy <b>2022</b> ,	
264	A database of refractive indices and dielectric constants auto-generated using ChemDataExtractor <b>2022</b> , 9, 192	1
263	Effect of rare-earth oxide additives on transparency and fluorescence of BiAlON ceramics. 2022,	0
262	Spectral and polarization based imaging in deep-ultraviolet excited photoelectron microscopy. <b>2022</b> , 93, 053701	
261	Targeted dielectric coating of silver nanoparticles with silica to manipulate optical properties for metasurface applications. <b>2022</b> , 126250	4
260	Residual stress of glass and crystalline oxide thin films responding to humidity. <b>2022</b> , 120, 193301	
259	Demonstration of Tunable Fano Resonances in a Meta-material Absorber Composed of Asymmetric Double Bars with Bent Arms. 1	
258	Precision size and refractive index analysis of weakly scattering nanoparticles in polydispersions <b>2022</b> , 19, 586-593	3
257	Polyhedral-Au@SiO2@Au CoreBhell Nanoparticle Reveals a Broadband and Tunable Strong Local Field Enhancement. <b>2022</b> , 126, 8165-8176	1
256	Improving the efficiency counting of Cherenkov detector by using high transmittance photonic crystal materials. <b>2022</b> , 54,	
255	Graphene-assisted tunable D-shaped photonic crystal fiber sensor in the visible and IR regions. <b>2022</b> , 39, 1490	2
254	A Bend-resistant Photonic Crystal Fiber with Large Effective Mode Area. <b>2022</b> , 71, 102902	

253	Inspection of an HSH-PCF for optical Communication with high Non-linearity, birefringence and negative dispersion. <b>2022</b> , 61, 11139-11147	0
252	Repulsive Casimir-Polder potentials of low-lying excited states of a multilevel alkali-metal atom near an optical nanofiber. <b>2022</b> , 105,	Ο
251	Source coherence-induced control of spatiotemporal coherency vortices.	О
250	Crescent-Shaped Shadow of Second Harmonic Generation in Dielectric Microsphere/TMD Monolayer Heterostructure.	1
249	A Theoretical Study of the Temperature Sensor Based on the LP01-LP02 Intermodal Interference in Optical Fiber with a Liquid Core. <b>2010</b> , 12, 10-13	2
248	The visual appearances of disordered optical metasurfaces 2022,	4
247	Nanostructured photosensitive layerfor Tamm-plasmon-polariton-based organic solar cells.	0
246	Formation of Colloidal Chains and Driven Clusters with Optical Binding.	
245	Tailorable Stimulated Brillouin Scattering in a Partially Suspended Aluminium Nitride Waveguide in the Visible Range.	
244	Enhancing Plasmon Excitation of Small Au Nanoparticles via Light Scattering from Metal-Oxide Supports.	O
243	Broadband Spectral Shaping of Regenerative Amplification with Extra-Cavity Waveplate for Cross Polarized Wave Generation. <b>2022</b> , 12, 5521	
242	Enhanced circular dichroism of cantilevered nanostructures by distorted plasmon.	O
241	Polarization Independent Metamaterial Absorber with Anti-Reflection Coating Nanoarchitectonics for Visible and Infrared Window Applications. <b>2022</b> , 15, 3733	1
	pp	
240	Extraction of silver losses at cryogenic temperatures through the optical characterization of silver-coated plasmonic nanolasers. <b>2022</b> , 30, 21664	
240	Extraction of silver losses at cryogenic temperatures through the optical characterization of	1
	Extraction of silver losses at cryogenic temperatures through the optical characterization of silver-coated plasmonic nanolasers. <b>2022</b> , 30, 21664  Long-Term Trend Analysis in the Solar Radiation and Climate Experiment (SORCE)/Spectral	1 0
239	Extraction of silver losses at cryogenic temperatures through the optical characterization of silver-coated plasmonic nanolasers. 2022, 30, 21664  Long-Term Trend Analysis in the Solar Radiation and Climate Experiment (SORCE)/Spectral Irradiance Monitor (SIM). 2022, 297,  Wide refractive index detection range surface plasmon resonance sensor based on D-shaped	

235 Photonic crystal fibers for various sensing applications. **2022**, 3-21

234	Towards <i>in-situ</i> diagnostics of multi-photon 3D laser printing using optical coherence tomography. <b>2022</b> , 3, 1	1
233	Self-Rolling SiO 2 /Au Based Epsilon-Near-Zero Metamaterials. 2200081	O
232	Efficient Low Threshold Frequency Conversion in AlGaAs-On-Insulator Waveguides. 3,	
231	AMORPHOUS SILICON CARBIDE HIGH CONTRAST GRATINGS AS HIGHLY EFFICIENT SPECTRALLY SELECTIVE VISIBLE REFLECTORS.	О
230	Nanoscale Optical Trapping by Means of Dielectric Bowtie. <b>2022</b> , 9, 425	2
229	Dual-parameter detection with an open-loop dual-core plasmonic optical fiber sensor. <b>2022</b> , 1, 1441	
228	Pulsewidth-dependent critical power for self-focusing of ultrashort laser pulses in bulk dielectrics.	1
227	Evaporation-Induced Self-Assembly of Metal Oxide Inverse Opals: From Synthesis to Applications.	4
226	Nonlinear pulse compression to 51 W average power GW-class 35 fs pulses at 2 µm wavelength in a gas-filled multi-pass cell.	1
225	Design of High-Sensitivity Surface Plasmon Resonance Sensor Based on Nanostructured Thin Films for Effective Detection of DNA Hybridization.	0
224	Focal shift and focal switch of broadband hollow Gaussian beams passing through an aperture-lens system. <b>2022</b> , 76,	
223	Environmentally sustainable electroplating of selective cobalt-chromium coating on stainless steel for efficient solar collectors. <b>2022</b> , 245, 111821	О
222	1.3-Octave Coherent Supercontinuum Generation of OAM Mode in Ring-Core Fiber with All-Normal Dispersion. <b>2022</b> , 1-1	
221	Integration of on-chip perovskite nanocrystal laser and long-range surface plasmon polariton waveguide with etching-free process.	2
220	Mode transitions and thickness measurements during deposition of nanoscale TiO2 coatings on tilted fiber Bragg gratings. <b>2022</b> , 1-5	O
219	Excitation of Hybrid Waveguide-Bloch Surface States with Bi2Se3 Plasmonic Material in the Near-Infrared Range. <b>2022</b> , 13, 1020	
218	Analytical formalism for perturbative chromatic dispersion.	

217	Role of Substrate Type in the Process of Polyelectrolyte Multilayer Formation. 2022, 14, 2566	O
216	Optical force between two coupled identical parallel optical nanofibers. 2022, 105,	
215	Sub-2-fs ultrashort optical pulses characterized by spectral phase interferometry for direct electric-field reconstruction.	
214	Modulation instability induced supercontinuum generation in defective core photonic crystal fiber. <b>2022</b> , 54,	
213	Electron dynamics in fused silica after strong field laser excitation detected by spectroscopic imaging pump-probe ellipsometry. <b>2022</b> , 106,	
212	Spectral tailoring of photon pairs from microstructured suspended-core optical fibers with liquid-filled nano channels.	
211	Simultaneous measurement of displacement and temperature using balloon-like hybrid fiber sensor.	
210	Infrared nanoplasmonic properties of hyperdoped embedded Si nanocrystals in the few electrons regime. <b>2022</b> ,	1
209	Large-area patterning for broadband, quasi-omnidirectional low-reflectance glass. 2022, 32, 085009	
208	Depletion of Polyelectrolytes near Like-Charged Substrates Probed by Optical Reflectivity.	O
207	Broadband metasurface aberration correctors for hybrid meta/refractive MWIR lenses.	1
206	Graphene-assisted synthesis NH3 gas sensor based on Silicon photonics crystal fiber and surface plasmon resonance. <b>2022</b> , 169654	
205	Observation of Two-dimensional Isotropic Double Dirac Cones in the Electromagnetic Dispersion Relation. <b>2022</b> , 91,	
204	Photonic Crystal Fiber Modulator Based on Surface Plasmon Resonance. <b>2022</b> , 169691	
203	Molybdenum Oxide Functional Passivation of Aluminum Dimers for Enhancing Optical-Field and Environmental Stability. <b>2022</b> , 9, 523	
202	Critical problems faced in Raman-based energy transport characterization of nanomaterials.	O
201	Enhancement of the contrast for a hexagonal boron nitride monolayer placed on a silicon nitride/silicon substrate. <b>2022</b> , 15, 086502	
200	Bulk Plasmon Polariton Modes in Hyperbolic Metamaterials for Giant Enhancement of the Transverse Magneto-Optical Kerr Effect. <b>2022</b> , 27, 5312	2

199	Local laser oxidation of titanium film for post-fabrication trimming of photonic integrated circuits.	1
198	Towards compact phase-matched and waveguided nonlinear optics in atomically layered semiconductors.	O
197	Quantitative Evaluation of the Phase Function Effects on Light Scattering and Radiative Transfer in Dispersed Systems. <b>2022</b> , 9, 584	0
196	Method to traceably determine the refractive index by measuring the angle of minimum deviation.	1
195	Surface plasmon resonance sensor based on D-shaped photonic crystal fiber for low refractive index detection. <b>2022</b> , 61,	0
194	Humidity-induced direct modification of optical response of plasmonic nanorod metamaterials.	
193	Avalanche ionization during UV filamentation in fused silica: suppression of blueshifted spectra extent. <b>2022</b> , 39, 2435	
192	Simulation of a Temperature-Compensated Voltage Sensor Based on Photonic Crystal Fiber Infiltrated with Liquid Crystal and Ethanol. <b>2022</b> , 22, 6374	O
191	Electromagnetic forces in the time domain. <b>2022</b> , 30, 32215	
190	Spectroscopic imaging ellipsometry of two-dimensional TMDC heterostructures. <b>2022</b> , 121, 071102	O
189	Design and research of multiparameter tunable optical filter based on phase-change Bragg grating. <b>2022</b> , 61,	
188	Computation of eigenfrequency sensitivities using Riesz projections for efficient optimization of nanophotonic resonators. <b>2022</b> , 5,	
187	Temporal-offset dual-comb vibrometer with picometer axial precision.	0
186	Numerical characterization of optical properties of tapered plasmonic structure on a cantilever pyramidal tip for plasmon nanofocusing. <b>2022</b> , 12, 085216	
185	Hybrid Plasmonic Waveguide Based Platform for Refractive Index and Temperature Sensing. <b>2022</b> , 34, 953-956	2
184	Achieving a macroscopic Nondiffracting length from a microscopic All-fiber Bessel beam generator. <b>2022</b> , 268, 169778	O
183	Achievement of low infrared emissivity photonic crystal design on [CdSe/SiO2]N periodic films. <b>2022</b> , 156, 108557	
182	A broadband SPR dual-channel sensor based on a PCF coated with sodium-silver for refractive index and temperature measurement. <b>2022</b> , 41, 105943	O

181	Surface exciton plasmon resonances (SEPR)Based sensors. <b>2023</b> , 160, 107273	1
180	Spatio-Spectro-Temporal Characterization of Ultrashort Vortex Pulses. <b>2022</b> ,	1
179	Molecular Mechanisms of Ph-Tunable Stability and Surface Coverage of Polypeptide Films.	О
178	Numerical Studies on Antiresonant Waveguide Assisted Metasurface and Its Application. <b>2022</b> , 10, 75949-75	955
177	Aluminum Nitride Grating Based Plasmonic Sensor Utilizing Enhanced Absorption. 2022, 257-264	0
176	Two Broadband Polarization Beam Splitters Based on Hybrid Lattice and Asymmetrical Elliptic Dual-Core Photonic Crystal Fiber. <b>2022</b> ,	О
175	High-Efficiency Broadband Polarization-Independent Reflective Grating with Double-Layer Dielectric Rectangle Groove in Littrow Mounting. <b>2022</b> , 12, 8612	О
174	Photonic Jets and Single-Photon Emitters. 2100365	O
173	(INVITED)Dispersion-shifted tellurite fibers for nonlinear frequency conversion. <b>2022</b> , 15, 100183	О
172	Modeling the optical properties of transparent1and absorbing dielectrics by means of Symbolic2Regression.	O
171	A Novel Buckle-Free Large Rib Microdisk with Submicrometer Thickness. 2200178	0
170	High broadband light absorption in ultrathin MoSြBolar cells.	О
169	Fused silica ablation by double ultrashort laser pulses with dual wavelength and variable delays.	О
168	Highly Sensitive Plasmonic Structures Utilizing a Silicon Dioxide Overlayer. 2022, 12, 3090	1
167	Interface Edge Mode Confinement in Dielectric-Based Quasi-Periodic Photonic Crystal Structure. <b>2022</b> , 9, 676	1
166	Broadband dispersion compensating ring-core fiber for orbital angular momentum modes. <b>2022</b> , 30, 35457	O
165	High Sensitivity Cryogenic Temperature Sensors Based on Arc-Induced Long-Period Fiber Gratings. <b>2022</b> , 22, 7119	1
164	Optical spectrum detection of synthetic microsphere resonator using a nanofiber. <b>2022</b> , 30, 35882	O

163	Prospects for Developing Low-Cost Optical Fiber Sensors for Liquid-Liquid Interface Detection. <b>2022</b> , 21, 338-350	О
162	Over-Two-Octave Supercontinuum Generation of Light-Carrying Orbital Angular Momentum in Germania-Doped Ring-Core Fiber. <b>2022</b> , 22, 6699	o
161	Power consumption analysis of an optical modulator based on different amounts of graphene. <b>2022</b> , 1, 2077	1
160	Vibrational sum frequency spectroscopy of thin film interfaces. <b>2022</b> , 17, 051202	1
159	Coupled topological edge states in one-dimensional all-dielectric heterostructures. <b>2022</b> , 30, 36900	О
158	Broadband Light Source for Optical Communication Applications Using Silicon Nanowire Embedded Pentagonal Photonic Crystal Fiber. <b>2023</b> , 143-154	O
157	Mid-Infrared Highly Efficient, Broadband, and Flattened Dispersive Wave Generation via Dual-Coupled Thin-Film Lithium-Niobate-on-Insulator Waveguide. <b>2022</b> , 12, 9130	0
156	A D-type dual side-polished, highly sensitive, plasma refractive index sensor based on photonic crystal fiber. 10,	O
155	A Combinatorial Study Investigating the Growth of Ultrasmall Embedded Silver Nanoparticles upon Thermal Annealing. <b>2022</b> , 38, 11983-11993	О
154	Spectral characteristics of gold nanoparticle doped optical fibre under axial strain. 2022, 12,	О
153	Reconfigurable and programmable optical devices with phase change materials Sb2S3 and Sb2Se3. <b>2022</b> ,	0
152	Designing a single mode anomalous dispersion silicon core fiberfor temporal multiplet formation.	О
151	Reflectance calibration of multimode optical fiber probes by probe-to-target distance reflectance profile modeling. <b>2022</b> , 203, 112002	0
150	Gas-pressure tuning of wavelength of photon pair emitted by Four-Wave-Mixing in Nanofibers. <b>2022</b> , 266, 11003	О
149	A Study of the Lossy Mode Resonances during the Synthesis Process of Zinc Telluride Films. <b>2022</b> , 22, 8108	0
148	Active control of dielectric singularities in indium-tin-oxides hyperbolic metamaterials. 2022, 12,	1
147	Volumetric evolution of elastic turbulence in porous media. <b>2022</b> , 950,	2
146	Numerical demonstration of low-reflective wire grid polarizers with a patterned Fe2O3 absorptive layer.	О

145	Broadband and perfect absorption in monolayer MoS2-based multilayered structure arranged in Kolakoski sequence. <b>2022</b> , 128,	Ο
144	Nanoparticle Shape Optimization for Tamm-Plasmon-Polariton-Based Organic Solar Cells in the Visible Spectral Range. <b>2022</b> , 9, 786	1
143	High sensitivity concave-shaped photonic crystal fiber sensor based on surface plasmon resonance. <b>2022</b> , 32, 126202	Ο
142	Strong effects of fast collisions between pulsed optical beams in a linear medium with weak cubic loss. <b>2022</b> , 170156	Ο
141	Magnetically Tunable Micro-Ring Resonators for Massive Magneto-Optical Modulation in Dense Wavelength Division Multiplexing Systems. <b>2022</b> , 22, 8163	1
140	Theoretical Analysis of Optical Properties for Amorphous Silicon Solar Cells with Adding Anti-Reflective Coating Photonic Crystals. <b>2022</b> , 9, 813	1
139	Multi-band polarization switch based on magnetic fluid filled dual-core photonic crystal fiber.	О
138	Holographic analysis of colloidal spheres sedimenting in horizontal slit pores. <b>2022</b> , 106,	Ο
137	Parametric Optimization of Hybrid Plasmonic Waveguide-Based SOI Ring Resonator Refractive Index Sensor.	1
136	Polarization-independent and ultra-sensitive biosensor with a one-dimensional topological photonic crystal. <b>2022</b> , 30, 42415	Ο
135	Advanced Lab-on-Tip ultrasound detectors: A numerical analysis. <b>2022</b> , 9, 100312	3
134	Optimization of plasmonic tapering nanostructures for strong and versatile angle-selective flat optics. <b>2022</b> ,	Ο
133	Multiperiodic photonic crystals for ultra-sensitive temperature monitoring and polarization switching. <b>2022</b> , 1-1	О
132	Highly Dispersive Optical Fiber For Orbital Angular Momentum Modes. 2022, 1-10	Ο
131	Aerosol-based deposition of broadband antireflective silica coating with closed mesoporous structure. <b>2023</b> , 250, 112078	Ο
130	Actinometry and Radiometry. <b>2022</b> , 134-176	O
129	Generation of Parabolic pulse by nonlinear pulse reshaping inside a Silicon on Insulator (SOI) Waveguide. <b>2022</b> , 2357, 012010	Ο
128	Two parameters detecting by using one Silicon core based fiber Bragg grating. 2022,	1

127	Photo-thermal effect with photonic crystals for photocatalysis and water desalination. <b>2022</b> , 16, 100215	0
126	PyMieLab_V1.0: A software for calculating the light scattering and absorption of spherical particles. <b>2022</b> , 8, e11469	O
125	Wurtzite Quantum Wires with Strong Spatial Confinement: Polarization Anisotropies in Single-Wire Spectroscopy. <b>2022</b> , 18,	0
124	Controlled fiber core mode and surface mode interaction for enhanced SERS performance.	O
123	A PCF Sensor Coated with Au-Graphene /Mxene for Low Refractive Index and Wide Detection Range Detection.	0
122	Phase Compensation Sensitized Wave Front Splitting Fiber Mach-Zehnder Interferometer. <b>2022</b> , 34, 1357-136	501
121	Transmission characteristics of DNA templated 1D photonic crystal system for 3D printing applications: Simulation. <b>2022</b> , 16, 100750	0
120	An investigation of Evanescent Wave-Induced Fluorescence Spectroscopy for Exploring High Refractive Index Media.	O
119	Subnanopore structural change of time-elapsed silica PECVD films elucidated by slow positron annihilation and ellipsometric porosimetry. <b>2018</b> , 7, 011205-011205	0
118	Experimental testing of a prototype cantilevered liquid-nitrogen-cooled silicon mirror. 2023, 30, 76-83	O
117	Highly Directive Silver Yagi-Uda Nanoantennas for Intra-/Inter-chip Nanolinks at 1550 nm. 2022,	0
116	Highly sensitive and stable probe refractometer based on configurable plasmonic resonance with nano-modified fiber core. <b>2023</b> , 220072-220072	O
115	A sandwich structure on Grapefruit microstructured fiber for measurement of non-coaxial torsion. <b>2023</b> , 75, 103164	0
114	Molybdenum precursor delivery approaches in atomic layer deposition of ⊞MoO3.	O
113	Quasi-achromatic rhomb compensator: Mueller matrix analysis versus azimuthal angle. <b>2023</b> , 764, 139600	0
112	Microcavities integrated in metal halide perovskite light-emitting field-effect transistors. 2023, 44, 106168	O
111	Reflected light microscopy of a gold oxide layer formed on a Au film by ultraviolet/ozone treatment. <b>2023</b> , 764, 139631	0
110	Detecting cancerous human liver cells with high performances using photonic crystals. <b>2023</b> , 650, 414557	О

109	Generation of a Synthetic Database for the Optical Response of One-Dimensional Photonic Crystals Using Genetic Algorithms. <b>2022</b> , 10, 4484	O
108	Double-parameter sensing of voltage and magnetic field based on photonic crystal fiber. 10,	O
107	Triply Hiding Optical Information via Excitation-Dependent Allochroic Photoluminescence Based on Cellulose Derivates. 2205697	О
106	Optical-caloric effect in diamond and vitreous silica. <b>2022</b> , 128,	O
105	Analysis of interface mode localization in disordered photonic crystal structure. 2022, 16,	O
104	Accurate compensation and prediction of thetemperature cross-sensitivity of tilted FBG claddingmode resonances.	O
103	Simulation of Self-Image Interference in Single Mode-No-Core-Single Mode Fiber with COMSOL Multiphysics [] . <b>2022</b> , 2411, 012019	O
102	Four-ray interference model for complete characterization of tubular anti-resonant hollow-core fibers. <b>2022</b> , 30, 48061	O
101	Mid-infrared refractive index photonic crystal fiber sensor based on surface plasmon resonance for ultra-high sensitivity. <b>2023</b> , 33, 016201	1
100	Intra-cavity immersion diffuser for low-coherence generation in dye and solid-state lasers. <b>2023</b> , 129,	O
99	Multi-color metasurface hologram based on depth-division multiplexing method.	O
98	Ultrahigh evaporative heat transfer measured locally in submicron water films. 2022, 12,	O
97	Plasmonic Sensors beyond the Phase Matching Condition: A Simplified Approach. <b>2022</b> , 22, 9994	O
96	Simulation on a dispersion-managed 4H-SiC on insulator waveguide for infrared supercontinuum generation. <b>2023</b> , 62, 34	O
95	Recent Progress of Supercontinuum Generation in Nanophotonic Waveguides. 2200205	1
94	On-chip integrated quantum emitter with <b>E</b> rap-enhance-guideEa simulation approach. <b>2022</b> , 30, 48051	O
93	Optical-quality assessment of a miniaturized intraocular telescope.	O
92	Multi-material design optimization of optical properties of particulate products by discrete dipole approximation and sequential global programming. <b>2023</b> , 66,	O

91	Plasmonic bound states in the continuum for unpolarized weak spatially coherent light.	O
90	Ultra-short polarization beam splitter based on rhombic structure dual-core photonic crystal fiber with a central hole filled nematic liquid crystal. <b>2023</b> , 40, 206	O
89	Flexible Displays with Multimode Reversible Switching between Transparent and Colorful States. 2202418	Ο
88	Suppressed-scattering windows for radiative cooling applications.	O
87	Effect of multi-interface patterns on the light-outcoupling of perovskite light-emitting diodes. <b>2023</b> , 122, 021106	O
86	Solving integral equations in free space with inverse-designed ultrathin optical metagratings.	O
85	AgCu/TiO2 hot-electron device for solar water splitting: the mechanisms of LSPR and time-domain characterization. <b>2023</b> ,	O
84	A fully fiber-integrated ion trap for portable quantum technologies. <b>2023</b> , 13,	1
83	Revisiting Optical Material Platforms for Efficient Linear and Nonlinear Dielectric Metasurfaces in the Ultraviolet, Visible, and Infrared.	0
82	Effect of 2-D nanomaterials on sensitivity of plasmonic biosensor for efficient urine glucose detection. 9,	O
81	Quantification of particle number concentration in liposomal suspensions by Laser Transmission Spectroscopy (LTS). <b>2023</b> , 222, 113137	O
80	Dispersive coherent Brillouin scattering spectroscopy. <b>2023</b> , 29, 100447	O
79	Molecular mechanisms of pH-tunable stability and surface coverage of polypeptide films. <b>2023</b> , 615, 156331	О
78	Compact and high-performance polarization beam splitter based on triple-waveguide coupler. <b>2023</b> , 161, 109159	O
77	Harmonic Generation and Impact of Phase Matching in Multimodal Multiphoton Microscopy. <b>2023</b> , 29, 1-9	О
76	Microfluidic for supporting Fiber-optic-based Surface Plasmon Resonance sensor. 2022,	O
75	Predicting the Structural Colors of Films of Disordered Photonic Balls. <b>2023</b> , 10, 58-70	0
74	Prozessbegleitender Nachweis ultradfiner Beschichtungen. <b>2023</b> , 63, 34-37	O

73	Effects of Curvature on Flexible Bragg Grating in Off-Axis Core: Theory and Experiment. 2023, 1-7	О
72	Thickness and refractive index measurements of a thin-film using an artificial neural network algorithm.	O
71	Ultraefficient on-Chip Supercontinuum Generation from Sign-Alternating-Dispersion Waveguides. 2200296	О
70	Compensation of Kerr-induced impairments in silicon nitride third-harmonic generators. <b>2023</b> , 31, 5229	O
69	Triple-clad W-type fiber mitigates multipath artifacts in multimodal optical coherence tomography. <b>2023</b> , 31, 4465	О
68	Improving the width of lossy mode resonances (LMRs) in double-clad fibers. <b>2023</b> , 1-6	O
67	Broadband mode converters in three-waveguide couplers based on quantumlike adiabatic transfer. <b>2023</b> , 107,	O
66	Absolute primary scintillation yield in gaseous xenon and in Xenon <b>T</b> rimethylamine mixtures. <b>2023</b> , 1049, 168038	O
65	Experimental study on the load-area relation of rough surfaces and comparison with theoretical model. <b>2023</b> , 99, 104934	1
64	Investigation of a Surface Layer Formed on Silica Glass as a Result of Mechanical-Chemical and Ionic Polishing. <b>2022</b> , 130, 573-584	O
63	Movable Optical Frequency Ruler with Optical Activity. <b>2023</b> , 10, 206	О
62	Solid-State Far-Ultraviolet C Light Sources for the Disinfection of Pathogenic Microorganisms Using Graphene Nanostructure Field Emitters. <b>2023</b> , 7,	O
61	Investigation of Silicon Core-Based Fiber Bragg Grating for Simultaneous Detection of Temperature and Refractive Index. <b>2023</b> , 23, 3936	O
60	Simulation of a Self-Referenced Meta-Grating Sensor With High Figure of Merit in NIR Communication Window. <b>2023</b> , 23, 8344-8351	O
59	Single-Layer Subwavelength Femtosecond-Laser-Induced Confined Nanocrystallization in Multistack Dielectrics. <b>2023</b> , 19,	О
58	Hybrid photon-enhanced thermionic emission and photovoltaic converter with concentrated solar power. <b>2023</b> , 254, 112279	O
57	Design of double-layer metal-dielectric reflecting polarizing beam splitter grating based on simplified mode method. <b>2023</b> , 280, 170789	О
56	Characterization of laser-induced optothermal effect in magnetic fluids based on a coreless-fiber-coupled microcavity Mach-Zehnder interferometric sensor. <b>2023</b> , 163, 109310	O

55	Polarization-insensitive refractive index sensor based on high-Q resonance in all-dielectric metasurface. <b>2022</b> ,	О
54	Design and analysis of wavelength tunable metamaterial reflector. <b>2023</b> , 10, 100366	О
53	Inverse-designed polarization multiplexing non-uniformly distributed gratings for one-dimensional beam steering. <b>2023</b> , 31, 6051	0
52	Proposal for a hybrid clock system consisting of passive and active optical clocks and a fully stabilized microcomb. <b>2023</b> , 31, 6228	O
51	Neural-network-powered pulse reconstruction from one-dimensional interferometric correlation traces. <b>2023</b> , 31, 11806	O
50	Design of ZnO/Ag dimer/porous silicon sandwich structures and theoretical investigation on its fluorescence emission mechanism. <b>2023</b> , 129,	O
49	Plasmon resonances of graphene-assisted core-bishell nanoparticles. <b>2023</b> , 98, 035509	0
48	Spectral Analysis Methods for Improved Resolution and Sensitivity: Enhancing SPR and LSPR Optical Fiber Sensing. <b>2023</b> , 23, 1666	О
47	Enhanced the sensitivity of one-dimensional photonic crystals infiltrated with cancer cells. <b>2023</b> , 10, 026202	0
46	Accurate modeling and measurement of pressure-induced group velocity dispersion variations in anti-resonant hollow-core fibers. <b>2023</b> , 48, 1506	О
45	Independent measurement of refractive index and temperature using D-gapped dual-channel structure in a photonic crystal fiber. <b>2023</b> , 55,	0
44	Design of a Broadband Fiber Optic Mode Coupler for Multimode Optical Coherence Tomography. <b>2023</b> , 10, 162	О
43	Hard-Templated Porous Niobia Films for Optical Sensing Applications. <b>2023</b> , 10, 167	0
42	Modified Distributed Bragg Reflectors for Color Stability in InGaN Red Micro-LEDs. <b>2023</b> , 13, 661	1
41	Ethyl Cellulose-Based Thermoreversible Organogel Photoresist for Sedimentation-Free Volumetric Additive Manufacturing. <b>2023</b> , 44,	0
40	Large Second-Order Nonlinearity in Poled Fused Silica*. <b>1992</b> ,	O
39	Selectively gas-filled anti-resonant hollow-core fibers for broadband high-purity LP11 mode guidance. <b>2023</b> , 48, 1622	0
38	Theoretical study on simultaneous measurement of seawater temperature and salinity based on dual fiber interferometers combined with nonlinear decoupling algorithm. <b>2023</b> , 211, 112596	О

37	A novel photovoltaic/thermal (PV/T) solar collector based on a multi-functional nano-encapsulated phase-change material (nano-ePCM) dispersion. <b>2023</b> , 280, 116797	2
36	A Numerical Exploration of Optical Soliton Reflection and Transmission At a Nonlinear/Dispersive Fiber Boundary. <b>1992</b> ,	О
35	Thickness measurements and uncertainty evaluation of a multilayer thin-film sample using auxiliary single-layer samples. <b>2023</b> , 60, 025007	O
34	Optimized Design of Antireflection Coating for Textured Silicon Solar Cells. 1992,	O
33	Power stability control based on white laser. 2023,	О
32	Electrostatic Interpretation of Phase Separation Induced by Femtosecond Laser Light in Glass. <b>2023</b> , 13, 393	O
31	Biocatalytic synthesis and ordered self-assembly of silica nanoparticles via a silica-binding peptide. 14, 280-290	0
30	Fabrication of high-aspect-ratio SiO2 nanopillars by Si thermal oxidation for metalenses in the visible region. <b>2023</b> , 62, SG1034	О
29	Strongly Enhanced Sensitivities of CMOS compatible Plasmonic Titanium Nitride Nanohole Arrays for Refractive Index Sensing under Oblique Incidence.	О
28	Efficient heat dissipation perovskite lasers using a high-thermal-conductivity diamond substrate.	О
27	Structural Insights on Ionizable Dlin-MC3-DMA Lipids in DOPC Layers by Combining Accurate Atomistic Force Fields, Molecular Dynamics Simulations and Neutron Reflectivity.	О
26	Dynamic screening of quasiparticles in WS2 monolayers. <b>2023</b> , 107,	О
25	Hybrid spatialEemporal Mueller matrix imaging spectropolarimeter for high throughput plant phenotyping. <b>2023</b> , 62, 2078	0
24	Step-Index (Semi-Immersed) Model for Photonic Nanojet and Experimental Characterization via Near-Field Optical Microscopy with Microcylinder. <b>2023</b> , 13, 1033	O
23	Plasmonic Metasurfaces for Superposition of Profile-Tunable Tightly Focused Vector Beams and Generation of the Structured Light. <b>2023</b> , 10, 317	1
22	Photoluminescence Redistribution of InGaN Nanowires Induced by Plasmonic Silver Nanoparticles. <b>2023</b> , 13, 1069	1
21	Ultrashort pulse selective laser ablation of multi-layer thin film systems. 2023,	0
20	Vanadium oxide metal-insulator phase transition in different types of one-dimensional photonic microcavities. 4,	О

19	Hierarchically Structured Deformation-Sensing Mechanochromic Pigments. 2206416	0
18	Extraction of the optical properties of waveguides through the characterization of silicon-on-insulator integrated circuits.	o
17	High-quality manipulable fiber-microsphere for super-resolution microscopy. 2023, 48, 2222	О
16	Measuring complex refractive index through deep-learning-enabled optical reflectometry. <b>2023</b> , 10, 025025	0
15	Direct sampling of ultrashort laser pulses using third-harmonic generation with perturbation in ambient air. <b>2023</b> , 48, 2154	0
14	Robust Si/Ge heterostructure metasurfaces as building blocks for wavelength-selective photodetectors. <b>2023</b> , 122, 121701	0
13	Excimer Laser Surface Patterning for Photoluminescence Enhancement of Silicon Nanocrystals. <b>2023</b> , 10, 358	0
12	Fringing Analysis and Simulation for the Vera C. Rubin Observatory Legacy Survey of Space and Time. <b>2023</b> , 135, 034503	0
11	Laser Damage Performance Study of Fundamental Frequency Dielectric Film Optical Elements. <b>2023</b> , 13, 571	0
10	Plasmonic Ring Resonator Sensor With High Sensitivity and Enhanced Figure of Merit Using an AgBiAg Bus Waveguide. <b>2023</b> , 22, 200-205	0
9	Spectral emission properties of a nitrogen-doped diamond (001) photocathode: Hot electron transport and transverse momentum filtering. <b>2023</b> , 107,	0
8	Tailoring the dielectric screening in WS2graphene heterostructures. <b>2023</b> , 7,	o
7	Wavelength-Independent Performance of Femtosecond Laser Dielectric Ablation Spanning Over Three Octaves. <b>2023</b> , 19,	0
6	Dielectric Cavity-Insulator-Metal (DCIM) Metamaterial Absorber in Visible Range. <b>2023</b> , 13, 1401	o
5	Analysis and Modeling of an Oval Shaped Silica PCF for Supercontinuum Generation. 2023,	0
4	A multi-mode super-fano mechanism for enhanced third harmonic generation in silicon metasurfaces. <b>2023</b> , 12,	0
3	Region-specified inverse design of absorption and scattering in nanoparticles by using machine learning. <b>2023</b> , 5, 024002	0
2	Active whispering-gallery microclock in pulsed-operation mode. <b>2023</b> , 107,	O

Broadband polarization-insensitive metalens with excellent achromaticity and high efficiency for the entire visible spectrum. **2023**, 122,

О